Low Mobility Cable Robot with Application to Robotic Warehousing

by

Sergio Javier Torres Méndez

A thesis
presented to the University of Waterloo
in fulfillment of the
thesis requirement for the degree of
Doctor of Philosophy
in
Mechanical Engineering

Waterloo, Ontario, Canada, 2014

AUTHOR'S DECLARATION

I hereby declare that I am the sole author of this thesis. This is a true copy of the thesis, including any required final revisions, as accepted by my examiners.

I understand that my thesis may be made electronically available to the public.

Sergio Javier Torres Méndez

Abstract

Cable-based robots consist of a rigid mobile platform connected via flexible links (cables, wires, tendons) to a surrounding static platform. The use of cables simplifies the mechanical structure and reduces the inertia, allowing the mobile platform to reach high motion acceleration in large workspaces. These attributes give, in principle, an advantage over conventional robots used for industrial applications, such as the pick and place of objects inside factories or similar exterior large workspaces. However, unique cable properties involve new theoretical and technical challenges: all cables must be in tension to avoid collapse of the mobile platform. In addition, positive tensions applied to cables may affect the overall stiffness, that is, cable stretch might result in unacceptable oscillations of the mobile platform.

Fully constrained cable-based robots can be distinguished from other types of cable-based robots because the motion and force generation of the mobile platform is accomplished by controlling both the cable lengths and the positive cable tensions. Fully constrained cable-based robots depend on actuator redundancy, that is, the addition of one or more actuated cables than end-effector degrees of freedom. Redundancy has proved to be beneficial to expand the workspace, remove some types of singularities, increase the overall stiffness, and support high payloads in several proposed cable-based robot designs. Nevertheless, this strategy demands the development of efficient controller designs for real-time applications.

This research deals with the design and control of a fully constrained cable-based parallel manipulator for large-scale high-speed warehousing applications. To accomplish the design of the robot, a well-ordered procedure to analyze the cable tensions, stiffness and workspace will be presented to obtain an optimum structure. Then, the control problem will be investigated to deal with the redundancy solution and all-positive cable tension condition. The proposed control method will be evaluated through simulation and experimentation in a prototype manufactured for testing.

Acknowledgements

First of all, I want to thank Almighty God, who has blessed and guided me to accomplish this Thesis. I would like to express my deepest appreciation to my supervisor Professor Amir Khajepour, who guidance and persistent support makes possible this dissertation.

I would like to thank my committee members: Professors John McPhee, Soo Jeon, Sanjeev Bedi, and Jeff Xi, for their comments and suggestions. I would also thank Edmon Chan (technical support), Jay Woo (components machine support), Kenneth Geertsema (software communication support), Jonathan Nivet (software communication support), Ankur Agrawal (software communication support), Gokhan Gungor (experimentation support), Professor Baris Fidan (control design support), Cochran (electrical technical support), and Mary McPherson (English tutorials).

Engineering machine shop: Rick Forgett, Karl Janzen, and Jorge Cruz, and Student machine shop: Phil Laycock and Andrew Urschel.

UW colleagues: Jonathan Spike, Jennifer Bastiaan, Abtin, Richard, Ayyoub, Reza, Hamed Jamshidifar, Masoud, Julio Noriega and Lulu Resendiz, Abel Dodero, Rury Takanayaki, Edgar Mateos and Vicky, Hosein Abyaneh, Arturo Caballero and Trinidad Badillo, March and Melody, Javier Rivera, and Rogelio Aguirre. Graduate office service: Martha Morales, Jian Zou, and Laurie Wilfong.

Mexico's family: My wife Beatriz del Carmen Aguilar Sanchez, my daughter Nancy Mayek Torres Aguilar, My parents Narcisa Mendez Ortega and Sergio Torres Ruiz, and my sister Luz Abril Torres Mendez, my aunt Leonor Mendez Ortega and cousin Victor Manuel Jimenez Mendez.

People of Instituto Tecnologico de Puebla: Maria Eugenia Lazcano, Maria del Carmen Romero Solares, Angela Garcia Vidal, Jose Antonio Duran Mejia, Carlos Gracia Franchini, Ismael Rebolledo Roman, Jesus Melgoza Palma, German Ardul Munoz Hernandez, Carlos Efren Jimenez Acosta, Alfredo Morales, Jose Rafael Mendoza Vazquez and Irma Delia Rojas, and Maria Evelinda Santiago Jimenez. Also, I would like to express my gratitude to Robert Simpson, Jose Munoz Mata, Juan de Jesus Arellano, Alberto Lagunes, and Jorge Baraona. Finally, I thank the support of the following funding agencies: Instituto Tecnologico de Puebla, DGEST, PROMEP, and University of Waterloo.

Dedicated to

Beatriz Aguilar Sanchez, wife

and

Nancy Mayek Torres Aguilar, daughter

pillars of my efforts

Table of Contents

List of Figures

List of Tables

Nomenclature

Acronyms

DOF	:	Degrees of Freedom
DC	:	Direct Current
PD	:	Proportional Derivative (controller)
PID	:	Proportional Integral Derivative (controller)
SMsat	:	Sliding Mode with saturation (controller)

Typeset Notations

δ	:	Scalar quantity
$\boldsymbol{\delta}$	:	Vector or matrix quantity
$\widehat{\boldsymbol{\delta}}$	:	Unitary vector quantity
$\underline{\boldsymbol{\delta}}$	:	Tensor quantity
$\{\ \}$	:	Vector elements
$[\ ]$	:	Matrix elements
$[\![\ ]\!]$	:	Dimensional unit
$[\ \times]$	:	Skew-symmetric matrix
$\dot{\delta}$	:	First time derivative
$\ddot{\delta}$	:	Second time derivative

Operators

dv	:	Absolute derivative
∂v	:	Partial derivative
$\cdot$	:	Dot product
$\times$	:	Cross product
$[\ ]^T$	:	Matrix or Vector transpose.
$[\ ]^{-1}$	:	Matrix inverse.
$[\ ]^{\dagger}$	:	Pseudoinverse or Moore-Penrose inverse

List of Symbols

$\mathbf{1}$	:	Identity matrix
$\mathbf{0}$	:	Zero vector or matrix
$\boldsymbol{R}$	:	Rotation transformation matrix
$\underline{\boldsymbol{I}}_p$	:	Inertia tensor of the mobile platform
$\boldsymbol{J}$	:	Jacobian matrix
$\boldsymbol{K}$	:	Stiffness matrix
$\boldsymbol{K_\tau}$	:	Stiffness matrix as a result of the cable tensions
$\boldsymbol{K_k}$	:	Stiffness matrix as a result of the cable stiffness
$\boldsymbol{A}$	:	Structure matrix
$\boldsymbol{\tau}$	:	Cable tensions vector
$\boldsymbol{\tau_w}$	:	Cable tensions to balance a external wrench
$\boldsymbol{\tau_o}$	:	Cable tensions to balance the internal forces and to make all cable tensions positive
$\boldsymbol{W}$	:	Wrench vector applied to the mobile platform
$\boldsymbol{F_e}$	:	External force vector applied to the mobile platform
$\boldsymbol{M_e}$	:	External moment vector applied to the mobile platform
$\boldsymbol{l}$	:	Cable position vector with respect to the reference frame
$\boldsymbol{p}$	:	Mobile platform position vector with respect to the reference frame
$\boldsymbol{r}$	:	Anchor position vector of the mobile platform with respect to the reference frame
$\boldsymbol{a}$	:	Anchor position vector of the static platform with respect to the reference frame
$\boldsymbol{\omega}$	:	Cable angular velocity vector
$\boldsymbol{G}$	:	Gravitational acceleration vector
$\boldsymbol{X}_p$	:	Mobile platform pose vector
$\boldsymbol{v}_p$	:	Mobile platform linear velocity vector with respect to the reference frame
$\boldsymbol{\omega}_p$	:	Mobile platform angular velocity vector with respect to the reference frame
$\boldsymbol{M}_p$	:	Inertia matrix of the mobile platform
$\boldsymbol{C}_p$	:	Coriolis, centrifugal and gravitational forces vector
$\boldsymbol{D}$	:	Design parameters vector of a cable-based robot
G_z	:	Gravitational acceleration, 9.81 m/s^2

n	:	Number of degrees of freedom
m	:	Number of cables of a cable-based robot
m_p	:	Mass of the mobile platform
f_{n_q}	:	The qth natural frequency
Γ	:	Workspace size of a cable-based robot

Chapter 1
Introduction

Global economic competition has motivated manufacturing industries to seek robots that perform faster movements, thereby reducing production time and cost and gaining a competitive advantage. According to Jeffrey A. Burnstein[1], President of the Robotic Industries Association (RIA), there is a strong trend towards non-automotive robot applications; indeed, arc welding showed a 52% gain in units, followed by material handling with 51%. Similarly, there is a growing interest in robotic applications in warehousing and distribution industries. Several industrial tasks require fast and precise repetitive movements, for instance, packaging, warehousing, machine loading and unloading, assembly, part transference, and material handling. Those tasks are called pick-and-place operations (PPO) and deal with grasping an object at one specific point, moving it to another predetermined place and then releasing it. Robot designs for this type of task are usually focused on both the initial and final points, but little attention is paid to the trajectory, as long as the robot does not suffer collisions [1]. Robots used in these tasks must move at high acceleration without affecting the operational accuracy and repeatability requirements of production systems. Another goal when designing a pick-and-place robot is smooth operation performance, that is, parts must be lifted, transferred, and deposited gently to eliminate damage and extend robot actuator life. If the motion is unstable during transitions, parts can slip from the robot's grasp. Several pick-and-place robot designs belong to the serial type, the most common being the Cartesian and SCARA robots. Current industrial demonstrations[2] have reported maximum velocities of between 3.5 m/s and 7.33 m/s, with values of ±0.04mm and ±0.15mm of repeatability, respectively, and 2g of maximum acceleration. However, cantilever structure and high inertia generate unwanted vibration, affecting operational properties.

Parallel manipulators are structures with several links connected to a mobile end effector. They form a closed chain between the static platform and the mobile platform and share the load among their actuators; thus, their stiffness is higher than that of the serial robots. However, studying them requires special methods and techniques. Parallel manipulators can use rigid links, flexible links or both. Substituting cables for rigid links in parallel robots reduces the mass of moving components, increasing the ratio of acceleration/force and the workspace of the robotic system. Moreover, adding one or more cables to the system (redundancy) is an inexpensive way to increase the system's

[1]http://www.robotics.org/content-detail.cfm/Industrial-Robotics-News/Robot-Sales-in-North-America-Jump-40-in-First-Half-of-2010/content_id/2283, accessed: August 2013

[2] http://www.atsautomation.com/automation/automationtech/st_superbot.asp, accessed: January 2012

mobility and rigidity. Nevertheless, cables can work only under tension, which might result in a robot workspace reduction, undesirable oscillations of the mobile platform, unstable configurations, and loss of controllability of the mobile platform. In order to avoid such difficulties, some solutions, developed in parallel robots and grasping mechanisms have been appropriately implemented to cable-based robots.

Several investigations have dealt with this unilateral force constraint and cable elastic properties with different solutions; for example, the application of a pretension to the cables to ensure manipulator rigidity, identification of tensionable regions, and optimal tension force distribution among cables. These approaches, however, have presented several difficulties for real applications; for example, in the recent work of Merlet [2], experimental results for four different cable-based robots have shown no agreement with the theoretical kinematic and singularity studies. Moreover, sources of accuracy errors such as cable length/tension measurement and internal/external dynamic uncertainties are not well studied for the control system design, resulting in discrepancies between simulations and experiments, Oh and Agrawal [3], and Miermeister et al. [4].

1.1 Objectives and contributions

This research investigates the design and control of a cable-based parallel manipulator for high-speed warehousing tasks, focusing on the study of redundancy, tensionability and stability. The research uses a redundant spatial eight-cable robot as a basis in large-scale applications. In summary, this research has four main objectives:

1) Investigate the kinematic and dynamic properties of a warehousing cable-based robot analyzing the issues/solutions related to singularities, redundancy solution, cable tension balance, stiffness and workspace formulations.

2) Optimization and design of a warehousing cable-based robot.

3) Develop a controller to achieve desirable accuracy and repeatability.

4) Prototype and test the warehousing cable-based robot.

1.2 Thesis organization

The complement of this Thesis is divided in five chapters, from Chapter 2 to Chapter 6. Chapter 2 presents a review of the cable-based robots which covers the relevant contributions concerning to the kinematic, dynamic and control approaches involved in the design of this type of mechanisms.

In Chapter 3 is established the theory for the design of cable-based robots with optimal workspace-stiffness. Based on this methodology the conceptual design of a cable-based robot with large workspace and high stiffness is presented. After that, the analytical workspace delineation curves of both the underconstrained and fully constrained cases are developed and analyzed. Finally, results of the proposed method are compared and discussed to the classical iterative methods.

Chapter 4 presents the controller development to achieve desirable accuracy and repeatability. A control topology is proposed and compared for robustness by means of simulations.

In Chapter 5, the experimental setup is presented. The controller developed in the last chapter is tested are discussed.

Finally, a summary of the Thesis results and contributions are presented in Chapter 6.

Chapter 2
Literature Review and Background

This chapter presents the relevant state of research for the study of cable-based robots. Although the inception of cable-based robots in the literature is recent, the production of hundreds of scientific publications justifies the use of a knowledge categorization. Moreover, cable-based robots investigations are frequently related to rigid-link parallel manipulators and grasping mechanisms, which extend even more the state of art of this type of robot [5] and [6]. This review presents the most important topics related to this research topic.

2.1 Design of cable-based robots

Cable-based robots are closed-chain mechanisms constituted of a mobile platform or end-effector connected through several cables to a static platform. These types of robots have received different names in the literature, cable-based robots, cable-driven manipulators, parallel wire robots, tendon-based parallel robots, wire-actuated parallel robots, or cable robots for short. Figure 2.1a shows a general scheme of a cable-based robot. Cable-based robots are characterized by their low-inertia and large-workspace attributes, both of which make them suitable for reconfigurable, huge-space, high load/power ratio, and high-speed applications.

The evolution of parallel rigid-link manipulators into parallel elastic-link robots has its basis in the mechanics of biological entities [7]; for example, eyes, head, hands, fingers, arms, feet and legs. For skeletal movement, tendons and muscles work together to transmit forces. On the other hand, only muscles are used to control the human orbit eye movement in almost pure rotation. All these cases require the contraction/relaxation coordination of multiple muscle-tendon units. Muscles show little inertia, and although two muscles can work in an antagonistic way, the stopping of one of these muscles does not generate ballistic motion.

On the other hand artificial antecedents of cable-based robots are usually based on two mechanical systems: parallel robots and grasping mechanisms. Definitions of cable-based robots are related to classical parallel manipulators, in which at least one closed-loop kinematic chain exists to allow the pose of a moving platform or end-effector. These classical robots first appeared in the 1960s, when Gough and Whitehall [8] developed a universal tire testing machine. Later, in the 1970s, Stewart [9] introduced his famous six degrees of freedom mechanism. One of the most successful

parallel manipulators used in high-speed pick and place operations is the Delta robot, designed by Clavel [10]. Industrial demonstrations[3], typically using a lightweight vacuum gripper, have shown a capacity of 160 pick cycles per minute, a maximum speed of 10 m/s at acceleration up to 10g, and ±0.1 mm of repeatability. Many more designs of parallel robot configurations have been developed and used in different tasks; Merlet and Gosselin [11] provide a detailed classification. Although cable-based robots are similar in structure and architecture to rigid-link parallel manipulators, their design development and mechanical analysis are quite different because of the elastic properties of cables. A parallel robot scheme is shown in Figure 2.1b.

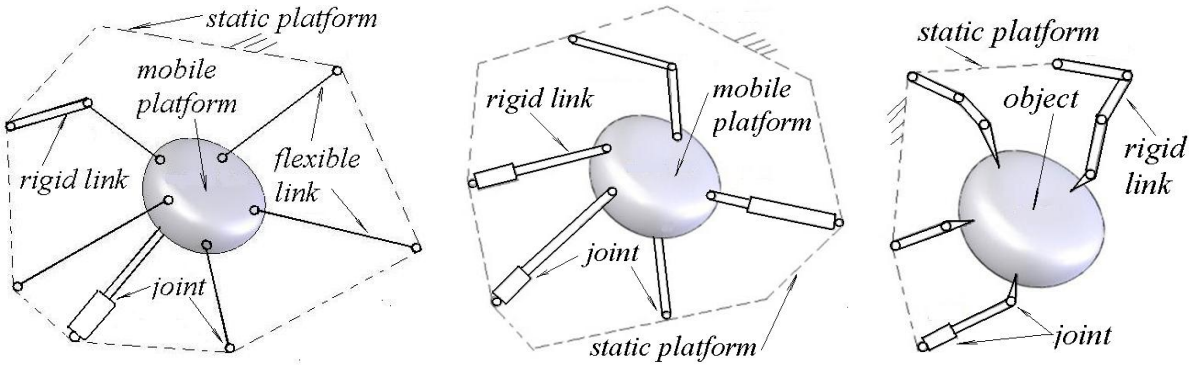

(a) (b) (c)

Figure 2.1: General schemes for analogous mechanisms: (a) Cable-based robot, (b) Parallel manipulator and (c) Grasping mechanism.

Grasping means the ability of an entity to constraint an object in a static configuration (the object is fixed with respect to the hand). The number of fingers defines the minimum number of point contacts on the object. In 1979, Okada [12] developed a three-finger hand actuated by cables, which connect each finger joint with a specific electrical actuator.

The force-closure grasp problem has been analyzed by Nguyen, first for a planar grasp [13], and after for a tridimensional grasp [14]. He realized that force-closure criteria can be developed in terms of the convexity theory to find the unlimited forces applied to actuators to balance the object to be grasped. Kawamura [15] and Pfeiffer [16] realized the importance of force control to achieve cooperative motions among fingers.

[3] http://www.adept.com/products/robots/parallel/quattro-s650h/technical-data

Grasping mechanisms must provide squeezing forces to fingers in order that they may hold an object, establishing an inverse force connection for cable-based robots. Then, several developments related to the transmission and distribution of force applied to grasping mechanisms can be inversely applied to cable-based robots and vice versa. Han et al. [17] added two more criteria to grasp analysis: the force-feasible and the force-optimal criteria. The first problem finds the bounded forces to balance the external forces applied to the object, and the second finds the optimal feasible forces. A model of a grasping mechanism is shown in Figure 2.1c.

2.1.1 Application examples

In cable-based robots, rigid links are replaced with cables. This reduces the robot weight because cables are almost massless and also eliminates the use of revolute joints. These advantages are attractive for diverse applications, some of which have been studied since the end of the nineteen century. Cable-based robot literature involving physical verification (a prototype or real robot) are included in Table 2.1, which lists the application and citations. Works on cable-based robots with only pure simulation are not included in this list.

Table 2.1: Summary of real applications of cable-based robots

Citation	General description of the task
[18], [19]	Tracking sensor
[20], [21], [22], [23], [24], [25], [26], [27], [28]	Aerial sensor
[29], [30], [31], [32], [33], [34]	Human environments interaction
[35], [36]	Highly repetitive movement training
[37], [38], [39], [40], [41], [42], [43]	Haptic systems
[44], [45], [46], [47]	Continuous path-operations
[48], [15], [49], [50], [51], [52], [53], [54], [55], [56], [57] ,[58]	Pick-and-place operations
[2], [59]	Reconfigurable and modular systems

2.2 Kinematic studies

Typically, a mobile box, part of a cable-based robot, is posed by controlling the length of cables through the actuation of fixed motors. Another strategy is to maintain constant cable lengths and control the motion of the anchor points at the fixed box. In both cases, the inverse kinematics deals with the problem of finding the actuated joint variables for a given mobile box pose. The inverse

kinematics is required for a joint space control, while the forward kinematics is used for simulation and sensor-based control. For fully constrained cable-based robots, the same inverse kinematic formulation used in rigid-link parallel manipulators is applicable; that is, cables can be modeled as massless, inextensible and straight rigid components [60], [61] and [62].

2.2.1 Classifications

Different strategies to classify cable-based robots can be found in the literature. The first method of classification was proposed by Kawamura and Ito [40]. They relate the number of degrees of freedom of a cable-based robot to the number of cables, establishing that n degrees of freedom of a mobile box of a cable-based robot will need $m=n+1$ cables. Based on this relationship, Ming and Higuchi [63] give a general classification; thus, for a Completely Restrained Positioning Mechanism (CRPM) with n degrees of freedom, $m \geq n+1$ cables are needed. If the gravity is included to constraint the mobile box, an Incompletely Restrained Positioning Mechanism (IRPM) is created. Later, Verhoeven et al. [60] include the term Redundantly Restrained Positioning Mechanism (RRPM) when the number of cables is greater than the number of degrees of freedom. However, the classification proposed by Yamamoto [64] and Bosscher [65] seems the most common: fully constrained and underconstrained cable-based robots.

In fully constrained cable-based robots the lengths of cables are used to determine the position and orientation of the mobile platform. Examples of these types of robots are the Charlotte [66] and FALCON-7 [67] robots. On the other hand, underconstrained robots need gravity in order to determine their position. The NIST robocrane [48] and the SkyCam [23] are examples of these robotic devices. The position of such robots must be determined under external perturbations in order to reach industrial operational properties, such as accuracy and repeatability.

The designs of cable-based robot manipulators reported in the literature are less frequent than those for parallel robots with rigid links. Among the first designs of cable-based robots are the NIST Robocrane [48], Landsberger robot [68], and FALCON-7 robot [67], shown in Figure 2.2.

These three cable-based robot configurations were used for a new generation of cable-based robot designs. The NIST Robocrane, also called by Yanai et al. [69] a Crane type manipulator, has a suspended mobile platform connected by six cables to a fixed platform. Based on the NIST Robocrane, the patented device SkyCam was developed by Brown [23].

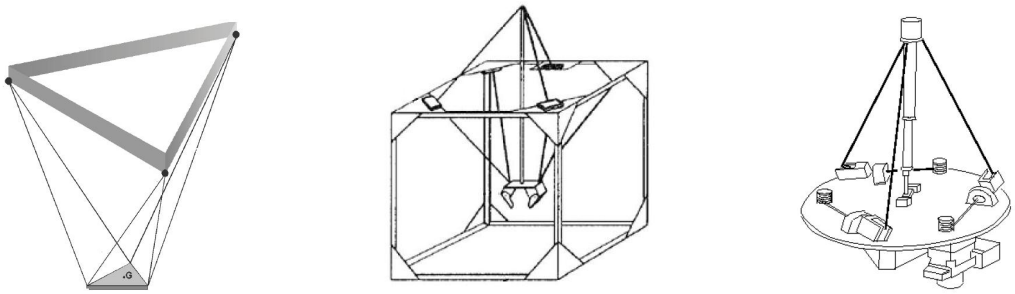

(a) (b) (c)

Figure 2.2: Cable-based type manipulators, (a) NIST robocrane [48], (b) FALCON-7 robot [67], and (c) Landsberger robot [68].

The SkyCam is a robotic device with a camera suspended from a four-cable-driven system with manual control. It is used in indoor locations such as stadiums and arenas. The FALCON-7 robot uses seven cables to completely restraint its mobile end-effector. This robot was used as a basis for the following cable-based robots: Charlotte robot [66], which has eight cables to fully constrain the movement of its mobile platform; WARP robot [49], WiRo robot [70], Marionette robot [62] and the C4 robot [71]. The Landsberger robot uses a rigid link, also called a spine, with three cables to improve its stiffness. The Landsberger robot motivated the creation of different designs called hybrid robots because they use rigid and flexible links; for example, the C3W4 [52], Betabot and Deltabot robots [72].

Tadokoro [42] classifies the cable-based robots according to the number of cables connected at the same position of an actuator unit. Tadokoro recognized the influence of these types of connecting combinations in the performance of the WARP robot, used for virtual reality applications. For example, a 5-2-1 combination means that a group of five actuators are located at the same place; another group is composed of two actuators, and the last group has only one actuator. Then, this cable-based design with eight active cables can present seventeen combinations with a minimum of three groups of actuation units.

2.2.2 Singularity conditions

Although the concept of singularity for serial and parallel robots (with rigid and flexible links) has different descriptions, the problem in principle is the same. Singularity studies refer to a particular

configuration of a mechanism in which its end-effector loses control and some joint velocities approach infinite. In consequence, singular configurations must be avoided or eliminated in order to maintain control of the robot. Thus, singularity analysis is indeed a measurement for evaluating a good or poor design.

Several papers have developed strategies to identify different types of singularities. Gosselin and Angeles [73] identify and classify different types of singularities for closed mechanisms and parallel manipulators. Later, Zlatanov et al. [74] presented a more general classification based on a velocity equation including the end-effector and joint velocities. Other researchers have been developing methods to analyze singularity-free workspaces and procedures to exclude and eliminate singularity configurations in parallel mechanisms.

Gosselin and Wang [75] found the singularity locations in planar parallel mechanisms, and one year later, the same authors [76] did the same for spherical parallel mechanisms. Dash et al. [77] established a path-planning strategy to avoid singularities, which are represented as obstacles. Kumar and Dash [78] reduced the singularities by changing the location of the actuators in a five-bar closed mechanism. Arakelian et al. [79] identified and minimized singularity zones by using the pressure angle as an indicator of force transmission. Kotlarski et al. [80] and Li et al. [81] eliminated singularities by adding appropriate redundant actuation to planar parallel and Stewart mechanisms.

Recent efforts to develop optimal design techniques to increase singularity-free workspaces of parallel robots are presented by [82], [83] and [84]. For cable-based robots, because of the unilateral driving capabilities of flexible cables, conventional rigid-link parallel robot methods cannot be directly applied to find all singularities. Yang et al. [85] prove that the use of the Jacobian, normally a non-square matrix, is valid only when all cables are in tension.

In general, a cable-based robot losses tensionability (positive tension cannot be exerted on all cables at the same time) when the mobile platform falls into the neighborhood of a singular configuration. Consequently, the control of the mobile box is impossible; that is, the mobile box makes only ineffectual *shaking* motions, even though the length of the cables has not changed, Hiller et al. [86]. Then, two types of singularities for cable-based robots can be identified: the rank-deficient Jacobian matrix (kinematic singularity) and the not fulfillment of tensionable solutions (force singularity) for all cables simultaneously along a desired path [87]. Several works are related to the avoidance and elimination of these two types of singularities. Su et al. [88] recommend changes in the cable-based robot design when there are near-singularity configurations that affect a system's

controllability: rearrangement of the attached point on the mobile box and modification of the location of the anchor points in the static box. Lahouar et al. [45] adapt the path planning methods of serial manipulator by modeling singularities as obstacles in an under-constrained spatial four-cable-driven robot. Qiu et al. [89] eliminate the force singularity of a large-scale cable robot by adding one more cable to the lower part of a large-scale crane design for radio telescope applications.

Alikhani et al. [90] study force singularities for the development of an optimal large-scale cable-based robot design. They separate the singular problem by identifying the contribution of the upper and the lower cables. They suggest that the lower cables are responsible for the pretension, and the upper cables affect the motion of the mobile box. Hassan and Khajepour investigate the singular configurations of hybrid cable-based robots [91].

2.2.3 Model formulation

In this section, a mathematical model of a fully constrained cable-based robot is presented. A schematic representation of such a robotic system is presented in Figure 2.3.

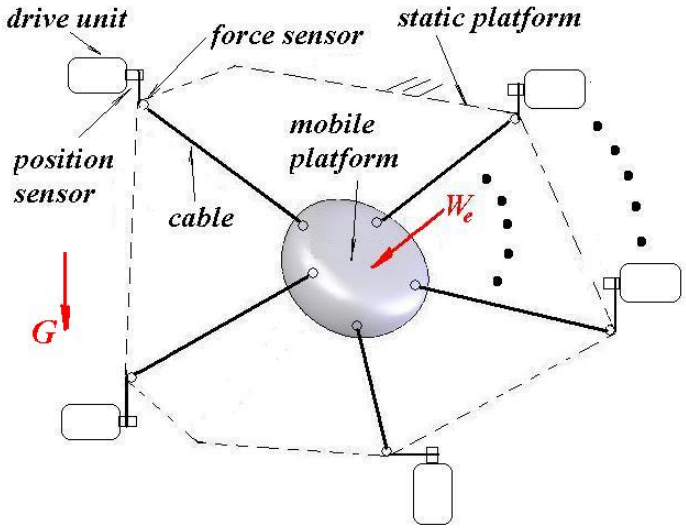

Figure 2.3: Components of a cable-based robotic system.

In this scheme, one end of each cable is attached to a mobile platform and the other side is connected to a drive unit. Typically, a drive unit consists of one or more pulleys which guide the cable to a drum which recollects/releases the cable in relation to the rotation of the shaft of a motor. Force and position sensors may be added to measure the tension and length of each cable. The goal is to move

the mobile platform to a desired pose by simultaneously changing the cable lengths and at the same time maintaining a positive cable tension. The theoretical model of this system is formulated assuming that each cable is always under positive tension for a given pose of the mobile platform.

An equivalent model, based on the above mentioned cable-based robotic system, is shown in Figure 2.4.

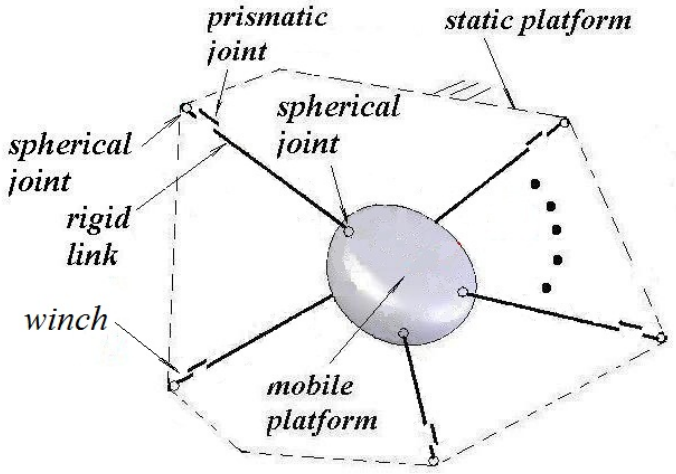

Figure 2.4: Equivalent cable-based robotic system.

This representation is characterized by assuming cables are massless (cables are thin and light), firmly stretched (cable slackness is ignored), and inelastic (any cable's elongation is compensated).

In this context, each cable is modeled as a subsystem composed of two moving elements, two spherical joints and one prismatic joint. Therefore, any cable subsystem has six degrees of freedom with five restraints to be added to the system to make cable lengths the active joints to control [63].

The system model is composed of $2m$ rigid links, one mobile platform, $2m$ spherical joints and $1m$ prismatic joints. Based on Grübler-Kutzbach's formula for spatial motions, the total number of DOF of the system is $n = 6(2m + 1) - m[2(6 - 3) + (6 - 1)] = m + 6$ DOF. However, regardless of the number of cables, a spatial mobile platform must have six DOF. This can be obtained by assuming that each cable twist is not affecting the pose of mobile platform; that is, m degrees of freedom can be reduced from the latter result; thus, $n = m + 6 - m = 6$. The same result can be obtained if each spherical joint between the winch and static box is substituted by a universal joint [92], [93]. This approach facilitates the creation of a virtual model in software packages as ADAMS and MAPLESim. Alternatively, for planar movements (three DOF) of the mobile platform, each

spherical joint must be replaced by a revolute joint whose axis of rotation must be perpendicular to the plane of motion of the mechanism.

Based on the previous model and assuming a mobile platform with six degrees of freedom, a general kinematic formulation is developed. Figure 2.5 shows the closure position vectors for cable *i* in a general spatial *m*-cable robot.

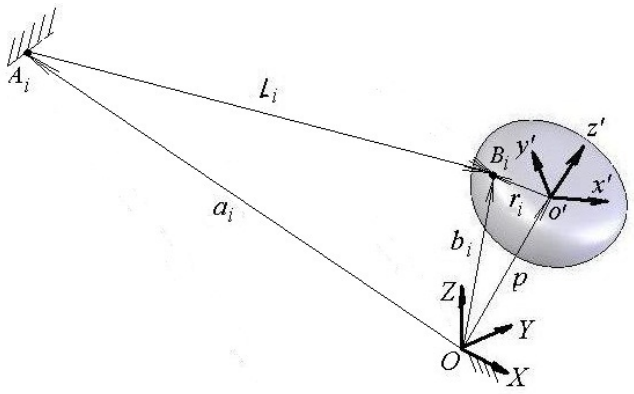

Figure 2.5: Kinematic position parameters.

A coordinate system x'y'z' is fixed at the mass center of the mobile platform *o'* and another, XYZ, is fixed at a reference point *O*. Vector $\boldsymbol{p} = [P_x \quad P_y \quad P_z]^T$ establishes the position of the mobile platform between these two coordinate systems. Vector $\boldsymbol{l_i}$ is the *i*th cable vector connecting the anchors points A_i and B_i at the static and mobile platform, respectively. Thus, constant vectors $\boldsymbol{a_i}$ and $\boldsymbol{r'_i}$ are placed with respect to the base and the mobile coordinate systems. Using the transformation $\boldsymbol{r_i} = \boldsymbol{R_{321}}\boldsymbol{r'_i}$, where $\boldsymbol{R_{321}}$ is the rotation transformation matrix with the sequence ZYX of the Euler angles $\boldsymbol{\theta_p} = [\alpha \quad \beta \quad \gamma]^T$ for the desired orientation of the mobile platform, it becomes:

$$\boldsymbol{R_{321}} = \begin{bmatrix} c(\alpha)c(\gamma) - s(\alpha)s(\gamma)s(\beta) & -s(\alpha)c(\beta) & c(\alpha)s(\gamma) + s(\alpha)s(\beta)c(\gamma) \\ s(\alpha)c(\gamma) + c(\alpha)s(\gamma)s(\beta) & c(\alpha)c(\beta) & s(\alpha)s(\gamma) - c(\alpha)s(\beta)c(\gamma) \\ -c(\beta)s(\gamma) & s(\beta) & c(\gamma)c(\beta) \end{bmatrix}$$

where $\boldsymbol{R_{321}} = \boldsymbol{R}(Z,\alpha)\boldsymbol{R}(X',\beta)\boldsymbol{R}(Y'',\gamma)$ is obtained with the three basic rotation transformation matrices around Z axis, X' axis, Y'' axis, and $c(\phi) = \cos(\phi)$ and $s(\phi) = \sin(\phi)$. Then, the mobile platform pose with respect to the reference frame can be denoted as $\boldsymbol{X_p} =$

$[P_x \quad P_y \quad P_z \quad \alpha \quad \beta \quad \gamma]^T$. The closure vector equation for the position of the mobile platform is obtained as:

$$\boldsymbol{l}_i = \boldsymbol{p} + \boldsymbol{r}_i - \boldsymbol{a}_i\,, \quad \forall\, i = 1,2 \ldots m. \tag{2.1}$$

The *i*th cable's length is obtained by applying the 2-norm Euclidian norm to Eq. (2.1) as

$$l_i = \|\boldsymbol{p} + \boldsymbol{r}_i - \boldsymbol{a}_i\|, \quad \forall\, i = 1,2 \ldots m. \tag{2.2}$$

Differentiating Eq. (2.1) results in

$$\dot{l}_i \hat{\boldsymbol{l}}_i + \boldsymbol{\omega}_i \times \boldsymbol{l}_i = \boldsymbol{v}_p + \boldsymbol{\omega}_p \times \boldsymbol{r}_i\,, \forall\, i = 1,2, \ldots m. \tag{2.3}$$

Equation (2.3) relates the cable velocities with the mobile box velocities; then, for any *i*th cable: $\dot{l}_i$ is the rate of change in the length; $\boldsymbol{\omega}_i$ is the angular velocity vector, $\hat{\boldsymbol{l}}_i$ is the cable unitary vector in the reference frame. For the mobile box, $\boldsymbol{v}_p = \dot{\boldsymbol{p}}$ and $\boldsymbol{\omega}_p$ are the linear and angular velocities with respect to reference frame. Expressing any cable unitary vector in its Cartesian components results in:

$$\hat{\boldsymbol{l}}_i = \frac{\boldsymbol{l}_i}{l_i} = \frac{\boldsymbol{l}_{i_X}}{l_i} + \frac{\boldsymbol{l}_{i_Y}}{l_i} + \frac{\boldsymbol{l}_{i_Z}}{l_i} = \left(\frac{l_{i_X}}{l_i}\right)\hat{\boldsymbol{l}}_{i_X} + \left(\frac{l_{i_Y}}{l_i}\right)\hat{\boldsymbol{l}}_{i_Y} + \left(\frac{l_{i_Z}}{l_i}\right)\hat{\boldsymbol{l}}_{i_Z} = \begin{bmatrix}\hat{l}_{i_X} & \hat{l}_{i_Y} & \hat{l}_{i_Z}\end{bmatrix}^T$$

Equation (2.3) can be written as $\dot{l}_i = \hat{\boldsymbol{l}}_i \cdot \left(\boldsymbol{v}_p + \boldsymbol{\omega}_p \times \boldsymbol{r}_i - \boldsymbol{\omega}_i \times \boldsymbol{l}_i\right) = \hat{\boldsymbol{l}}_i \cdot \boldsymbol{v}_p + (\boldsymbol{r}_i \times \hat{\boldsymbol{l}}_i) \cdot \boldsymbol{\omega}_p$, or in matrix form

$$\begin{Bmatrix}\dot{l}_1 \\ \dot{l}_2 \\ \vdots \\ \dot{l}_m\end{Bmatrix} = \begin{bmatrix}\hat{l}_{1_X} & \hat{l}_{1_Y} & \hat{l}_{1_Z} & (\boldsymbol{r}_1 \times \hat{\boldsymbol{l}}_1)_X & (\boldsymbol{r}_1 \times \hat{\boldsymbol{l}}_1)_Y & (\boldsymbol{r}_1 \times \hat{\boldsymbol{l}}_1)_Z \\ \hat{l}_{2_X} & \hat{l}_{2_Y} & \hat{l}_{2_Z} & (\boldsymbol{r}_2 \times \hat{\boldsymbol{l}}_2)_X & (\boldsymbol{r}_2 \times \hat{\boldsymbol{l}}_2)_Y & (\boldsymbol{r}_2 \times \hat{\boldsymbol{l}}_2)_Z \\ \vdots & \vdots & \vdots & \vdots & \vdots & \vdots \\ \hat{l}_{m_X} & \hat{l}_{m_Y} & \hat{l}_{m_Z} & (\boldsymbol{r}_m \times \hat{\boldsymbol{l}}_m)_X & (\boldsymbol{r}_m \times \hat{\boldsymbol{l}}_m)_Y & (\boldsymbol{r}_m \times \hat{\boldsymbol{l}}_m)_Z\end{bmatrix} \begin{Bmatrix}v_{p_X} \\ v_{p_Y} \\ v_{p_Z} \\ \omega_{p_X} \\ \omega_{p_Y} \\ \omega_{p_Z}\end{Bmatrix} \tag{2.4}$$

Equation (2.4) has the well known form of

$$\frac{d\boldsymbol{l}}{dt} = \boldsymbol{J}\frac{d\boldsymbol{X}_p}{dt} \tag{2.5}$$

where $\boldsymbol{J}$ represents the Jacobian matrix. In general, the rank-deficient Jacobian matrix results in geometrical singularities of a robot, frequently related to configurations near the boundaries of the

robot workspace and loss of full motion. Thus, for fully constrained cable-based robots ($m>n$) and supposing all cables are always in tension by the application of positive cable tensions, a non-singular configuration satisfies the condition:

$$rank\, \boldsymbol{J} = n, \text{if } \boldsymbol{J} \in \mathbb{R}^{m \times n} \text{ where } n < m. \tag{2.6}$$

2.3 Force formulations

Force analysis of cable-based robots is related to the study of a particular pose of the mobile platform, where all-positive cable tension conditions must be maintained to balance a given wrench by solving the dynamics or static equations with or without additional constraints, for example, bounded cable tensions. In consequence, this analysis is imperative for design and control development. A cable-based robot can be seen as a set of rigid and flexible elements, which under certain circumstances (straight cables and rigid joints) can be modeled as a multibody rigid system. Under this situation, the dynamic model is easily formulated by using Newton-Euler motion equations that incorporate the static model, ensuring always positive driving forces. Lagrange's formulation with Lagrange's multipliers give a better knowledge of the cables tensions [94], and together result in ordinary differential algebraic equations. However, by its physical-meaning, clarity, and ease of applicability, the Newton-Euler formulation seems to be the most popular approach to deriving the dynamic equations of cable-based robots [46], [95] and [93]. Further works have dealt with the problem of finding accurate and easy-to-solve dynamic models in order to clarify and predict different scenarios quickly and cheaply. Bedoustani et al. [96] include the elastic and damping effects of cables in an overall dynamic model of an aerostat large-scale cable-based robot. Miermeister and Pott [51] present a dynamic model with friction of the cable-based robot IPAnema. Du et al. [97] analyze the cable sag effect in the dynamic model of a large-scale undetermined cable-based robot.

A variety of conditions and methods have been proposed for evaluating whether a given configuration meets all-positive cable tension requirements. Force-closure (vector-closure or wrench-closure) analysis gives conditions in which a given configuration can support any arbitrary wrench applied to the mobile platform if unbounded positive cable tensions are allowed [15] and [98]. Supposing a non-singular pose, Ming and Higuchi [63] solved the force equation by using the pseudoinverse formulation and determine the force-closure condition if the nullspace of the structure matrix (a transpose of the Jacobian matrix) is always positive. Proof of the force-closure is given in

[99] and [100] by analyzing the nullspace of the structure matrix. This proof is based on the existence of a positive vector in the nullspace of the structure matrix, which results in a positive tension solution in the homogenous term (internal force) of the pseudoinverse solution. This internal force can be used to balance any negative tension (as a result to balance any wrench) without changing the wrench. A particular case of the latter solution was established by [101] for cable-based robots with one redundant cable, where the force-closure can be satisfied if the components of the nullspace vector of the structure matrix are all positive or negative. Diao and Ma [102] present another method to verify the force-closure condition by checking that all hyperplanes of the structure matrix are separating hyperplanes of the structure matrix. This method to check force-closure is based on convex sets analysis; thus, a force-closure exists if the convex hull of the set of the columns of the structure matrix lies in the general neighbourhood of the origin [103] and [104]. Hassan and Khajepour [58] developed a method based on convex analysis and the Dykstra algorithm to check force-closure conditions.

The inclusion of bounded cable tensions affects the assumption of an unbounded wrench applied to a mobile platform (force-closure condition). Thus, the feasible-wrench condition is established when a given constant static wrench is applied to a mobile platform subjected to a given interval of tensions. The feasible-wrench condition gives a more realistic result than the force-closure condition; in consequence, this analysis must be included in any design and control analysis. The methods used to analyze the force-closure condition can be extended to study the feasible-wrench condition by adding the wrench and the tension limits. Pham et al. [105] developed a recursive algorithm to find an equivalent one-dimension system of the higher dimension of the nullspace of the structure matrix. Pott et al. [106] used the minimum norm solution (pseudoinverse) to the difference between the median of the given limits tensions and the actual tension. According to Gosselin and Grenier [107], the performance of these tension solutions is better. Moreover, they evaluated several feasible-wrench formulations based on different norms.

2.3.1 Stiffness

Stiffness/compliance can be related respectively to the rigidity/flexibility of a mechanical system (with elastic components). For practical applications, low rigidity is related to poor positioning accuracy, trajectory errors and loss of controllability; therefore, stiffness modeling, low-stiffness workspace identification and the enhancement of stiffness is required before such effects (mobile box

oscillations) can be compensated with a control system [108]. Examples of these studies in several mechanical systems can be found in [109] for parallel robots, [110] serial robots, and [111] grasping mechanisms. In general, stiffness measures the resistance of a robotic system to a displacement as a result of applying an external force to its end-effector along a degree of freedom. In the case of cable-based robots, all cables are frequently modeled as massless springs having only axial deformations with the same and constant stiffness [112]. Other models include the elasticity property of the cable material and the variation of the cross-sectional area, Merlet [113]. On the other hand, the mobile box is modeled with infinite stiffness (a rigid body); however, it might present finite rotational and translational stiffness. Thus, several approaches to calculate the overall stiffness have been studied. Behzadipour and Khajepour [114] use an equivalent four-spring model for each cable to analyze the effects of antagonistic forces in the overall stiffness of cable-based robots.

Yu et al. [115] use the stiffness definition in order to find the Cartesian and joint stiffness; further simulations verify that redundancy changes the stiffness mapping of the robotic system. Using the differential transformation principle, Liu et al. [116] find the stiffness matrix expression for an eight-cable robot used as an airplane wind tunnel tester. This expression includes both effects: cable tensions and the robot configuration. The authors enhance the stiffness in three directions by using an optimal cable tension distribution method. Yang et al. [117] divide the stiffness study of a spherical joint cable-based robot into two parts: the structural parameters (only driving and transmission systems are considered flexible) and the cable tensions, realizing that the overall stiffness is related to the mobile box pose, cable stiffness and cable tensions. Stiffness studies provide a basis for stability analysis and the development of robust control strategies.

2.3.2 Stability

Because of the constraint affinities (unidirectional forces) between grasping mechanisms and cable-based robots; studies of frictionless grasping stability can be extended to cable-based robot studies. Howard and Kumar [118] classify the grasp equilibrium and develop conditions to determine frictionless stable grasping. Svinin et al. [119] consider grasping stability as a force distribution problem, which can be stabilized by a simple control law. Hanafusa and Adli [120] and Svinin et al. [121] extended the grasping stability conditions for parallel manipulators. They establish that a parallel manipulator is stable around an equilibrium point if its stiffness matrix is positive definite.

Using two planar parallel manipulators as examples, Svinin shows that singular configurations can be stable or not, depending on the force distribution and the form of the singular configuration.

A general stability definition for cable-based robots is given by Bosscher and Ebert-Uphoff [65] as the ability of a cable-based robot to resist external disturbances applied to the mobile box at a given equilibrium pose during infinitesimal motions of the mobile box. Behzadipour and Khajepour [114] establish the concept of stabilizability as a particular property for cable-based robots if antagonistic cable forces are used to increase the overall stiffness of the system. Then, a cable-based robot becomes stabilizable if the total stiffness matrix (obtained from the contribution of the elastic and antagonistic stiffness of each cable) is positive definite.

2.3.3 Model conception

The force analysis deals with the problem of finding the forces (cable positive tensions) for a specific equilibrium point of the system. This analysis begins with the static equilibrium followed by a dynamic study by the addition of the translational motion (Newton's equation) and the rotational motion about the mass center (Euler's equation), as is shown in Figure 2.6.

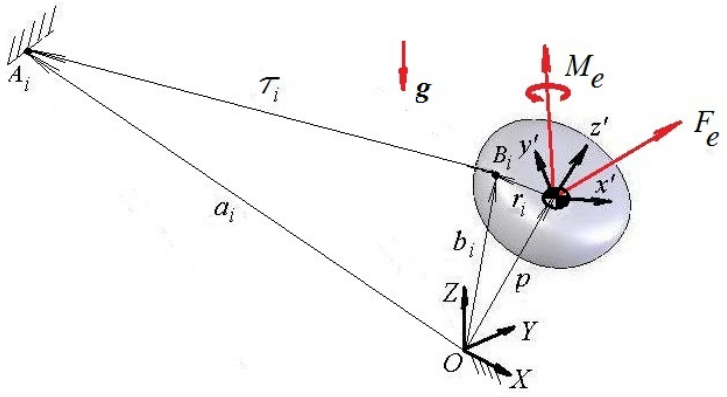

Figure 2.6: Static parameters.

In this analysis, the external forces and moments are assumed constant and acting along the center of mass of the mobile platform. Thus, the mobile box static equations are:

$$\sum_{i=1}^{m} \boldsymbol{\tau}_i + \boldsymbol{F}_e + m_p \boldsymbol{G} = \boldsymbol{0} \tag{2.7a}$$

$$\sum_{i=1}^{m} (\boldsymbol{r}_i \times \boldsymbol{\tau}_i) + \boldsymbol{M}_e = \boldsymbol{0} \tag{2.7b}$$

where $\boldsymbol{F}_e$ and $\boldsymbol{M}_e$ are the external forces and moments applied to the mobile platform; m_p is the mobile platform mass; and $\boldsymbol{G}$ is the gravitational acceleration vector. Tensions applied to the cables can be written as $\boldsymbol{\tau}_i = -\tau_i \hat{\boldsymbol{l}}_i$; then equations (2.7a) and (2.7b) can be written as

$$\boldsymbol{F}_e + m_p \boldsymbol{G} = \sum_{i=1}^{m} \tau_i (\hat{\boldsymbol{l}}_{i_X} + \hat{\boldsymbol{l}}_{i_Y} + \hat{\boldsymbol{l}}_{i_Z}) \tag{2.8a}$$

$$\boldsymbol{M}_e = \sum_{i=1}^{m} \tau_i \left[(\boldsymbol{r}_i \times \hat{\boldsymbol{l}}_i)_X + (\boldsymbol{r}_i \times \hat{\boldsymbol{l}}_i)_Y + (\boldsymbol{r}_i \times \hat{\boldsymbol{l}}_i)_Z \right] \tag{2.8b}$$

Assuming the gravitational acceleration is acting along the vertical Z axis $\boldsymbol{G} = [0 \quad 0 \quad -G_z]^T$. Thus, the matrix form is shown by

$$\begin{Bmatrix} F_{e_X} \\ F_{e_Y} \\ F_{e_Z} - m_p G_z \\ M_{e_X} \\ M_{e_Y} \\ M_{e_Z} \end{Bmatrix} = \begin{bmatrix} \hat{l}_{1_X} & \hat{l}_{2_X} & \cdots & \hat{l}_{m_X} \\ \hat{l}_{1_Y} & \hat{l}_{2_Y} & \cdots & \hat{l}_{m_Y} \\ \hat{l}_{1_Z} & \hat{l}_{2_Z} & \cdots & \hat{l}_{m_Z} \\ (\boldsymbol{r}_1 \times \hat{\boldsymbol{l}}_1)_X & (\boldsymbol{r}_2 \times \hat{\boldsymbol{l}}_2)_X & \cdots & (\boldsymbol{r}_m \times \hat{\boldsymbol{l}}_m)_X \\ (\boldsymbol{r}_1 \times \hat{\boldsymbol{l}}_1)_Y & (\boldsymbol{r}_2 \times \hat{\boldsymbol{l}}_2)_Y & \cdots & (\boldsymbol{r}_m \times \hat{\boldsymbol{l}}_m)_Y \\ (\boldsymbol{r}_1 \times \hat{\boldsymbol{l}}_1)_Z & (\boldsymbol{r}_2 \times \hat{\boldsymbol{l}}_2)_Z & \cdots & (\boldsymbol{r}_m \times \hat{\boldsymbol{l}}_m)_Z \end{bmatrix} \begin{Bmatrix} \tau_1 \\ \tau_2 \\ \vdots \\ \tau_m \end{Bmatrix} \tag{2.9}$$

In a compact representation, (2.9) can be written as

$$\boldsymbol{W} = \boldsymbol{A}\boldsymbol{\tau} \tag{2.10}$$

where $\boldsymbol{W} \in \mathbb{R}^n$ is the wrench vector to balance under static equilibrium. It is easy to observe a relationship between equations (2.4) and (2.9) as $\boldsymbol{A} = \boldsymbol{J}^T$. Matrix $\boldsymbol{A}$ is called the structure matrix and depends on the parameters of the robot and the pose of the mobile platform. Cable tensions to balance wrench can be found by inverting $\boldsymbol{A}$ ensuring all cable tensions are always positive. However, for fully constrained cable-based robots, the number of cables *m* is larger than the degrees of freedom *n* of the mobile platform; in consequence, $\boldsymbol{A} \in \mathbb{R}^{n \times m}$ and it may have infinite cable tensions solutions (underdetermined linear system). A free-singular pose of the mobile platform means that condition

(2.6) is satisfied, which results in that $\boldsymbol{A}$ has full row-rank. Assuming the last condition, the solution of Eq. (2.10) can be obtained as

$$\boldsymbol{\tau} = \boldsymbol{\tau}_w + \boldsymbol{\tau}_o \tag{2.11}$$

where $\boldsymbol{\tau}_w \in \mathbb{R}^m$ is a solution and $\boldsymbol{\tau}_o \in \mathbb{R}^m$ is the homogenous solution. Thus, $\boldsymbol{A\tau}_o = \boldsymbol{0}$ and $\boldsymbol{A\tau} = \boldsymbol{A\tau}_w + \boldsymbol{A\tau}_o = \boldsymbol{W}$; which indicates that any vector from the null space of $\boldsymbol{A}$ added to $\boldsymbol{\tau}_w$ is indeed a solution of Eq. (2.10). If minimum cable tension solutions are desired in order to reduce the size of the drivers, the pseudoinverse matrix is the most common formulation to use. Then, (2.11) is given by

$$\boldsymbol{\tau} = \boldsymbol{A}^{\dagger}\boldsymbol{W} + (\boldsymbol{I} - \boldsymbol{A}^{\dagger}\boldsymbol{A})\boldsymbol{\vartheta} \tag{2.12}$$

where $\boldsymbol{A}^{\dagger} \in \mathbb{R}^{m\times n}$ is called the Moore-Penrose inverse or pseudoinverse of $\boldsymbol{A} \in \mathbb{R}^{n\times m}$ where $\boldsymbol{AA}^{\dagger}\boldsymbol{A} = \boldsymbol{A}$, and $\boldsymbol{A}^{\dagger} = \boldsymbol{A}^T(\boldsymbol{AA}^T)^{-1}$, and $\boldsymbol{I} \in \mathbb{R}^{m\times m}$ is the identity matrix. The first term of Eq. (2.12) represents a vector with the minimum 2-norm solution without considering the cable tension constraints, and therefore the cable tensions might be negative. The second term is an arbitrary vector from the nullspace of $\boldsymbol{A}$ depending on $\boldsymbol{\vartheta} \in \mathbb{R}^m$. Equation (2.12) can be rewritten as

$$\boldsymbol{\tau} = \boldsymbol{A}^{\dagger}\boldsymbol{W} + \boldsymbol{Nh} \tag{2.13}$$

where $\boldsymbol{Nh}$ is an arbitrary vector of cable tensions to balance the redundant cables among all the cables without affecting the pose of the mobile platform (internal forces). This vector is used to make all cable tension positive. $\boldsymbol{N} \in \mathbb{R}^{m\times(m-n)}$ is the nullspace or kernel of $\boldsymbol{A}$, and $\boldsymbol{h} \in \mathbb{R}^{(m-n)}$ must be determined such that all cable tensions be positive (minimum requirement). Thus, the problem is reduced to select a criterion to find a unique value(s) of $\boldsymbol{h}$ subjected to $\tau_i \geq 0 \; \forall \; i = 1,2 \ldots m$. The latter is called force-closure condition with the assumption that unlimited actuator forces can be applied to the cables in order to support any arbitrary wrench. The force-closure condition is satisfied when the homogenous term of the structure matrix is always strictly positive [63], that is

$$\forall \; \boldsymbol{N} \in null(\boldsymbol{A}), \exists \; \boldsymbol{Nh} \in \mathbb{R}_+^m \text{ , where } \boldsymbol{A} \in \mathbb{R}^{n\times m} \text{ and } n < m \tag{2.14}$$

However, in real applications, cable tensions are bounded by lower and upper cable tension limits because lower tension limits maintain cables taut ensuring a minimum overall stiffness of the robot, and upper tension limits avoid excessive deformation of the cables and the use of big actuators. Here,

the minimum 2-norm solution is used to select $\boldsymbol{h}$ which minimizes the tensions among all cables while all cable tensions remain bounded; in other words

$$\begin{aligned} &\text{minimize } \mathrm{F} = \left(\sum_{\mathrm{i}=1}^{\mathrm{m}} \tau_i^2\right)^{1/2}. \\ \text{Subjected to} \quad &\boldsymbol{W} = \boldsymbol{A\tau} \\ \text{and} \quad &0 < \tau_{i,\min} \leq \tau_i \leq \tau_{i,\max} \;\; \forall \; i = 1,2,\dots m. \end{aligned} \tag{2.15}$$

On the other hand, feasible wrenches are those constant static forces/moments applied to the mobile platform that can be balanced by all positive cable tensions, which might be subjected to a set of cable tension limits. Conditions to determine the feasibility of balancing a wrench [58], [122], are as follows:

$$\begin{aligned} &\exists \left\{\boldsymbol{\tau} \middle| \boldsymbol{\tau} = \boldsymbol{A}^{\dagger}\boldsymbol{W} + \boldsymbol{Nh}, \boldsymbol{Nh} \in \mathbb{R}_{+}^{\boldsymbol{m}}, \text{where } n < m \right\} \cap \\ &\{\boldsymbol{\tau} | 0 < \tau_{i,min} \leq \tau_i \leq \tau_{i,max} \;\; \forall \, i = 1,2,\dots,m\} \end{aligned} \tag{2.16}$$

In other words, this condition establishes that there is at least a solution to Eq. (2.13) which intersects the convex set delimited by the cable tension limits. This convex set is essentially a hyperbox in $\mathbb{R}_{+}^{m}$. Then, two infeasible wrench situations can occur; the inability of a certain pose of the mobile platform to satisfy the force-closure condition and the impossibility of finding a set of cable tensions to fulfill the set of cable limits for a given wrench applied to the mobile platform. These conditions can be used to generate different workspaces.

2.4 Workspace analysis approaches

Several methods to quantify, qualify, expand, and design cable-based robot workspaces have been developed during the last ten years. Ebert-Uphoff and Voglewede [5] and Bosscher and Ebert-Uphoff [123] give different definitions of workspaces for cable-based robots assuming that the cables are massless and straight. According to these authors, two groups of workspace can be identified: static and dynamic. A static workspace is a particular case of the dynamic workspace, where accelerations of the mobile box can be assumed to be small, and thus, quasi-static motion analysis is valid; examples of studies of static workspaces can be found in [99] and [53]. Works related to dynamic workspaces can be found in [124] and [125], where the dynamic effects of the cables and motors are neglected and only the inertial effects of the mobile box for a given set of accelerations are

included. Workspace analysis methods can be identified by the inclusion of the following criteria: kinematic and force singularities, external wrenching applied to the mobile box, stiffness, interference, and gravitational force. Thus, several shapes and sizes of workspaces can be identified and depicted. The process of selecting an appropriate criterion may be reduced by identifying the existing correlation between the workspace with the type of cable-based robot and the task to be accomplished. Moreover, depending on the type of criterion selected, it is possible to propose changes in the configuration of a cable-based robot in order to expand its workspace. Bruckmann et al. [112] suggest starting the workspace analysis with the force singularity condition (wrench-closure workspace); that is, the identification of all possible mobile-box poses where cable tensions are bounded by predefined minimum and maximum tension values. Then, any of the above mentioned criteria can be added.

Based on the last paragraph, an appropriate definition for the workspace of a cable-based robot [126] and [60], can be established as a set of all poses of the mobile box subjected to a given external wrench (force/torque), which must be balanced with positive bounded cable tensions and might include one of the following limitations: geometric free-singularity configurations, enough structural rigidity and free-collision cable configurations. This analysis can be done with a discretization approach, follow by a continuous approach for verification purposes. Discrete approaches are based on a grid resolution of the area or volume, and therefore, each pose of the mobile box must be analyzed. In contrast, continuous approaches use analytical techniques to generate the whole workspace of a cable-based robot; for instance, Stump and Kumar [122] use convex analysis to develop closed form expressions to define the workspace boundaries of a planar and a spatial robots; however, these results are based on unbounded positive cable tensions. After a workspace analysis is done, the next step is to develop strategies to optimize this workspace by expanding or improving some of the above mentioned criteria. Gosselin and Bouchard [26] extend the orientation workspace of an underconstrained cable-based robot to capture the shapes of solid objects with a camera mounted in the mobile box. The latter is achieved by the addition of a gravity-activated mechanism mounted in this mobile box. Including a desired stiffness in the workspace is another additional criterion analyzed by several authors. Verhoeven et al. [60] find the workspace subjected to a minimum stiffness value condition of a planar cable-based robot. Behzadipour and Khajepour [114] map a stable workspace by including the antagonistic forces in the overall stiffness model. Liu et al. [116] and Yu et al. [115] analyze the enhancement of stiffness maintaining an optimal cable tension

distribution. Hassan and Khajepour [127] analyze different anchor points of a large-scale fully constrained cable-based robot by mapping the fundamental natural frequency in the wrench-closure workspace.

2.4.1 Iterative model description

Stiffness modelling allows knowing whether the mobile box is stabilizable, thus avoiding erratic motions and lack of system control. The overall stiffness formulation of a cable-based robot is based on the elastic properties and tensions of cables, considering the mobile platform and the actuators as rigid elements. Thus, the stiffness matrix relates the infinitesimal changes of external forces and moments applied to the mobile platform and the linear and rotational small displacements of the mobile platform. Applying derivatives to Eq. (2.10) with respect to a pose of the mobile platform $\boldsymbol{X}_p$, the stiffness matrix is obtained as

$$\boldsymbol{K} = \frac{d\boldsymbol{W}}{d\boldsymbol{X}_p} = \frac{d}{d\boldsymbol{X}_p}(\boldsymbol{A}\boldsymbol{\tau}) = \frac{d}{d\boldsymbol{X}_p}(\boldsymbol{J}^T\boldsymbol{\tau}) .$$

Then

$$\boldsymbol{K} = \frac{d\boldsymbol{J}^T}{d\boldsymbol{X}_p}\boldsymbol{\tau} + \boldsymbol{J}^T\frac{d\boldsymbol{\tau}}{d\boldsymbol{X}_p} .$$

The term $\frac{d\boldsymbol{\tau}}{d\boldsymbol{X}_p}$ can be written as

$$\left(\frac{d\boldsymbol{\tau}}{d\boldsymbol{l}}\right)\left(\frac{d\boldsymbol{l}}{d\boldsymbol{X}_p}\right) = [\mathrm{diag}(k_1, \dots, k_m)]\,\boldsymbol{J}$$

Thus,

$$\boldsymbol{K} = \frac{d\boldsymbol{J}^T}{d\boldsymbol{X}_p}\boldsymbol{\tau} + \boldsymbol{J}^T[\mathrm{diag}(k_1, \dots, k_m)]\,\boldsymbol{J}$$

Using the four-spring model proposed by Behzadipour and Khajepour [114], the stiffness of a cable-based robot can be expressed as

$$\boldsymbol{K} = \boldsymbol{K}_\tau + \boldsymbol{K}_k \tag{2.17}$$

where $\boldsymbol{K}_\tau$ is the stiffness matrix as a consequence of the tensions applied to the cables, and $\boldsymbol{K}_k$ is the stiffness matrix resulting from cable stiffness. The stiffness matrices can be expressed as

$$\boldsymbol{K}_{\tau} = \sum_{i=1}^{m} \frac{\tau_i}{l_i} \begin{bmatrix} \mathbf{1} - \hat{\boldsymbol{l}}_i \hat{\boldsymbol{l}}_i^{\,T} & (\mathbf{1} - \hat{\boldsymbol{l}}_i \hat{\boldsymbol{l}}_i^{\,T})[\boldsymbol{r}_i\times]^T \\ [\boldsymbol{r}_i\times](\mathbf{1} - \hat{\boldsymbol{l}}_i \hat{\boldsymbol{l}}_i^{\,T}) & [\boldsymbol{r}_i\times]\left(\mathbf{1} - \hat{\boldsymbol{l}}_i \hat{\boldsymbol{l}}_i^{\,T}\right)[\boldsymbol{r}_i\times]^T - [\hat{\boldsymbol{l}}_i\times][\boldsymbol{r}_i\times]^T \end{bmatrix}$$

$$\boldsymbol{K}_{k} = \sum_{i=1}^{m} k_i \begin{bmatrix} \hat{\boldsymbol{l}}_i \hat{\boldsymbol{l}}_i^{\,T} & \hat{\boldsymbol{l}}_i \hat{\boldsymbol{l}}_i^{\,T}[\boldsymbol{r}_i\times]^T \\ [\boldsymbol{r}_i\times]\hat{\boldsymbol{l}}_i \hat{\boldsymbol{l}}_i^{\,T} & [\boldsymbol{r}_i\times]\hat{\boldsymbol{l}}_i \hat{\boldsymbol{l}}_i^{\,T}[\boldsymbol{r}_i\times]^T \end{bmatrix}$$

where k_i is the *i*th cable stiffness; $[\boldsymbol{r}_i\times]$ means the cross product operator, and $\mathbf{1}$ is the identity matrix. A sufficient condition for the stabilizability of a static cable-based robot is that the stiffness matrix must be positive definite.

The robot stiffness matrix is used to map the deflections of the mobile platform with respect to a set of the applied forces/moments. Alternatively, robot natural frequencies can be used as another measure for robot's design. Assuming no friction in drums, the natural frequencies of the robot are obtained from:

$$(f_{n_q})_{\boldsymbol{X}_p} = \frac{\sqrt{\mathrm{eig}_q(\,\boldsymbol{M}_p^{-1}\boldsymbol{K}_{\boldsymbol{X}_p})}}{2\pi} \quad [\![Hz]\!] \tag{2.18}$$

where $\boldsymbol{K}_{\boldsymbol{X}_p}$ is the robot stiffness matrix at a particular pose $\boldsymbol{X}_p$ of the mobile platform, $\mathrm{eig}_q(\,\boldsymbol{M}_p^{-1}\boldsymbol{K}_{\boldsymbol{X}_p})$ is the *q*th eigenvalue and $(f_{n_q})_{\boldsymbol{X}_p}$ is the *q*th natural frequency at a particular pose of the mobile platform, and $\boldsymbol{M}_p$ is the inertial matrix of the mobile platform.

Consequently, a design optimization problem can be formulated with respect to a performance index; for example, the fundamental frequency (minimum natural frequency), must be maximized in the overall robot workspace in order to enhance the robot stiffness subjected to the positive cable tension constraints; that is:

$$\max_{\boldsymbol{D}} \left\{ \min_{\boldsymbol{X}_p \,\epsilon\, V} f_{n_q}(\boldsymbol{D}, \boldsymbol{X}_p) \right\}$$
$$\text{Subjected to} \quad 0 < \tau_{\min} \le \tau_i \le \tau_{\max} \quad \forall \; i = 1,2,\dots,m \text{ cables} \tag{2.19}$$

where $\boldsymbol{D}$ is the design parameters vector which has a relevant influence on the robot stiffness; $\tau_{\min}$ is the minimum cable tension; $\tau_{\max}$ is the maximum tensions, and τ_i is the tension in the *i*th cable.

The workspace of a cable-based robot can be obtained by scanning every possible pose of the mobile platform and applying the equations developed in the previous chapter. Then, any criteria can be successively added, such as gravity, external forces/moments, and stiffness. The following algorithm is implemented in a MATLAB program (Appendix A) to calculate the cable tensions and workspace of a cable-based robot.

1. Input of robot parameters and selection of a criterion (force-closure or feasible-wrench).
2. For each pose of the mobile platform:
   - 2a. Check free-singularity condition using Eq. (2.6). If it is satisfied, go to next step, otherwise go to step 2e.
   - 2b.
     - Case 1: (Force-closure condition) Given any arbitrary wrench, find all cable positive tensions with unbounded maximum tension. Check force-closure condition with Eq. (2.14). If there exists such condition, find cable tensions with Eq. (2.15) and go to step 2c; otherwise go to step 2e.
     - Case 2: (Positive feasible-wrench condition) Given a constant static wrench, find all cable positive tensions with bounded maximum tension. Check feasibility condition with Eq. (2.14). If there exists such condition, find cable tensions with Eq. (2.16) and go to step 2c; otherwise go to step 2e.
     - Case 3: (Feasible-wrench condition) Given a constant static wrench, find all cable positive tensions subjected to a set of bounded cable tensions (minimum and maximum tensions) with Eq. (2.16). Check feasibility condition. If there exists such condition, go to step 2c; otherwise go to step 2e.
   - 2c. Calculate the overall stiffness matrix with Eq. (2.17). Check the stiffness matrix is a definite positive matrix. If there exists such condition go to the next step, otherwise go to step 2e.
   - 2d. Mark this pose as part of the positional workspace of the cable-based robot.

2e. End of the loop: if there exists more poses to check, go to step 2a; otherwise go to step 3.

3. End.

This algorithm analyzes each pose of the mobile platform inside the static workspace. Given the parameters of the cable-based robot, the Jacobian matrix is obtained by using Eq. (2.4); then, the null-space of the structure matrix is used to calculate the tensions of all cables.

2.5 Control topologies

In Bruckmann et al. [93] and without loss of generality, the objective of a cable-based robot's control is to adjust the length (position control) and tension (force control) of each actuated cable for a desired pose or trajectory of a mobile platform subjected to external disturbances (forces/moments). Several disturbance types can be modeled such as static, impulsive, random and cyclical, and where they are located (actuators, cables, mobile box and anchor points). However, static and punctual disturbances located in the mobile box and the actuators are the more common models under study, assuming the cables are massless [128]. Static disturbances are constant wrenches, for instance, an invariable object weight. On the other hand, impulsive disturbances happen when wrench values suddenly change, for example, during a collision between the mobile box and the object to be grasped. In the case of redundant cable-based robots, these control studies are based on parallel manipulators. Indeed, it has proved that almost all control methodologies for parallel mechanisms can be applied to cable-based robots by adding the positive cable tension conditions to the overall control scheme [48], [129] and [130].

The use of redundant cables could eliminate or decrease some types of singularities and enhance the overall stiffness. However, this extension has its own difficulty finding an optimal distribution of all cable tensions between a minimum and a maximum value for each configuration. Thus, several approaches have been developed in order to solve the main cable-based robots' control problems: the unilateral tension and the redundantly actuation of cables. Feedback linearization and time optimal control are examples of these approaches [131]. Feedback linearization, also known as inverse dynamics control or computed torque technique, is used to calculate the actuator forces based on the dynamic forces obtained from the dynamic model of the cable-based robot. This technique is commonly coupled with Proportional-Derivative (PD) controllers, and more recently with robust and adaptive controllers [132] and [133]. Kawamura et al. [15] apply a PD feedback controller in the joint

space coordinate (cable length coordinates) with gravitational compensation to the FALCON-7 robot. Su et al. [88] establish that once it is proved that there are no singularities in a cable-based robot, the use of a robust control for tracking is appropriate. Thus, a Proportional-Integrative-Derivative (PID) control scheme is implemented to control each cable independently based on a comparison between the measured lengths (using a laser positioning system of the mobile box) against the desired lengths (calculated using the kinematic model). This control scheme is not based on a dynamic model and needs an expensive sensory system. Ghasemi et al. [134], Hiller, and Hirsch [92] apply the input-output linearization feedback technique to simulate different motions of the mobile box. They apply an optimal feedback linearization technique on variant objective functions. Gholami et al. [135] propose an efficient inverse dynamics controller in the joint space for a redundant cable-driven robot. This algorithm does not need to measure the end-effector position and to solve the robot forward kinematics, which make it suitable for real time applications. However, this controller is evaluated only by simulations. Yu et al. [115] develop an active task stiffness control scheme of an unconstrained cable-based robot, improving the trajectory tracking of its mobile box and disturbance rejection performance. A minimum-time task realization must be achieved for cable-based robots doing pick-and-place operations. This type of problem implies positive cable tension conditions in the formulation of the overall motion trajectory planning strategy of a cable-based robot. The strategy must deal with the computational time for real-time applications. Therefore, efficient methods (controller closed-loop algorithms) for real-time redundant cable-driven robot applications are still under study. Indeed, a balance between the minimum-time and the real-time task realization is an objective in many investigations.

2.5.1 Dynamic model generation

The system dynamics model is derived by assuming that cables are massless and straight. Also, the nonlinear effect of friction is ignored to reduce the dynamic equations' complexity. In that sense, the Newton-Euler's equations of the mobile platform are obtained by

$$\sum_{i=1}^{m}(\boldsymbol{\tau}_i) + \boldsymbol{F}_e + m_p\boldsymbol{G} = m_p\dot{\boldsymbol{v}}_p \tag{2.20}$$

$$\sum_{i=1}^{m}(\boldsymbol{r}_i \times \boldsymbol{\tau}_i) + \boldsymbol{M}_e = \underline{\boldsymbol{I}}_p \cdot \dot{\boldsymbol{\omega}}_p + \boldsymbol{\omega}_p \times (\underline{\boldsymbol{I}}_p \cdot \boldsymbol{\omega}_p) \tag{2.21}$$

where $\boldsymbol{F}_e$ and $\boldsymbol{M}_e$ are unknown but bounded forces and moments (perturbations) applied to the mobile platform, $\underline{\boldsymbol{I}}_p$ is the inertial tensor of the mobile platform about its mass center in the reference coordinates; $\dot{\boldsymbol{v}}_p$, $\dot{\boldsymbol{\omega}}_p$ are the linear and the angular acceleration of the mobile platform, respectively. In a compact form, equations (2.20) and (2.21) can be rewritten by

$$\boldsymbol{M}_p \ddot{\boldsymbol{X}}_p + \boldsymbol{C}_p - \boldsymbol{W}_p = \boldsymbol{A}\boldsymbol{\tau} \tag{2.22}$$

where $\boldsymbol{M}_{p(n\times n)} = \begin{bmatrix} (m_p\ \mathbf{1})_{n_T \times n_T} & \mathbf{0}_{n_T \times n_R} \\ \mathbf{0}_{n_R \times n_T} & (\underline{\boldsymbol{I}}_p)_{n_R \times n_R} \end{bmatrix}$ is the inertial matrix, n_T and n_R are the number of translational and rotational DOF of the mobile platform, respectively, such that $n = n_T + n_R$; $(\ddot{\boldsymbol{X}}_p)_{n\times 1} = [(\dot{\boldsymbol{v}}_p)_{n_T \times 1} \quad (\dot{\boldsymbol{\omega}}_p)_{n_R \times 1}]^T$ is the acceleration vector of a mobile platform pose; $\boldsymbol{C}_{p(n\times 1)} = \left[(m_p \boldsymbol{G})_{n_T \times 1} \quad \left([\boldsymbol{\omega}_p \times](\underline{\boldsymbol{I}}_p\, \boldsymbol{\omega}_p)\right)_{n_R \times 1}\right]^T$ includes the Coriolis, centrifugal and gravitational forces, where $[\boldsymbol{\omega}_p \times]$ means the cross product operator; $\boldsymbol{W}_{p(n\times 1)} = [(\boldsymbol{F}_e)_{n_T \times 1} \quad (\boldsymbol{M}_e)_{n_R \times 1}]^T$ is the wrench vector to balance under dynamic equilibrium; and $(\boldsymbol{A}\boldsymbol{\tau})_{n\times 1}$ has the same meaning as Eq. (2.10).

Chapter 3
Design and Optimization of a Cable-based Warehousing Robot

The design problem of a cable-based robot for large-workspace and high-stiffness applications such as warehousing is addressed in this chapter. This chapter presents the problem of defining the layout design of a fully constrained cable-based robot for warehousing applications so that its workspace fulfills the tensionable condition and maximum robot stiffness for a given set of minimum and maximum tension limits. The chapter begins with the optimal design study of the robot based on the theoretical formulations presented in Chapter 2. Section 3.2 introduces the conceptual designs of a planar and a spatial cable robot with pure translational moving capabilities, followed by an investigation on their workspaces expansion.

3.1 Design formulation

Warehousing tasks require that a robot end-effector grasp parts located on the ground, move them upwards and automatically place them in shelves. Moreover, this operation demands a stable translational motion of the mobile platform, such that the mobile platform always moves aligned with the ground. In that sense, any rotational motion of the mobile platform must be nullified to achieve a pure translational robot design. In addition, warehousing tasks require high speed and stable motions of a mobile platform along straight distances. In consequence, requirements such as high stiffness, small inertia and large workspace must be included in the design plan.

An initial design configuration can be selected with respect to the size of the feasible workspace. The approximated size of a feasible workspace can be obtained by the number of poses that are marked in the above algorithm. A feasible workspace size might be affected by the size of the static and mobile platform, and where their respectively anchor points are located. Then, a minimum number of design parameters with relevant influence on the size of the feasible workspace must be selected from a set of parameters with a predetermined configuration. The remaining parameters must be specified by the designer based on the practical application of the robot. In other words,

$$\begin{aligned} &\max_{\boldsymbol{D}_\Gamma} \ \Gamma(\boldsymbol{D}_\Gamma, \boldsymbol{C}), \ \ \boldsymbol{D}_\Gamma \subset \boldsymbol{C} \\ &\text{Subjected to} \quad 0 < \tau_{\min} \le \tau_i \le \tau_{\max} \ \ \forall \ i = 1, 2, \dots, m \end{aligned} \tag{3.1}$$

where $\boldsymbol{D}_\Gamma$ is the design parameters vector which has a relevant influence on the workspace size Γ from the parameter vector $\boldsymbol{C}$; $\tau_{\min}$ is the minimum cable tension; $\tau_{\max}$ is the maximum admissible tensions, and τ_i is the tension in the *i*th cable. The low force actuation objective is achieved by including the condition established in Eq. (2.16) into formulation (3.1).

A larger feasible workspace might be a good criterion to select a configuration; however, this is not enough for practical applications. For example, high stiffness poses of the mobile platform are preferred to reduce oscillations.

Consequently, a design optimization problem can be formulated with respect to the lowest natural frequency or fundamental frequency for a given design payload mass. That is, the minimum value of the fundamental frequency in the overall robot feasible workspace must be maximized in order to enhance the overall robot stiffness. This is expressed as:

$$\max_{\boldsymbol{D}_f} \left\{ \min_{\boldsymbol{X}_p \,\epsilon\, \boldsymbol{\Gamma}} f_{n_1}\left(\boldsymbol{D}_f, \boldsymbol{X}_p, \boldsymbol{C}\right) \right\}, \;\; \boldsymbol{D}_f \subset \boldsymbol{C} \tag{3.2}$$

where $\boldsymbol{D}_f$ is the vector of design parameters which have a relevant influence on the robot stiffness.

3.1.1 Topology selection

A warehousing robot must be simple with a large workspace, and capable of heavy-payloads and high-speed operation. In consequence, hybrid designs (with rigid and flexible links), and architectures with moving actuators/pulleys are not considered in this study. Similarly, designs with purely point-mass end effectors are also excluded because they are limited to do linear-force tasks; that is, they cannot resist external moments.

A pure planar translational mobile platform can be obtained by adding at least one parallelogram mechanism (minimum condition) to the system, as is shown in Figure 3.1a. The evaluation of these designs permits to establish some crucial differences.

The first design is the simplest one because of its minimum component requirements; however, its asymmetry might affect the appropriate cable tensions balance, which could generate undesired vibrations in the mobile platform. This problem is reduced in the symmetrical design with the addition of an extra pair of cables working as a parallelogram mechanism.

These designs use the same number of motors and might have similar workspaces. On the other hand, the last candidate design (Figure 3.1c) uses four independent cables and one parallelogram mechanism. This configuration allows an expansion of the workspace and a better distribution of a payload among all the cables. Nevertheless, these advantages are possible with the addition of one extra motor to the system. In this work the symmetric design is selected for analysis.

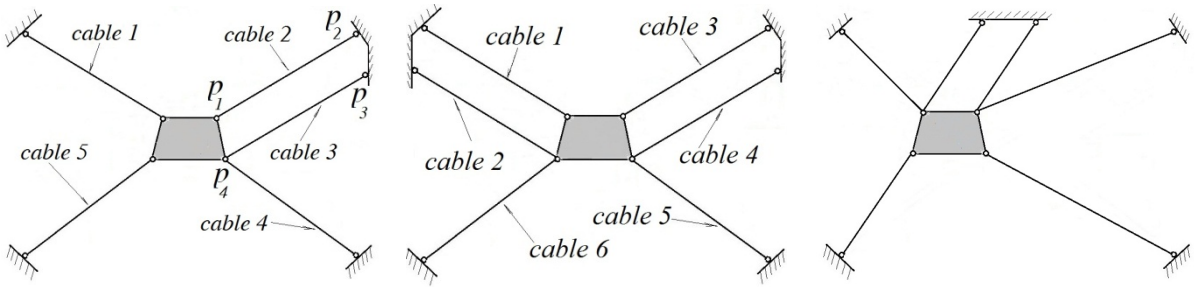

(a) (b) (c)

Figure 3.1: Pure planar translational topologies with: (a) minimum parallel mechanisms condition, (b) parallel mechanism redundancy, and (c) independent cable redundancy.

Assuming the distances $\overline{P_1P_2}$ and $\overline{P_3P_4}$ are equivalent, a parallelogram mechanism is developed between cables two and three. This parallelogram mechanism always guarantees the parallelism between the sides $\overline{P_1P_4}$ and $\overline{P_2P_3}$, resulting in a fixed orientation motion of the mobile platform provided the cables are in tension. In consequence, this design has $n = 3 - 1 = 2$ translational DOFs. Thus, four motors are used to control the position of the mobile platform by pulling three independent cables, and one pair of dependent cables. This dependent pair of cables must be equally collected/released such that the equivalent cable lengths condition is always maintained.

The candidate shown in Figure 3.1b utilizes an extra parallelogram mechanism, which might result in a symmetrical design actuated by four motors.

Symmetrical designs allow a better balance among the wrench and the cable tensions. In general, warehousing tasks do not have preferences for some kinematic and force directions, allowing the use of symmetrical designs. In addition, symmetry is useful for reducing the number of design parameters. Therefore, the candidate shown in Figure 3.1b is selected as the topology to be optimized.

3.1.2 Optimization

The optimization procedure is divided in two stages. Firstly, an equivalent planar optimized design is obtained by analyzing the sensitivity of its geometrical parameters with respect to its feasible workspace and stiffness. In the final stage the optimized planar configuration is extended to its spatial version, where a set of geometrical parameters is selected to evaluate the changes of the overall stiffness. For simplicity, only the weight of the mobile platform is considered as external force.

Based on the configuration shown in Figure 3.1b, two planar configurations are optimized to obtain their maximum feasible workspace size. For a further spatial analysis, this study defines the planar size of the mobile platform and the location of the bottom anchor points connected to the mobile platform. In both planar configurations, the upper cables are working as parallel mechanisms and the bottom ones are used to constrain the motion of the mobile platform.

The anchor points on the mobile platform of the bottom cables are symmetrical. They are located along the bottom length of the mobile platform for a non-crossing cable configuration, Figure 3.2a. Conversely, Figure 3.2b shows a crossing cable configuration, where the anchor points of the bottom cables are connected to the upper length of the mobile platform.

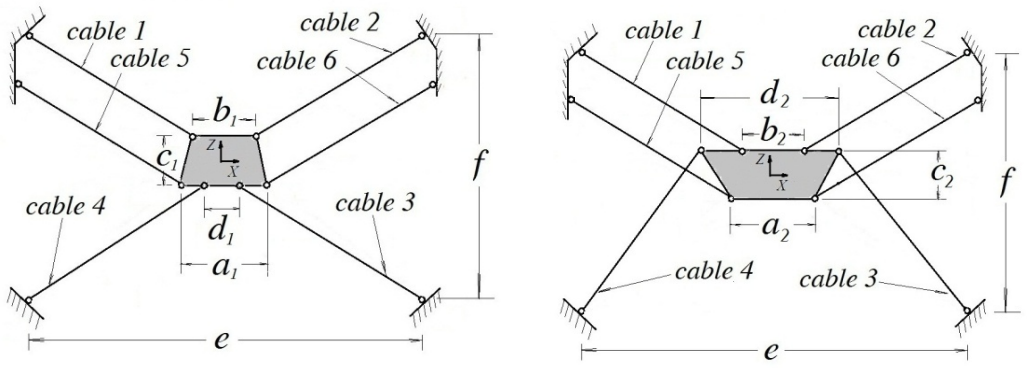

(a) (b)

Figure 3.2: Design parameters for: (a) no-crossing and (b) crossing cables configurations.

To allow for a fair comparison between both configurations, the static platforms are defined by the same parameters e and f by assuming that a rectangular shape for the static platform. The size of

each mobile platform is defined by the parameters a_1, b_1, c_1, d_1, and a_2, b_2, c_2, d_2, respectively. These parameters represent the bottom length, upper length, and high dimensions.

Parameters d_1 and d_2 define the anchor points along the bottom and upper side of the mobile platform for the non-crossing and crossing cable configuration, respectively. Thus, there are a total of six parameters that must be determined in each configuration to completely establish the design configuration of the planar cable-based robot; that is,

$$\boldsymbol{C}_i = [a_i, b_i, c_i, d_i, e, f]^T \quad \forall\, i = 1, 2 \tag{3.3}$$

The following geometrical parameters of the mobile platform and their anchor points connected to the bottom cables must be determined:

$$\boldsymbol{D} = [a, b, c, d]^T \tag{3.4}$$

where the subscripts are dropped as long as the parameters are referenced to both configurations.

A minimum set of horizontal and vertical lengths of the mobile platform is established in function of the maximum size of the components to be translated ($b_{\min}$ and $c_{\min}$). To reduce the number of design parameters, let parameter b be fixed at a predefined minimum value and let parameters d_1 and d_2 have the same value as parameters a_1 and b_2, respectively. Table 3.1 summarizes the values of these parameters and others used in this study.

Table 3.1: Initial parameters for planar configurations

Symbol	Description	Value
$b_{\min}$	Mobile platform upper length (m)	1.0
$c_{\min}$	Mobile platform height (m)	0.1
e	Static platform length (m)	15.0
f	Static platform height (m)	5.0
$\tau_{\min}$	Cables minimum tension (N)	200.0
$\tau_{\max}$	Cables maximum tension (N)	2000.0
k	Cable stiffness (N/m x cable length)	30000.0
m_p	Mobile platform mass (Kg)	50.0

Parameters d_1 and d_2 are analyzed to determine their effects on the workspace and stiffness in each configuration. These variations are condensed in Figure 3.3.

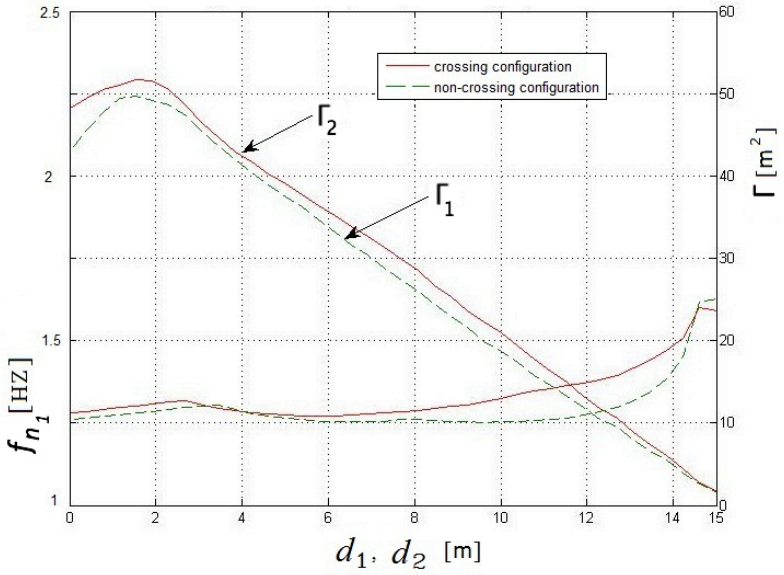

Figure 3.3: Variations of the workspace and natural frequency as a function of parameters $\boldsymbol{d_1}$ and $\boldsymbol{d_2}$.

Adopting the largest size of the workspace as the highest optimization priority, optimal parameters $a = a^*$ and $c = c^*$ can be obtained from Eq. (3.1) and used to establish the remaining parameters. It is worthy to note that parameter c has an active but inverse effect on the size of the workspace and the overall stiffness of both configurations.

In general, the crossing planar configuration presents a larger workspace's size and a better overall stiffness than the non-crossing configuration. Moreover, when parameter d_2 is increased, both the size of the feasible workspace and the fundamental frequency are enhanced. On the other hand, parameter d_1 which belongs to the non-crossing configuration must reduce its value to achieve a maximum size feasible workspace, while its fundamental frequency is decreasing. In consequence, the crossing configuration is selected for a further spatial study. Based on the optimal parameters obtained from the planar case, Figure 3.4 shows a spatial version with twelve cables. In this configuration there are four sets of cables that are each activated by an actuator, respectively. Each set of cables consists of cables 1, 5, 7, and 11; 2, 6, 8, and 12; 3 and 9; and 4 and 10. The upper set of

cables maintain the same orientation of the mobile platform, while the bottom set of cables are used to fully constraint the motion of the mobile platform along the XZ plane.

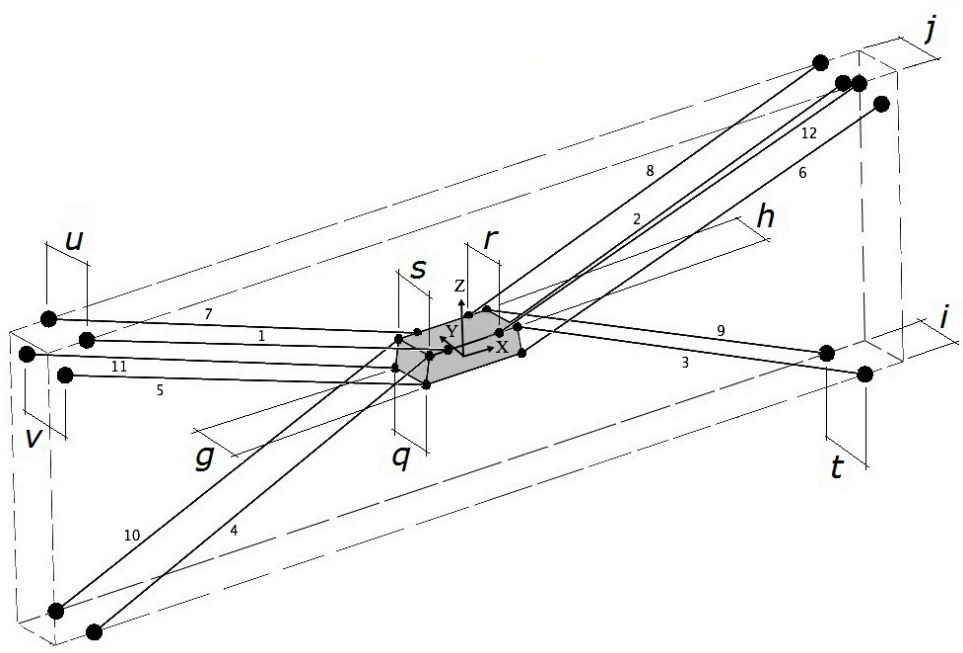

Figure 3.4: Design parameters of the tridimensional robot configuration with planar motion.

The design optimization objective is twofold: firstly, eliminate the interference among the bottom and upper set of cables, and secondly, to increase the overall stiffness by keeping the maximum workspace established in the previous planar configuration analysis. There are ten parameters to be analyzed: $g,\ h, i, j, q, r, s, t, u,$ and v which represent the extension of the planar robot along its Y axis. In order to reduce the number of parameters to be analyzed, it is assumed that parameters g, h, i and j are defined by a maximum value defined by the task requirement; that is, the maximum wide of the components to be translated. Thus, the number of design parameters to be determined reduces to six; that is,

$$\boldsymbol{C} = [q, r, s, t, u, v]^T \tag{3.5}$$

Parameters q, r, s represent the anchor distances along the width of the mobile platform, while parameters t, u, v define the anchor points along the width of the static platform.

Interference among upper and bottom cables might be eliminated by accepting inverse triangular connections. These type of cable arrangements have been explored in [127] to increase the cable-

based robot overall stiffness. Thus, two sets of parameters: q, v and s, t are studied to evaluate their minimum lowest natural frequency changes. In other words,

$$\min_{X_p \in \Gamma} f_{n_1} = F(q, v, \boldsymbol{X}_p) \text{ s.t. } g = h = i = j = g_{\min}$$

$$0 \leq q \leq g, \qquad 0 < v < j \tag{3.6a}$$

and

$$\min_{\boldsymbol{X}_p \in \Gamma} f_{n_1} = F(s, t, \boldsymbol{X}_p) \text{ s.t. } g = h = i = j = g_{\min}$$

$$0 \leq s \leq h, 0 < t < i \tag{3.6b}$$

By assuming a minimum width of the mobile platform of $g_{\min} = 1.0$ m, plots for formulations (3.6a) and (3.6b) are presented in Figure 3.5a and Figure 3.5b, respectively.

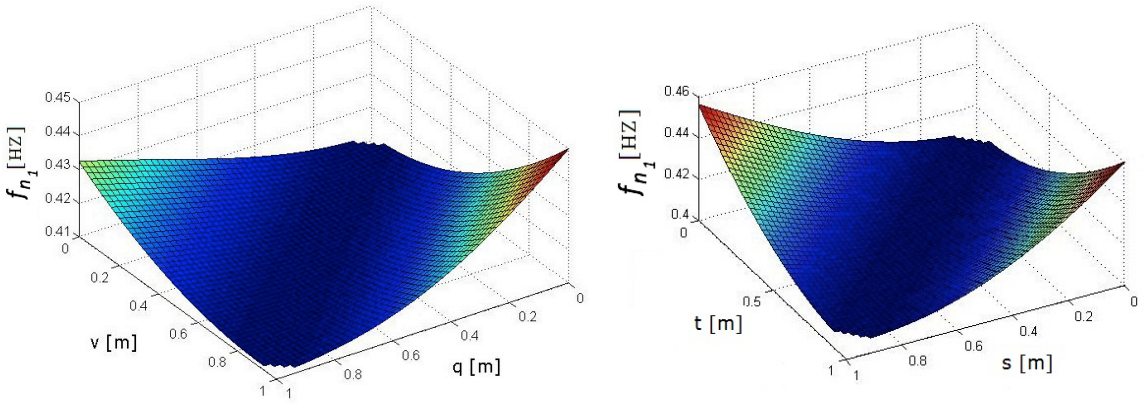

(a) (b)

Figure 3.5: Minimum lowest natural frequencies as a function of parameters: (a) *q* and *v*, and (b) *s* and *t*.

A maximum value of the fundamental frequency is obtained when v reaches its upper limit and q its minimum value, respectively. On the other hand, two similar maxima are achieved when inversely s and t reach their upper and lower limits. Then, the optimal parameters of q and v are selected to achieve a maximum stiffness, and parameters s and t are selected such that the interference is eliminated.

Similarly, to define the last anchor points, a sensitivity study can be developed for parameters r and u. This formulation is expressed as:

$$\min_{\boldsymbol{X}_p \,\epsilon\, \Gamma} f_{n_1} = F\left(r, u, \boldsymbol{X}_p\right) \text{ s.t. } g = h = i = j = g_{\min}$$
$$q = 0, v = j, s = h, t = 0 \tag{3.7}$$
$$0 \le r \le h, \qquad 0 < u < j$$

Figure 3.6 shows the stiffness sensitivity compared to variations of parameters r and u.

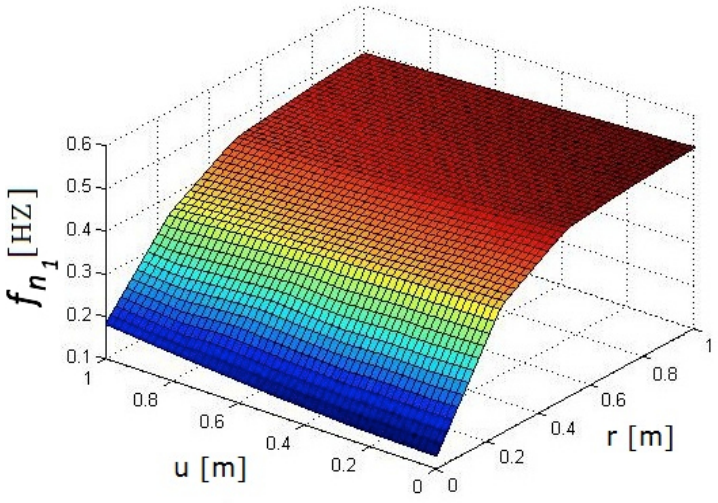

Figure 3.6: The fundamental natural frequency as a function of parameters r and u.

The increase in the fundamental frequency is achieved when parameter r approximates to its upper limit and u is near to its minimum value. Finally, Table 3.2 shows the optimized parameters of the twelve-cable robot.

Table 3.2: Optimal parameters for spatial configuration

Symbol	Description	Value
a	Mobile platform bottom length (m)	1.86
b	Mobile platform upper length (m)	1.0
c	Mobile platform height (m)	0.47
d	Mobile platform upper anchor length (m)	1.71

e	Static platform length (m)	15.0
f	Static platform height (m)	5.0
g	Mobile platform bottom width (m)	1.0
h	Mobile platform upper width (m)	1.0
i	Static platform bottom width (m)	1.0
j	Static platform upper width (m)	1.0
q	Mobile platform bottom anchor length (m)	0.0
r	Mobile platform upper-inside anchor length (m)	1.0
s	Mobile platform upper-outside anchor length (m)	1.0
t	Static platform bottom anchor length (m)	0.0
u	Static platform upper-up anchor length (m)	0.0
v	Static platform upper-down anchor length (m)	1.0
$\tau_{\min}$	Cables minimum tension (N)	200.0
$\tau_{\max}$	Cables maximum tension (N)	2000.0
k	Cable stiffness (N/m x cable length)	30000.0
m_p	Mobile platform mass (Kg)	50.0

This configuration achieves a maximum feasible workspace $\Gamma = 51.82$ m^2 with no interference and a minimum value of its fundamental natural frequency of $f_{n_1} = 0.49$ Hz. An analysis of the fundamental frequencies along the feasible workspace is depicted in Figure 3.7. Also, it is shown a maximum inscribed rectangular workspace with an area of 45.82 m^2.

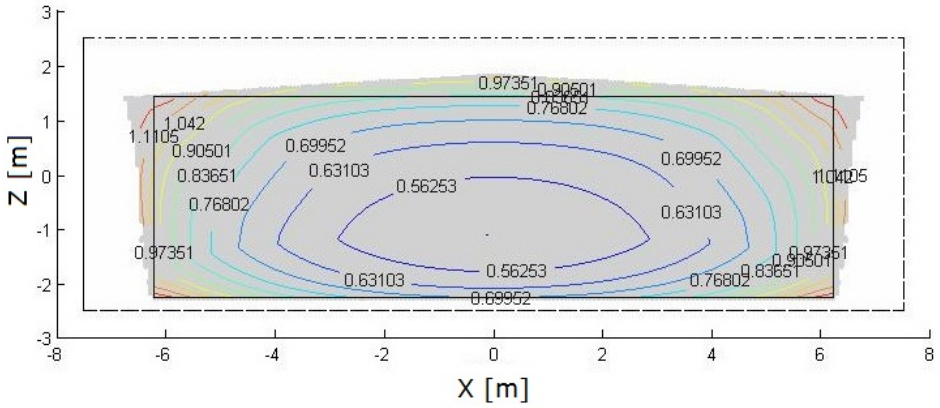

Figure 3.7: Fundamental natural frequencies of the optimal robot configuration.

The maximum values of the fundamental frequencies are located at the boundaries of the feasible workspace, where the maximum cable tensions and minimum cable lengths are located.

3.2 Configuration description

The general structure of the proposed cable-based robotic system is shown in Figure 3.8. A suspended box is constrained to move inside of a static box by the action of twelve cables. The twelve cables are symmetrically grouped into eight top cables and four bottom cables.

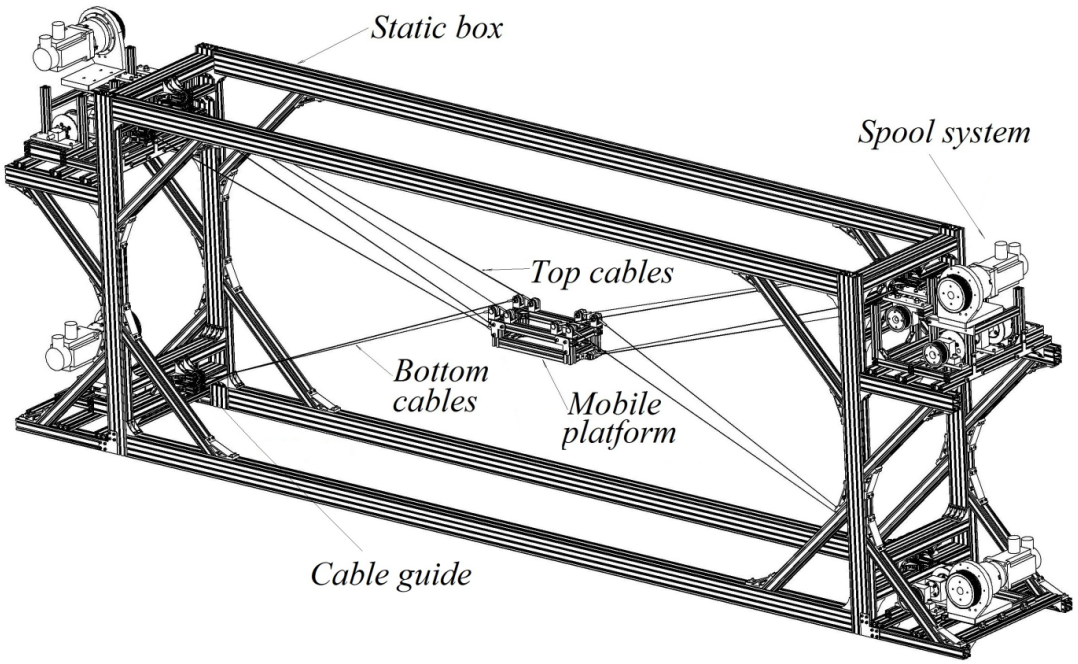

Figure 3.8: Main components of the proposed optimal robot configuration.

The top cables support the weight of the mobile platform and restrict planar fixed-orientation poses of the mobile platform. Their counterparts, the bottom cables, are used to provide the required positive tension among cables. In other words, the top cables are sufficient to translate the mobile platform as an under-constrained robot relying only on the gravity force to maintain positive tension. Thus, the bottom cables effectively provide an adaptive gravity force to balance any external wrench (including forces and torques) and give rigidity to the whole system. Cables pass through pulley guides. They are wrapped around drums, which are activated by four motors. Motors are

symmetrically located in each corner of the static structure. One of the top motors controls the length of four cables simultaneously, while one of the bottom motors controls the tension of two cables concurrently.

A detail of one of the four top cables is shown in Figure 3.9. Each cable length is defined by the distance between its anchor points A to B, such that $l_i = \overline{A_i B_i},\ \forall\, i = 1,2 \ldots 12$. Note that each cable of the top and bottom cable pair has a coincident static anchor point, respectively, that is, $A_i = A_{i+6}$, $\forall\, i = 1,2 \ldots ,4$. Conversely, the middle cable pair arrives to a common anchor point in the mobile platform, that is $B_i = B_{i+6},\ \forall\, i = 4,5$.

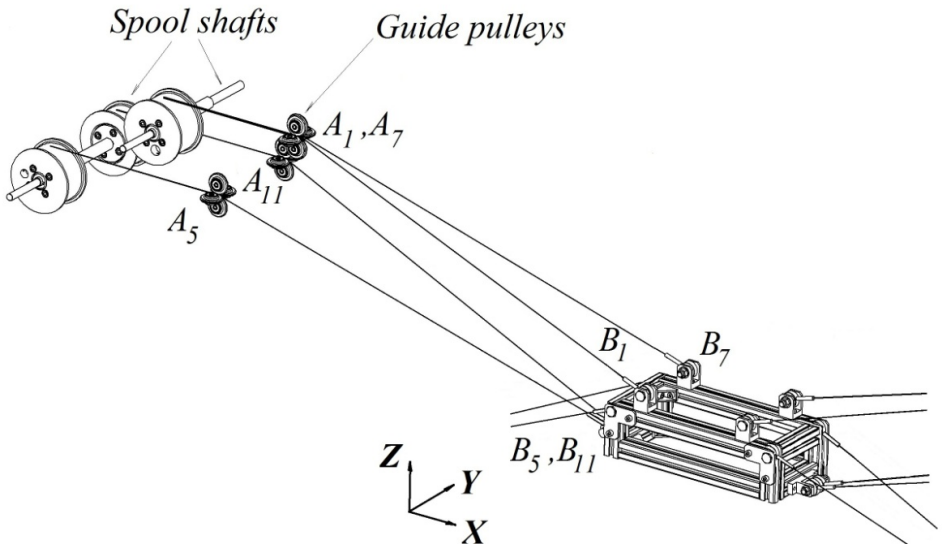

Figure 3.9: Detail of one of the top set of cables.

Symmetrical locations of no-coincident anchor points make the length of each cable in each cable pair equal to one another, that is, $l_i = l_{i+6},\ \forall\, i = 1,2 \ldots 6$. These conditions eliminate two rotations and one translation of the mobile platform, with one rotation remaining to be removed.

The top set of cables reveals a dependent motion based on a projected parallelogram mechanism. The projected distances along the motion plane between anchor points $\overline{A_1 B_1}$ and $\overline{A_7 B_7}$ is equivalent and defined as l_{r1}. Similarly, the projected distances for $\overline{A_5 B_5}$ and $\overline{A_{11} B_{11}}$ are the same and defined as l_{r5}, as is shown in Figure 3.10, and computed as follows

$$l_{ri} = \begin{cases} \sqrt{{l_i}^2 - \left(\frac{h}{2}\right)^2} & \forall\, i = 1,..,4 \\ \sqrt{{l_i}^2 - \left(\frac{g}{2}\right)^2} & \forall\, i = 5,6 \end{cases} \tag{3.8}$$

Thus, a projected parallelogram mechanism is obtained if the following conditions hold, $l_{r1} = l_{r5}$ and $l_{r1} \parallel l_{r5}$. Therefore, these dependent cables must be uniformly collected or released so that the projected cable lengths condition is always maintained.

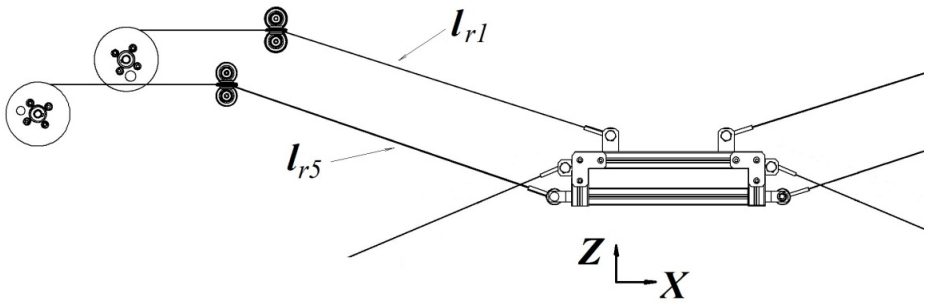

Figure 3.10: Projection of one of the top set of cables.

The above conditions eliminate any rotation, as well as one perpendicular translation of the mobile platform by assuming all cables are taut. Consequently, this design has two translational DOF.

3.2.1 Kinematics

The inverse position deals with the problem of finding the cable lengths by a given position of the center of the mobile platform $\boldsymbol{p}$, with respect to the reference system. According to Figure 3.11, a coordinate system $x'y'z'$ is fixed at the mass center of the mobile platform, o', and another, XYZ, is fixed at a reference point $\boldsymbol{O}$.

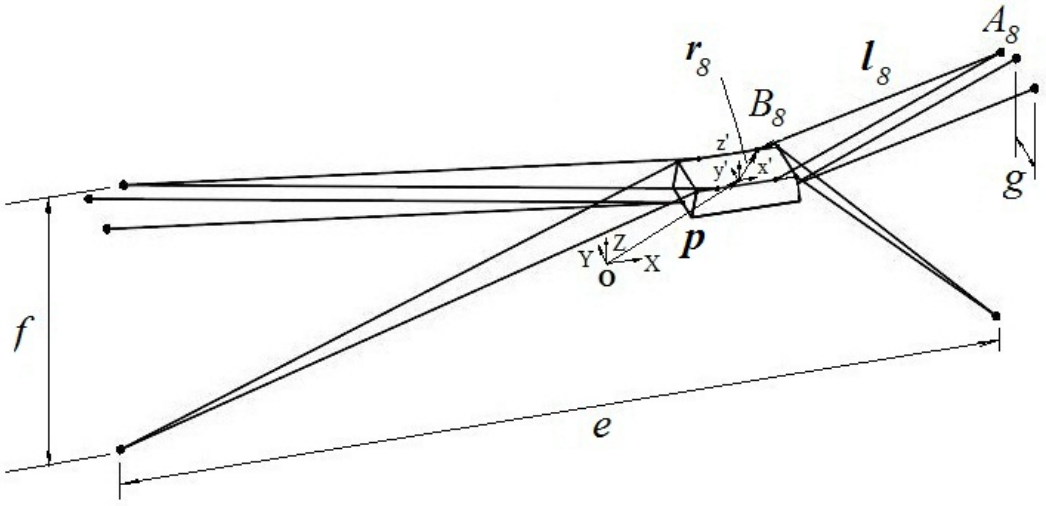

(a)

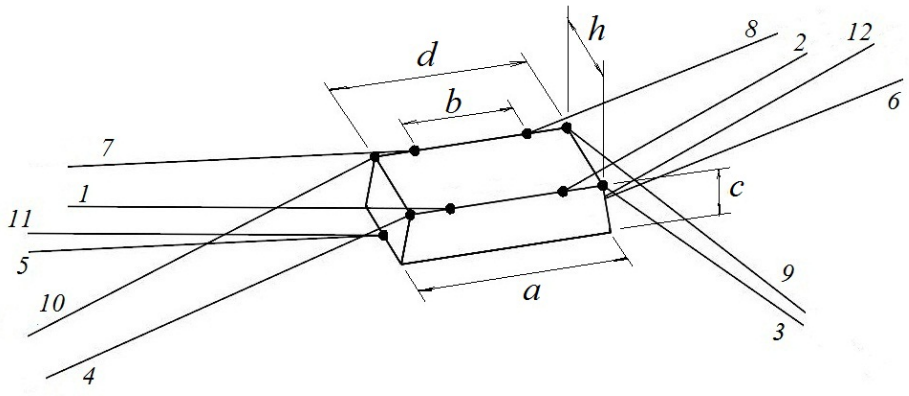

(b)

Figure 3.11: Geometric parameters related to: (a) the static box and (b) the mobile platform.

Vector $\boldsymbol{p}$ establishes the position of the mobile platform between these two coordinate systems. Vector $\boldsymbol{l}_i$ is the *i*th cable vector connecting the anchors points A_i and B_i at the static and mobile platforms, respectively. Thus, constant vectors $\boldsymbol{a}_i$ and $\boldsymbol{r}'_i$ are placed with respect to the base and the mobile coordinate systems.

Using the transformation $\boldsymbol{r}_i = \boldsymbol{R}_{321}\boldsymbol{r}_i'$, where $\boldsymbol{R}_{321}$ is the rotation transformation matrix with the sequence ZYX of the Euler angles $\boldsymbol{\theta}_p = [\alpha \quad \beta \quad \gamma]^T$, for the desired orientation of the mobile platform, where $\boldsymbol{R}_{321} = \boldsymbol{R}(Z,\alpha)\boldsymbol{R}(X',\beta)\boldsymbol{R}(Y'',\gamma)$ is obtained with the three basic rotation transformation matrices around the Z axis, X' axis, and Y'' axis. For planar translational motions, the rotation transformation becomes an identity matrix. The closure vector equation for the position is:

$$\boldsymbol{l}_i = \boldsymbol{p} + \boldsymbol{r}_i - \boldsymbol{a}_i\,, \quad \forall \quad i = 1,2,\dots 12 \tag{3.9}$$

The *i*th cable's length is obtained by applying the Euclidian norm to Eq. (3.9) as:

$$l_i = \|\boldsymbol{p} + \boldsymbol{r}_i - \boldsymbol{a}_i\|, \quad \forall \quad i = 1,2,\dots 12 \tag{3.10}$$

Each pair of cables consists of an isosceles triangular shape, of which conditions can be expressed as:

$$l_i = \|\boldsymbol{l}_i\| = \|\boldsymbol{l}_{i+6}\| \quad \forall \quad i = 1,2,\dots 6 \tag{3.11}$$

Also, the upper cables are forming two projected parallelogram mechanisms which are related as:

$$l_{ix} = \|\boldsymbol{l}_{ix}\| = \left\|\boldsymbol{l}_{(i+4)x}\right\| \quad \forall \quad i = 1,2 \tag{3.12}$$

$$l_{iz} = \|\boldsymbol{l}_{iz}\| = \left\|\boldsymbol{l}_{(i+4)z}\right\| \quad \forall \quad i = 1,2 \tag{3.13}$$

For purely translational motions on the plane XZ, the coordinates of the mobile platform are expressed as $\boldsymbol{X}_p = [P_x \quad 0 \quad P_z \quad 0 \quad 0 \quad 0]^T$. Conditions (3.11) to (3.13) allow the analysis of the first six cables instead of the twelve cables. Then, substituting constraints (3.11) to (3.13) into (3.10), the inverse kinematic equations are:

$$l_1 = \left(\left(P_x - \frac{b}{2} + \frac{e}{2}\right)^2 + \left(-\frac{h}{2}\right)^2 + \left(P_z + c - y_{cp} - \frac{f}{2}\right)^2\right)^{1/2} \tag{3.14a}$$

$$l_2 = \left(\left(P_x + \frac{b}{2} - \frac{e}{2}\right)^2 + \left(-\frac{h}{2}\right)^2 + \left(P_z + c - y_{cp} - \frac{f}{2}\right)^2\right)^{1/2} \tag{3.14b}$$

$$l_3 = \left(\left(P_x + \frac{d}{2} - \frac{e}{2}\right)^2 + \left(-\frac{h}{2}\right)^2 + \left(P_z + c - y_{cp} + \frac{f}{2}\right)^2\right)^{1/2} \tag{3.14c}$$

$$l_4 = \left(\left(P_x - \frac{d}{2} + \frac{e}{2}\right)^2 + \left(-\frac{h}{2}\right)^2 + \left(P_z + c - y_{cp} + \frac{f}{2}\right)^2\right)^{1/2} \tag{3.14d}$$

$$l_5 = \left(\left(P_x - \frac{b}{2} + \frac{e}{2}\right)^2 + \left(\frac{g}{2}\right)^2 + \left(P_z + c - y_{cp} - \frac{f}{2}\right)^2\right)^{1/2} \tag{3.14e}$$

$$l_6 = \left(\left(P_x + \frac{b}{2} - \frac{e}{2}\right)^2 + \left(\frac{g}{2}\right)^2 + \left(P_z + c - y_{cp} - \frac{f}{2}\right)^2\right)^{1/2} \tag{3.14f}$$

where y_{cp} represents the vertical distance to locate the center of mass of the mobile platform measured from its base. For example, if the mobile platform is considered as a trapezoidal prism, this value can be obtained as $y_{cp} = \frac{(2d+a)c}{3(d+a)}$.

Differentiating Eq. (3.10) results in $\dot{l}_i\hat{\boldsymbol{l}}_i + \boldsymbol{\omega}_i \times \boldsymbol{l}_i = \boldsymbol{v}_p + \boldsymbol{\omega}_p \times \boldsymbol{r}_i$, $\forall i = 1,2,\ldots,12$, which relates the cable velocities with the mobile box velocities; as such, for any *i*th cable, $\dot{l}_i$ is the rate of change in the length; $\boldsymbol{\omega}_i$ is the angular velocity vector, $\hat{\boldsymbol{l}}_i$ is the cable unitary vector in the reference frame. For the mobile box, $\boldsymbol{v}_p$ and $\boldsymbol{\omega}_p$ are the linear and angular velocities, respectively. In matrix form the inverse velocity can be expressed as:

$$\frac{d\boldsymbol{l}}{dt} = \boldsymbol{J}\frac{d\boldsymbol{X}_p}{dt} \tag{3.15}$$

where $\boldsymbol{J}$ represents the Jacobian matrix. Differentiating constraints (3.11) to (3.13) results in

$$\dot{l}_i = \dot{l}_{(i+6)} \quad \forall \quad i = 1,2 \dots 6 \tag{3.16}$$

$$\dot{l}_i = \dot{l}_{(i+4)} \quad \forall \quad i = 1,2 \tag{3.17}$$

Conditions (3.16) and (3.17) permit the use of the first four cables to obtain a representative differentiating inverse kinematic equation for purely translational movements, such as:

$$\begin{bmatrix} \dot{l}_1 \\ \dot{l}_2 \\ \dot{l}_3 \\ \dot{l}_4 \end{bmatrix} = \begin{bmatrix} \frac{P_x - \frac{b}{2} + \frac{e}{2}}{l_1} & \frac{P_z + c - y_{cp} - \frac{f}{2}}{l_1} \\ \frac{P_x + \frac{b}{2} - \frac{e}{2}}{l_2} & \frac{P_z + c - y_{cp} - \frac{f}{2}}{l_2} \\ \frac{P_x + \frac{d}{2} - \frac{e}{2}}{l_3} & \frac{P_z + c - y_{cp} + \frac{f}{2}}{l_3} \\ \frac{P_x - \frac{d}{2} + \frac{e}{2}}{l_4} & \frac{P_z + c - y_{cp} + \frac{f}{2}}{l_4} \end{bmatrix} \begin{bmatrix} v_{px} \\ v_{pz} \end{bmatrix} \tag{3.18}$$

In general, the rank-deficient Jacobian matrix, expressed in Eq. (2.6), results in geometrical singularities of a robot. Frequently, these singularities are related to configurations near the boundaries of the robot's workspace and the loss of full motion. Conditions of free-singularity poses are established as:

$$l_i > 0 \quad \forall \quad i = 1,2,..,4 \tag{3.19a}$$

$$\frac{-3f(a+d) - 2c(2a+d)}{6(a+d)} < P_z < \frac{3f(a+d) - 2c(2a+d)}{6(a+d)} \tag{3.19b}$$

The inverse acceleration of the mobile platform can be obtained by differentiating Eq. (3.15) which results in

$$\frac{d^2\boldsymbol{l}}{dt^2} = \boldsymbol{J}\,\frac{d^2\boldsymbol{X}_p}{dt^2} + \dot{\boldsymbol{J}}\,\frac{d\boldsymbol{X}_p}{dt} \tag{3.20}$$

where:

$$\dot{\boldsymbol{J}} = [\dot{\boldsymbol{J}}_1 \quad \dot{\boldsymbol{J}}_2]$$

$$\dot{\boldsymbol{J}}_1 = \frac{l_i(\boldsymbol{v}_p + \boldsymbol{\omega}_p \times \boldsymbol{r}_i) - \dot{l}_i \boldsymbol{l}_i}{l_i^2}$$

$$\dot{\boldsymbol{J}}_2 = \frac{l_i\left((\boldsymbol{\omega}_p \times \boldsymbol{r}_i) \times \boldsymbol{l}_i + \boldsymbol{r}_i \times \boldsymbol{v}_p\right) - \dot{l}_i(\boldsymbol{r}_i \times \boldsymbol{l}_i)}{l_i^2}$$

For purely translational motions of the mobile platform, the acceleration equations are:

$$\begin{bmatrix} \ddot{l}_1 \\ \ddot{l}_2 \\ \ddot{l}_3 \\ \ddot{l}_4 \end{bmatrix} = \begin{bmatrix} \frac{P_x - \frac{b}{2} + \frac{e}{2}}{l_1} & \frac{P_z + c - y_{cp} - \frac{f}{2}}{l_1} \\ \frac{P_x + \frac{b}{2} - \frac{e}{2}}{l_2} & \frac{P_z + c - y_{cp} - \frac{f}{2}}{l_2} \\ \frac{P_x + \frac{d}{2} - \frac{e}{2}}{l_3} & \frac{P_z + c - y_{cp} + \frac{f}{2}}{l_3} \\ \frac{P_x - \frac{d}{2} + \frac{e}{2}}{l_4} & \frac{P_z + c - y_{cp} + \frac{f}{2}}{l_4} \end{bmatrix} \begin{bmatrix} a_{px} \\ a_{pz} \end{bmatrix} + \tag{3.21}$$

$$\begin{bmatrix} \frac{l_1 v_{px} - \dot{l}_{r1}\left(P_x - \frac{b}{2} + \frac{e}{2}\right)}{l_1^2} & \frac{l_1 v_{pz} - \dot{l}_{r1}\left(P_z + c - y_{cp} - \frac{f}{2}\right)}{l_1^2} \\ \frac{l_2 v_{px} - \dot{l}_{r2}\left(P_x + \frac{b}{2} - \frac{e}{2}\right)}{l_2^2} & \frac{l_2 v_{pz} - \dot{l}_{r2}\left(P_z + c - y_{cp} - \frac{f}{2}\right)}{l_2^2} \\ \frac{l_3 v_{px} - \dot{l}_{r3}\left(P_x + \frac{d}{2} - \frac{e}{2}\right)}{l_{r3}^2} & \frac{l_3 v_{pz} - \dot{l}_{r3}\left(P_z + c - y_{cp} + \frac{f}{2}\right)}{l_3^2} \\ \frac{l_4 v_{px} - \dot{l}_{r4}\left(P_x - \frac{d}{2} + \frac{e}{2}\right)}{l_4^2} & \frac{l_4 v_{pz} - \dot{l}_{r4}\left(P_z + c - y_{cp} + \frac{f}{2}\right)}{l_4^2} \end{bmatrix} \begin{bmatrix} v_{px} \\ v_{pz} \end{bmatrix}$$

The forward position problem is related to obtaining the center of the mobile platform $\boldsymbol{p}$, when any of the two cable lengths, l_1 or l_7, and l_2 or l_8 are known. In this analysis, it is assumed that the anchor points are fixed and also known. As such, based on the first two expressions of Eq. (3.14), the position of the mobile platform can be found by:

$$P_x = \frac{l_1^2 - l_2^2}{2(e-b)} \tag{3.22a}$$

$$P_z = \frac{f - 2(c - y_{cp}) \pm \sqrt{2(l_1^2 + l_2^2 + be) - (4P_x^2 + b^2 + h^2 + e^2)}}{2} \tag{3.22b}$$

There are two solutions for the vertical position of the mobile platform. If the motion is constrained to be inside of the static structure, the sign of the radical in Eq. (3.22b) should be negative.

3.2.2 Static Force Analysis

The forces (cable positive tensions) for a specific equilibrium point of the system are developed by assuming the external forces and moments are constant and acting along the center of mass of the mobile platform. In particular, the general structure matrix of the WCR can be formulated as $\boldsymbol{A} = [\,\boldsymbol{a}_1 \quad \cdots \quad \boldsymbol{a}_{12}]$, where each column is represented by $\boldsymbol{a}_i = [\hat{\boldsymbol{l}}_i \quad (\boldsymbol{r}_i \times \hat{\boldsymbol{l}}_i)]^T$. The cable tensions are defined as $\boldsymbol{\tau} = [\tau_1 \quad \cdots \quad \tau_{12}]^T$ and the planar wrench as $\boldsymbol{W} = [F_x \quad (F_z - m_p G_z) \quad M_y]^T$. A reduced static system of equations can be established by assuming the cable tension relations shown in Figure 3.12.

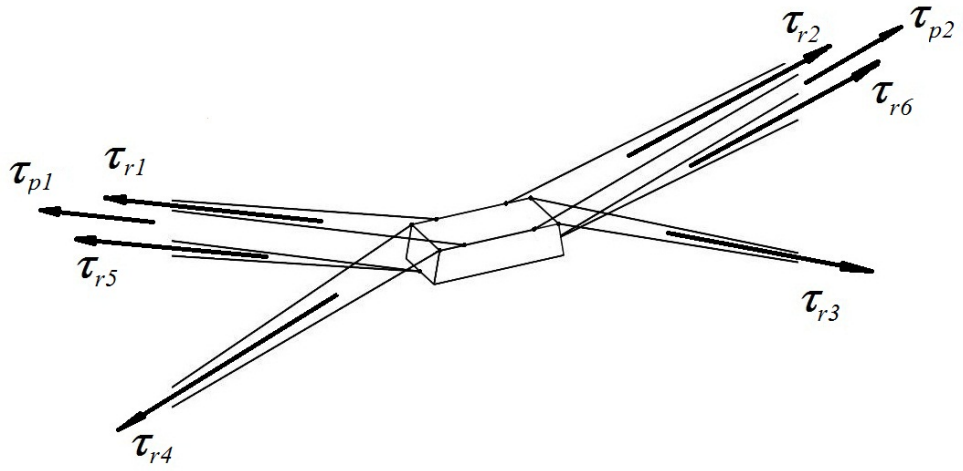

Figure 3.12: Cable tensions in the robot configuration.

A resultant tension on each pair cable of the robot can be determined as:

$$\tau_{ri} = \tau_i + \tau_{i+6} \;\; \forall \; i = 1,2,\dots,6 \tag{3.23}$$

Let each cable tension in every cable pair have equal tension; that is $\tau_i = \tau_{i+6} \;\; \forall \; i = 1,2,\dots,6$. Then, $\tau_i = \tau_{i+6} = \frac{\tau_{ri}}{2} \;\; \forall \; i = 1,2,\dots,6$. In addition, top cables used for the projected parallel mechanism, are related by:

$$\tau_{pi} = \tau_{ri} + \tau_{r(i+4)} \;\; \forall \; i = 1,2 \tag{3.24}$$

Under conditions (3.23) and (3.24), and assuming motions of the mobile platform along plane XZ ($P_y = 0$), a reduced formulation for the structure matrix and the cable tensions are obtained as:

$$\boldsymbol{A}_c = \begin{bmatrix} \frac{q_1}{2l_1} & \frac{q_2}{2l_2} & \frac{q_3}{2l_3} & \frac{q_4}{2l_4} & \frac{q_1}{2l_5} & \frac{q_2}{2l_6} \\ \frac{q_5}{2l_1} & \frac{q_5}{2l_2} & \frac{q_6}{2l_3} & \frac{q_6}{2l_4} & \frac{q_5}{2l_5} & \frac{q_5}{2l_6} \\ \frac{q_7}{4l_1} & \frac{q_8}{4l_2} & \frac{q_9}{4l_3} & \frac{q_{10}}{4l_4} & \frac{q_{11}}{4l_5} & \frac{q_{12}}{4l_6} \end{bmatrix}, \qquad \boldsymbol{\tau}_c = \begin{bmatrix} \tau_{r1} \\ \tau_{r2} \\ \tau_{r3} \\ \tau_{r4} \\ \tau_{r5} \\ \tau_{r6} \end{bmatrix} \tag{3.25}$$

where

$$q_1 = -2P_x + (b - e),\, q_2 = -2P_x - (b - e)$$

$$q_3 = -2P_x - (d - e),\, q_4 = -2P_x + (d - e)$$

$$q_5 = -2P_z - 2\big(c - y_{cp}\big) + f,\, q_6 = -2P_z - 2\big(c - y_{cp}\big) - f$$

$$q_7 = 2\big(c - y_{cp}\big)q_1 + bq_5,\, q_8 = 2\big(c - y_{cp}\big)q_2 - bq_5$$

$$q_9 = 2\big(c - y_{cp}\big)q_3 - dq_6,\, q_{10} = 2\big(c - y_{cp}\big)q_4 + dq_6$$

$$q_{11} = a\, q_5 - 2y_{cp}\, q_1,\, q_{12} = -a\, q_5 - 2y_{cp}\, q_2$$

Assuming non-singular poses, Eq. (3.25) can be used to delimit the positions of the mobile platform such that all cables are in tension.

3.3 Workspace delineation

Feasible planar regions are defined by establishing which cable pair is slack. Indeed, according to [136] and [50], the analysis of workspace boundaries with one or more cables that have lost tension admits the analytical solution of a reduced system of static equations. The all-positive workspace boundaries of the underconstrained and fully constrained robot configurations are studied in the following sections.

3.3.1 Underconstrained case

Based on the configuration shown in Figure 3.11, let us assume that bottom cables 3, 4, 9 and 10 are slack; in consequence, the mobile platform is suspended by the remaining eight cables 1, 2, 5, 6, 7, 8, 11, and 12. Assuming conditions (3.23) and (3.24) and nonsingular motions of the mobile platform along plane XZ, a reduced structure matrix based on Eq. (3.25) can be expressed as follows

$$\boldsymbol{A}_s = \begin{bmatrix} \frac{q_1}{2l_1} & \frac{q_2}{2l_2} & \frac{q_1}{2l_5} & \frac{q_2}{2l_6} \\ \frac{q_5}{2l_1} & \frac{q_5}{2l_2} & \frac{q_5}{2l_5} & \frac{q_5}{2l_6} \\ \frac{q_7}{4l_1} & \frac{q_8}{4l_2} & \frac{q_{11}}{4l_5} & \frac{q_{12}}{4l_6} \end{bmatrix} \tag{3.26}$$

The equivalent cable tensions of each top cable pair are grouped in $\boldsymbol{\tau}_s = [\tau_{s1} \quad \tau_{s2} \quad \tau_{s5} \quad \tau_{s6}]^T$, as is shown in Figure 3.13.

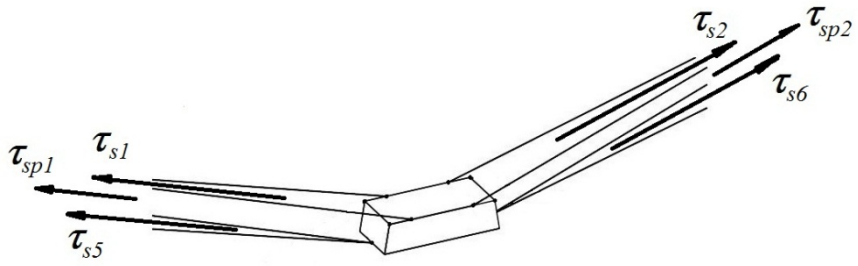

Figure 3.13: Underconstrained planar configuration.

Considering only the effect of the mobile platform mass, the wrench is represented as $\boldsymbol{W} = [0 \quad -m_p G_z \quad 0]^T$ (the complete equations are given in the appendix). Thus, the all-positive workspace, $\boldsymbol{\Gamma}_s$ can be obtained by analyzing slackness conditions with constant orientation of the mobile platform ($\theta_y = 0$), and by solving the all-positive cable tension redundancy. Indeed, the loss of one cable makes $\boldsymbol{A}_s$ square, which might admit an exact positive tension solution for the remaining three cable pairs. When cable pair 1 has no tension, then $\tau_{s1} = 0$ and the system transforms into an equivalent three-tension system. The unique solution, $\boldsymbol{\Gamma}_{s1}$, is defined by the feasible area of curves $\boldsymbol{\delta}_0 > 0$, $\boldsymbol{\delta}_2 > 0$, and $\boldsymbol{\delta}_6 > 0$. Symmetrically, the area defined by curves $\boldsymbol{\varepsilon}_0 < 0$, $\boldsymbol{\varepsilon}_1 < 0$ and $\boldsymbol{\varepsilon}_5 < 0$ represents the feasible workspace, $\boldsymbol{\Gamma}_{s2}$, when cable 2 is slack ($\tau_{s2} = 0$). Curve equations are shown below.

$$
\begin{aligned}
\boldsymbol{\delta}_0 &= \tfrac{1}{8}(e-b)(2cq_2 + (a-b)q_5)q_5. \\
\boldsymbol{\delta}_2 &= -\tfrac{1}{8}a(q_1 + q_2)q_5. \\
\boldsymbol{\delta}_5 &= \tfrac{1}{8}(2cq_2 + (a-b)q_5)q_2. \\
\boldsymbol{\delta}_6 &= \tfrac{1}{8}(bq_1 + aq_2)q_5 - \tfrac{1}{4}cq_1q_2. \\
\boldsymbol{\varepsilon}_0 &= -\tfrac{1}{8}(e-b)\big((a-b)q_5 - 2cq_1\big)q_5. \\
\boldsymbol{\varepsilon}_1 &= \boldsymbol{\delta}_2. \\
\boldsymbol{\varepsilon}_5 &= \tfrac{1}{8}(aq_1 + bq_2)q_5 + \tfrac{1}{4}cq_1q_2. \\
\boldsymbol{\varepsilon}_6 &= \tfrac{1}{8}\big((a-b)q_5 - 2cq_1\big)q_1.
\end{aligned}
\tag{3.27}
$$

Conditions $\boldsymbol{\delta}_0 > 0$ and $\boldsymbol{\varepsilon}_0 < 0$ ensure that the structure matrices are not singular, by assuming that all cables have a length that is different than zero. Additional nonsingular conditions are observed when:

$$
\begin{aligned}
b &\neq e \\
P_z &\neq \left(\frac{f}{2} - c + y_{cp}\right)
\end{aligned}
\tag{3.28}
$$

$$P_x \neq \pm\left(\left(\frac{a-b}{2c}\right)P_z + \left(\frac{2ac - af - 2ay_{cp} + bf + 2y_{cp} - 2ce}{4c}\right)\right)$$

These curves are the function of the geometrical parameters and the position of the mobile platform. Any pose of the mobile platform on curves $\boldsymbol{\delta}_6$ or $\boldsymbol{\varepsilon}_5$ makes the system lose tension on either cable 5 or 6, transforming the system into a two-cable robot. As long as the mobile platform stays on the aforementioned curves, the orientation will be maintained. However, beyond this limit; that is, inside the regions delimited by curves $\boldsymbol{\delta}_5$, $\boldsymbol{\delta}_6$, $\boldsymbol{\varepsilon}_5$ and $\boldsymbol{\varepsilon}_6$, the two-cable system cannot hold the fixed orientation.

The loss of one cable makes $\boldsymbol{A}_s$ square, which admits an exact positive tension solution for the remaining three cable pairs, as long as the position of the mobile platform belongs to $\boldsymbol{\Gamma}_{s1}$ or $\boldsymbol{\Gamma}_{s2}$. Thus, cable tensions can be obtained for any value of $P_z < \left(\frac{f}{2} - c + y_{cp}\right)$, as:

$$\overline{\tau}_{si} = \begin{cases} \delta_i\left(\dfrac{l_i\, m_p\, G_z}{\delta_0}\right) & \forall\, i = 2,5,6.\ \ 0 < P_x < \delta_6 \\ \\ \varepsilon_i\left(\dfrac{l_i\, m_p G_z}{\varepsilon_0}\right) & \forall\, i = 1,5,6.\ \ \varepsilon_5 < P_x \leq 0 \end{cases} \tag{3.29}$$

These results provide information about the amount of tension applied at each top projected parallel cable set by

$$\tau_{spi} = \overline{\tau}_{si} + \overline{\tau}_{s(i+4)}\ \ \forall\, i = 1,2 \tag{3.30}$$

with the tension orientation as follows:

$$\boldsymbol{\tau}_{spi} = \tau_{spi}[\hat{l}_{ix} \quad 0 \quad \hat{l}_{iz}]^T \quad \forall \quad i = \quad 1,2 \tag{3.31}$$

The delineation of the workspace $\boldsymbol{\Gamma}_s$ requires the redundancy solution of the four cable tensions. Here, the redundancy solution of the suspended planar cable robot is achieved by the inclusion of two virtual cables. This approach allows an analytical solution to the problem presented in (2.15) and (2.16). The location of virtual cables in the mobile platform permits a better understanding of the

problem. The virtual cables represent the action of the top parallel cables on the mobile platform. Figure 3.14 shows the virtual cables acting on the suspended cable robot.

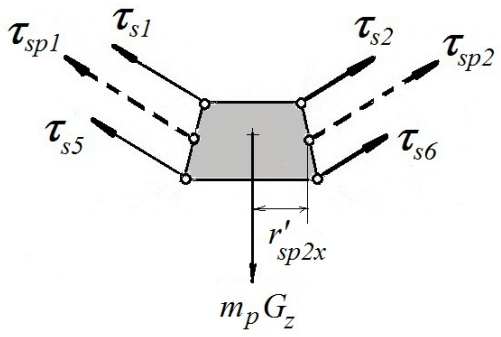

Figure 3.14: Virtual cables acting in the suspended planar cable robot.

The orientation and magnitude of these virtual cables are known from equations (3.30) and (3.31). The virtual anchor points can be written in function of the anchor horizontal distance r'_{sp2x}, by using geometrical parameters of the mobile platform and moment balance equations as follows:

$$r'_{sp2z} = \rho\left(r_{6x} - r'_{sp2x}\right) - y_{cp} \tag{3.32}$$

$$r'_{sp1z} = \rho\left(r'_{sp1x} - r_{5x}\right) - y_{cp} \tag{3.33}$$

$$r'_{sp1x} = \frac{r'_{sp2x}(\rho + \theta_2) - \rho(r_{5x} + r_{6x})}{(\rho - \theta_1)} \quad \forall\ \rho \neq \theta_1 \tag{3.34}$$

where

$$\rho = \frac{2c}{(a-b)}, \quad \forall\ a > b, c > 0$$

$$\theta_i = \frac{\hat{l}_{iz}}{\hat{l}_{ix}}, \quad \forall\ \hat{l}_{ix} \neq 0, i = 1, 2.$$

In other words, the virtual anchor points are changing accordingly to find a positive cable tension solution. Thus, cable tensions can be expressed in function of these virtual anchor points as:

$$\begin{bmatrix}\tau_{s1}\\ \tau_{s5}\end{bmatrix} = \left(\frac{\tau_{sp1}}{r_{1x}r_{5z} - r_{1z}r_{5x}}\right)\begin{bmatrix} r_{5z} & -r_{5x}\\ -r_{1z} & r_{1x}\end{bmatrix}\begin{bmatrix}r'_{sp1x}\\ r'_{sp1z}\end{bmatrix} \tag{3.35a}$$

$$\begin{bmatrix}\tau_{s2}\\ \tau_{s6}\end{bmatrix} = \left(\frac{\tau_{sp2}}{r_{2x}r_{6z} - r_{2z}r_{6x}}\right)\begin{bmatrix} r_{6z} & -r_{6x}\\ -r_{2z} & r_{2x}\end{bmatrix}\begin{bmatrix}r'_{sp2x}\\ r'_{sp2z}\end{bmatrix} \tag{3.35b}$$

The distances r_{ix} represent the known anchor points on the mobile platform, as are defined in Eq. (3.9). The solution of equations (3.19a) and (3.19b) are function of the geometrical parameter r'_{sp2x} which values for positive tensions can be found between the following limits

$$r_{2x} < r'_{sp2x} < r_{6x} \tag{3.36}$$

The minimum two-norm cable tension problem expressed in Eq. (2.15) can be rewritten as:

$$\text{minimize } \mathrm{F}^2 = \tau_{sp1}^2 + \tau_{sp2}^2 - 2(\tau_{s1}\tau_{s5} + \tau_{s2}\tau_{s6}) \tag{3.37}$$

By substituting equations (3.35a) and (3.35b) into Eq. (3.37), a quadratic equation is obtained which admits a minimum value by equaling its derivative to zero,

$$\frac{\partial(\tau_{s1}\tau_{s5} + \tau_{s2}\tau_{s6})}{\partial(r'_{sp2x})} = 0 \tag{3.38}$$

Solution of Eq. (3.38) gives the optimal value of the virtual location r'_{sp2x} for the minimum cable tensions in sense of the two-norm definition as

$${}^{*}r'_{sp2x} = -\frac{N}{2D} \tag{3.39}$$

where

$$D = \left(\frac{\tau_{sp1}}{(r_{1x}r_{5z} - r_{1z}r_{5x})}\right)^2 \left(\frac{(\theta_2 + \rho)}{(\theta_1 - \rho)}\right)^2 (\rho r_{1x} - r_{1z})(r_{5z} - \rho r_{5x}) - \left(\frac{\tau_{sp2}}{r_{2x}r_{6z} - r_{2z}r_{6x}}\right)^2 (\rho\, r_{2x} + r_{2z})(\rho\, r_{6x} + r_{6z})$$

$$\begin{aligned} N = \left(\frac{\tau_{sp1}}{(r_{1x}r_{5z} - r_{1z}r_{5x})}\right)^2 \left(\frac{1}{(\theta_1 - \rho)}\right)^2 (\theta_2 + \rho)\big(&2r_{1x}r_{5x}^2\theta_1\rho^2 + 2r_{1x}r_{5x}r_{6x}\rho^3 - 2r_{1x}r_{5z}r_{6x}\rho^2 \\ &- r_{1x}r_{5z}\theta_1 y_{cp} - 2r_{1x}r_{5x}\rho^2 y_{cp} + r_{1x}r_{5z}\rho y_{cp} + 2r_{1x}r_{5x}\theta_1\rho y_{cp} + 2r_{1z}r_{5x}r_{5z}\rho \\ &- 2r_{1z}r_{5x}r_{6x}\rho^2 - r_{1z}r_{5x}\theta_1 y_{cp} + r_{1z}r_{5x}\rho y_{cp} + 2r_{1z}r_{5z}r_{6x}\rho - r_{1z}r_{5x}^2\theta_1\rho \\ &- r_{1x}r_{5x}r_{5z}\rho^2 - r_{1z}r_{5x}^2\rho^2 - r_{1x}r_{5x}r_{5z}\theta_1\rho\big) \\ &+ \left(\frac{\tau_{sp2}}{r_{2x}r_{6z} - r_{2z}r_{6x}}\right)^2 (\rho\, r_{6x} - y_{cp})(2\rho\, r_{2x}r_{6x} + r_{2x}r_{6z} + r_{2z}r_{6x}) \end{aligned}$$

The all-positive tensions workspace $\mathbf{\Gamma}_s$ can be delineated by analyzing equations (3.19a) and (3.19b) for different conditions on cable tensions. For example, for force-closure conditions:

$$\boldsymbol{\tau}_{si} > 0, \ \ \forall \ i = 1,2,5,6 \tag{3.40}$$

Also for feasible conditions:

$$\mathbf{0} < \boldsymbol{\tau}_{\min} \leq \boldsymbol{\tau}_{si} \leq \boldsymbol{\tau}_{\max}, \ \ \forall \ i = 1,2,5,6 \tag{3.41}$$

The stiffness matrix of the suspended configuration shown in Figure 3.13 is analyzed. As is expressed in Eq. (2.17), the values inside the stiffness matrix are affected by the cable tensions and the cable stiffness. Let us consider the stiffness matrix which results of the tensions applied to cables, that is:

$$\boldsymbol{K}_{\tau s} = \left(\frac{d\boldsymbol{A}_s}{d\boldsymbol{X}_p}\right)\boldsymbol{\tau}_s \tag{3.42}$$

Equation (3.42) expressed that the stiffness can be enhanced by selecting large values in the cable tension vector $\boldsymbol{\tau}_s = [\tau_{s1} \quad \tau_{s2} \quad \tau_{s5} \quad \tau_{s6}]^T$. Moreover, based on the equations (3.35a) and (3.35b), each top cable tension value is directly proportional to the amount of tension applied at each top

projected parallel cable set, τ_{sp1} and τ_{sp2}. The amount of tension applied at each top cable set, expressed in Eq. (3.30), can be expressed as

$$\tau_{sp1} = m_p G_z \left(l_1 \left(\frac{\varepsilon_1}{\varepsilon_0}\right) + l_5 \begin{cases} \left(\frac{\delta_5}{\delta_0}\right) & \text{if } \ 0 < P_x < \delta_6 \\ \left(\frac{\varepsilon_5}{\varepsilon_0}\right) & \text{if } \ \varepsilon_5 < P_x \leq 0 \end{cases} \right) \tag{3.43a}$$

$$\tau_{sp2} = m_p G_z \left(l_2 \left(\frac{\delta_2}{\delta_0}\right) + l_6 \begin{cases} \left(\frac{\delta_6}{\delta_0}\right) & \text{if } \ 0 < P_x < \delta_6 \\ \left(\frac{\varepsilon_6}{\varepsilon_0}\right) & \text{if } \ \varepsilon_5 < P_x \leq 0 \end{cases} \right) \tag{3.43b}$$

Then, for the suspended configuration, the stiffness matrix can be increased by adding a gravitational vertical force to the mobile platform. Indeed, stiffness has a direct relationship to the values of the minimum and maximum allowable cable tensions. It is observed by [131] and [116] that the increment of $\tau_{\min}$ improves the stiffness of the robot; however, it might reduce the workspace size as well. Consequently, high stiffness configurations must be evaluated with respect to the variations in the workspace size.

In that sense, the method to distribute the tension among cables plays an important role; in fact, different norms used in the minimization of the cable tension vector affects the cable tension redundancy resolution, as is probed by Gosselin and Grenier [107].

3.3.2 Fully-constrained case

The fully constrained planar robot, shown in Figure 3.2b, is analyzed in this section. The all-positive workspace is obtained by establishing a reduced structure matrix of Eq. (3.9) and analyzing the slackness in each one of the bottom pair cables with constant orientation of the mobile platform. Specifically, top cables 1, 2 together with the bottom pair cables 3 and 4 define the reduced structure matrix. Then, assuming a lack of tension on cables 3 and 4, and considering only gravitational effects, the unique solution of the three-cable system defines the feasible workspace $\boldsymbol{\Gamma}_c$ delineated by curves $\boldsymbol{\alpha}_0 < 0$, $\boldsymbol{\alpha}_1 < 0$ and $\boldsymbol{\beta}_2 > 0$. The equations of these curves are:

$$\boldsymbol{\alpha}_0 = -\frac{1}{8}\left(2c - f + 2P_z - 2y_{cp}\right)(2bce + 2bdf - bef + 2beP_z - 2bey_{cp} + 4bfP_x - 2cde - def - 2deP_z + 2dey_{cp}).$$

$$\boldsymbol{\alpha}_1 = \frac{1}{4}bce - \frac{1}{2}bcP_x + \frac{1}{4}bdf - \frac{1}{8}bef + \frac{1}{4}beP_z - \frac{1}{4}bey_{cp} + \frac{1}{4}bfP_x - \frac{1}{2}bP_xP_z + \frac{1}{2}bP_xy_{cp} - \frac{1}{4}cde + \frac{1}{2}cdP_x - \frac{1}{8}def - \frac{1}{4}deP_z + \frac{1}{4}dey_{cp} + \frac{1}{4}dfP_x + \frac{1}{2}dP_xP_z - \frac{1}{2}dP_xy_{cp}.$$

$$\boldsymbol{\alpha}_2 = \frac{1}{4}bce - \frac{1}{2}bcP_x + \frac{1}{4}bdf - \frac{1}{8}bef + \frac{1}{4}beP_z - \frac{1}{4}bey_{cp} + \frac{1}{4}bfP_x - \frac{1}{2}bP_xP_z + \frac{1}{2}bP_xy_{cp} - \frac{1}{4}cde - \frac{1}{2}cdP_x - \frac{1}{8}def - \frac{1}{4}deP_z + \frac{1}{4}dey_{cp} - \frac{1}{4}dfP_x - \frac{1}{2}dP_xP_z + \frac{1}{2}dP_xy_{cp}.$$

$$\boldsymbol{\alpha}_3 = \frac{1}{2}bP_x\left(2c - f + 2P_z - 2y_{cp}\right).$$

$$\boldsymbol{\beta}_0 = \frac{1}{8}\left(2c - f + 2P_z - 2y_{cp}\right)(2bce + 2bdf - bef + 2beP_z - 2bey_{cp} - 4bfP_x - 2cde - def - 2deP_z + 2dey_{cp}).$$

$$\boldsymbol{\beta}_1 = -\frac{1}{4}bce - \frac{1}{2}bcP_x - \frac{1}{4}bdf + \frac{1}{8}bef - \frac{1}{4}beP_z + \frac{1}{4}bey_{cp} + \frac{1}{4}bfP_x - \frac{1}{2}bP_xP_z + \frac{1}{2}bP_xy_{cp} + \frac{1}{4}cde - \frac{1}{2}cdP_x + \frac{1}{8}def + \frac{1}{4}deP_z - \frac{1}{4}dey_{cp} - \frac{1}{4}dfP_x - \frac{1}{2}dP_xP_z + \frac{1}{2}dP_xy_{cp}.$$

$$\boldsymbol{\beta}_2 = -\frac{1}{4}bce - \frac{1}{2}bcP_x - \frac{1}{4}bdf + \frac{1}{8}bef - \frac{1}{4}beP_z + \frac{1}{4}bey_{cp} + \frac{1}{4}bfP_x - \frac{1}{2}bP_xP_z + \frac{1}{2}bP_xy_{cp} + \frac{1}{4}cde + \frac{1}{2}cdP_x + \frac{1}{8}def + \frac{1}{4}deP_z - \frac{1}{4}dey_{cp} + \frac{1}{4}dfP_x + \frac{1}{2}dP_xP_z - \frac{1}{2}dP_xy_{cp}.$$

$$\boldsymbol{\beta}_4 = \boldsymbol{\alpha}_3.$$

(3.44)

The pose of the mobile platform on curves $\boldsymbol{\alpha}_1$ or $\boldsymbol{\beta}_2$ has the consequence of tension loss in cables 1 or 2, resulting in a two-cable system. The fixed orientation of the mobile platform is maintained as long as the platform is moving on the mentioned curves. The minimum two-norm cable tension problem expressed in Eq. (2.15) can be rewritten as:

$$\text{minimize } \mathrm{F}^2 = \left(\tau_{sp1}^2 + \tau_{sp2}^2 + \tau_3^2 + \tau_4^2\right) - 2(\tau_1\tau_5 + \tau_2\tau_6) \tag{3.45}$$

Finding the minimum of $\mathrm{F}(\boldsymbol{\tau})$ implies to maximize the negative term $2(\tau_1\tau_5 + \tau_2\tau_6)$ and keep all the cable tension positive; that is,

$$\max(\tau_1\tau_5 + \tau_2\tau_6)$$
$$\text{Subjected to} \quad \tau_i > 0 \quad \forall \; i = 1, 2, \ldots, m \tag{3.46}$$

An iterative method can be used to solve Eq. (3.46).

3.4 Numerical results

The following examples are based on the geometric parameters given in Table 3.3 under different conditions of force applied on the mobile platform for the underdetermined and fully-constrained robot cases.

Table 3.3: Parameters of the suspended planar robot

Symbol	Value in meters
a	0.370
b	0.200
c	0.094
d	0.340
e	3.000
f	1.000
g	0.200
h	0.160

Geometric parameters are shown in Figure 3.11.

3.4.1 Suspended cable-based robot

The influence of the gravitational force is analyzed for both planar cases, by assuming a mobile platform mass $m_p = 1$ Kg. The curves described in Equation (3.11) are delineated in Figure 3.15.

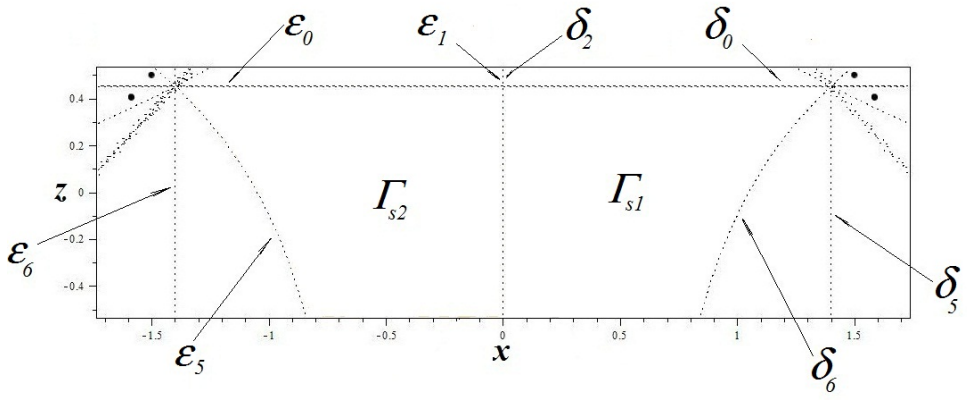

Figure 3.15: Delineation of workspace $\boldsymbol{\Gamma_{s1}}$ by $\boldsymbol{\delta_0 > 0}$, $\boldsymbol{\delta_6 > 0}$ and $\boldsymbol{\delta_2 > 0}$, and workspace $\boldsymbol{\Gamma_{s2}}$ by $\boldsymbol{\varepsilon_0 < 0}$, $\boldsymbol{\varepsilon_1 \leq 0}$, and $\boldsymbol{\varepsilon_5 < 0}$.

When cable 1 has no tension, the robot transforms into a three-cable system. Then, the right side workspace, $\boldsymbol{\Gamma}_{s1}$, is defined by the area delimited by conditions $\boldsymbol{\delta}_0 > 0$, $\boldsymbol{\delta}_2 > 0$, and $\boldsymbol{\delta}_6 > 0$. Symmetrically, the left workspace, $\boldsymbol{\Gamma}_{s2}$, is contained inside the curves $\boldsymbol{\varepsilon}_0 < 0$, $\boldsymbol{\varepsilon}_1 < 0$ and $\boldsymbol{\varepsilon}_5 < 0$ when cable 2 is slack.

Additional curves $\boldsymbol{\delta}_5 > 0$ and $\boldsymbol{\varepsilon}_6 < 0$ define the positive tension in cables 5 and 6, respectively. Conditions $\boldsymbol{\delta}_0 > 0$ and $\boldsymbol{\varepsilon}_0 < 0$ ensure that the structure matrices are not singular, by assuming that all cables have a minimum length different from zero.

The cable tension redundancy solution expressed by equations (3.35) and (3.40) are delineated by assuming that a minimum cable tension condition greater than zero is acceptable; that is, $\tau_{\min} > 0$. Moreover, there is no limit to the amount of tensions that are introduced; that is, $\tau_{\max}$ is unbounded.

In Figure 3.16, regions defined by curves $\boldsymbol{\tau}_{s1} > 0$ and $\boldsymbol{\tau}_{s2} > 0$ define the all-positive tension workspace $\boldsymbol{\Gamma}_s$. Regions between $\boldsymbol{\tau}_{s1} > 0$ and $\boldsymbol{\tau}_{s6} > 0$, and $\boldsymbol{\tau}_{s2} > 0$ and $\boldsymbol{\tau}_{s5} > 0$, define regions where the tension of at least one cable loses tension.

A point on either the curves $\boldsymbol{\tau}_{s1}$ or $\boldsymbol{\tau}_{s2}$ makes cable one or two slack. Then, beyond these limits, the all-positive tension condition is not hold, and the four-pair-cable system is transforming in the three-cable planar system. In consequence, any point outside the curves $\boldsymbol{\tau}_{s1} > 0$ and $\boldsymbol{\tau}_{s2} > 0$, implies the use of equations (3.11) to obtain the cable tensions.

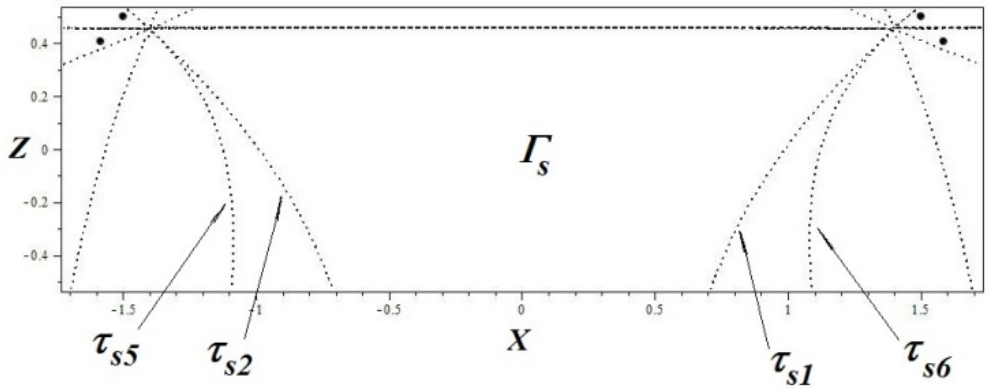

Figure 3.16: The all-positive cable tension area $\boldsymbol{\Gamma_s}$ delineated by curves $\boldsymbol{\tau_{s1} > 0}$ and $\boldsymbol{\tau_{s2} > 0}$.

In Figure 3.17, the regions defined between right curves $\boldsymbol{\tau_{s1} > 0}$ and $\boldsymbol{\delta_6 > 0}$, and left curves $\boldsymbol{\tau_{s2} > 0}$ and $\boldsymbol{\varepsilon_5 > 0}$ represent positions of the mobile platform when cable one or two is slack, respectively.

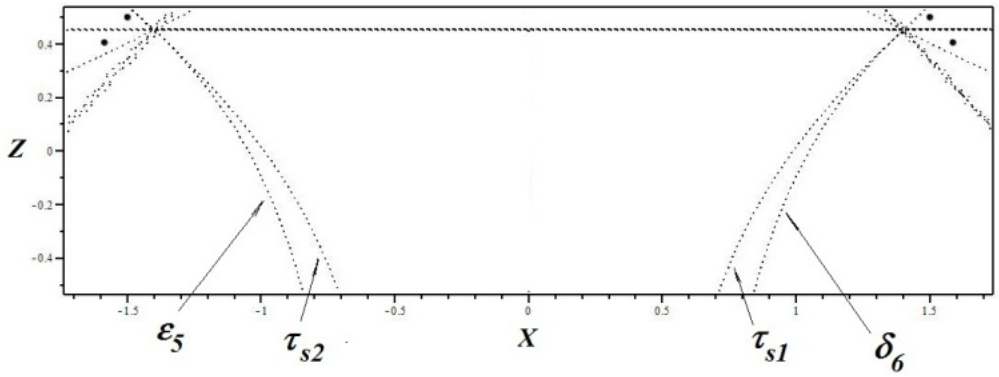

Figure 3.17: Curves $\boldsymbol{\tau_{s1} > 0}$ and $\boldsymbol{\tau_{s2} > 0}$, and $\boldsymbol{\delta_6 > 0}$ and $\boldsymbol{\varepsilon_5 > 0}$.

A validation of the above results is shown in Figure 3.18. An iterative algorithm is used to compare the analytical results. The all-positive area has a reduction of 34% with respect to the available workspace assuming an unbounded maximum cable tension.

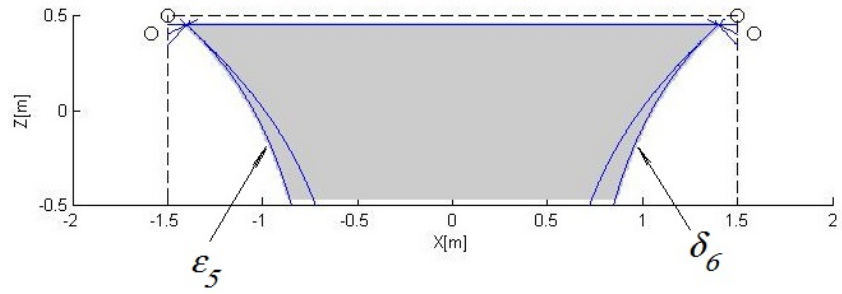

(a)

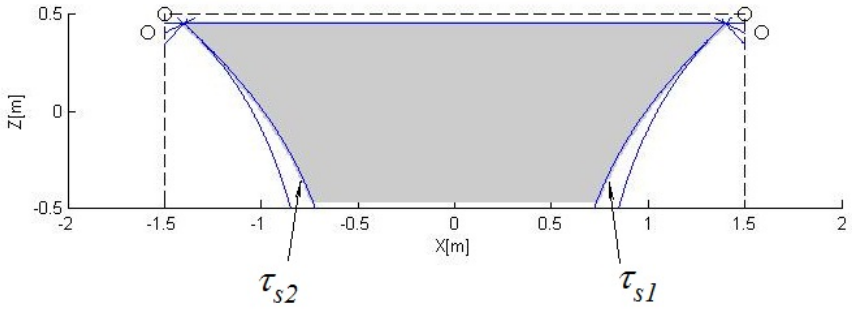

(b)

Figure 3.18: Workspaces of the suspended cable robot: (a) Area when $\boldsymbol{\tau_{min} \geq 0}$ and delineated by curves $\boldsymbol{\varepsilon_5 < 0}$ and $\boldsymbol{\delta_6 > 0}$, (b) The all-positive cable tension area when $\boldsymbol{\tau_{min} > 0}$ and delineated by curves $\boldsymbol{\tau_{s1} > 0}$ and $\boldsymbol{\tau_{s2} > 0}$.

An increase of the minimum cable tension; e.g. $\tau_{\min} \geq 5$ N, results in a reduction in the size of the workspace by a reduction of the bottom right and left poses of the mobile platform, expressed by curves $\boldsymbol{\tau}_{s1} \geq \tau_{\min}$ and $\boldsymbol{\tau}_{s2} \geq \tau_{\min}$, Figure 3.19a. On the other hand, a bounded value in the maximum cable tension; e.g. $\tau_{\max} \leq 20$ N, makes the workspace a reduction on the top poses of the mobile platform, depicted by curves $\boldsymbol{\tau}_{s1} \leq \tau_{\max}$ and $\boldsymbol{\tau}_{s2} \leq \tau_{\max}$, as is shown in Figure 3.19b. Also a 20% of change in the mass of the mobile platform is shown in both figures.

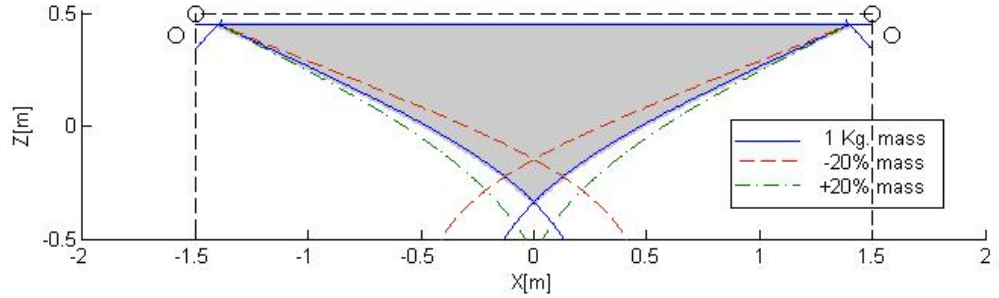

(a) $\tau_{\min} \geq 5$ N and $\tau_{\max}$ unbounded.

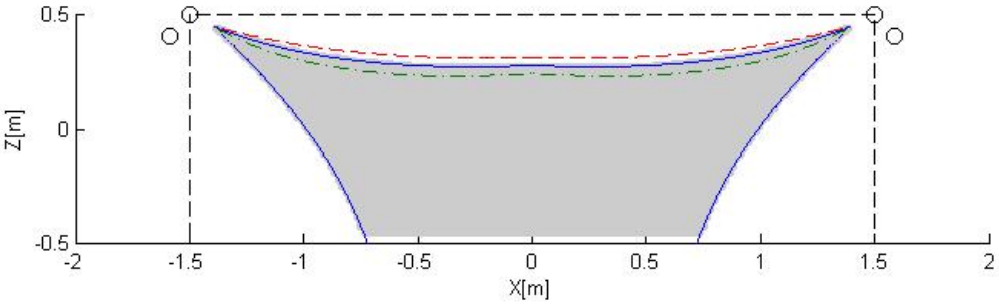

(b) $\tau_{\max} \leq 20$ N and $\tau_{\min} > 0$ N.

Figure 3.19: Workspaces of the suspended cable robot when the mass of the mobile platform changes $\pm 20\%$.

Selection of the minimum cable tension $\tau_{\min}$ has an influence in the size of the workspace compare to the maximum cable tension $\tau_{\max}$. Moreover, a change in the mass of the mobile platform makes an impact on the workspace when is influenced by $\tau_{\min}$ as well. The value selection of $\tau_{\max}$ is related with the actuation capacity and limited by the top position of the workspace.

Next, the influence of the natural frequency into the workspace size is studied in the suspended robot case. Each numerical simulation is based on the parameters provided in Table 3.2, with a maximum allowable cable tension, $\tau_{\max} = 200$ N, and a cable stiffness $k_i = 300{,}000$ N/m per 1 m cable length. The study incorporates the variations of the mass of the mobile platform from 0.1 to 20 Kg, and the minimum admissible cable tension from 0.1 to 40 N, to measure the changes of the

lowest minimum natural frequency, as well as the variations of the workspace size. This is shown in Figure 3.20 and Figure 3.21, respectively.

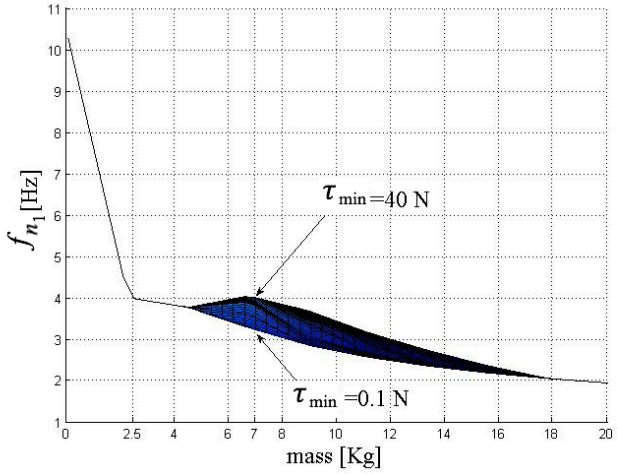

Figure 3.20: Variation of the lowest minimum natural frequency of the unconstrained robot.

Small changes in payloads lighter than 2.5 Kg have a significant impact on the minimum natural frequency regardless the values of the admissible minimum cable tensions. On the contrary, payloads beyond 2.5 Kg allow a smooth but constant reduction of the minimum natural frequency.

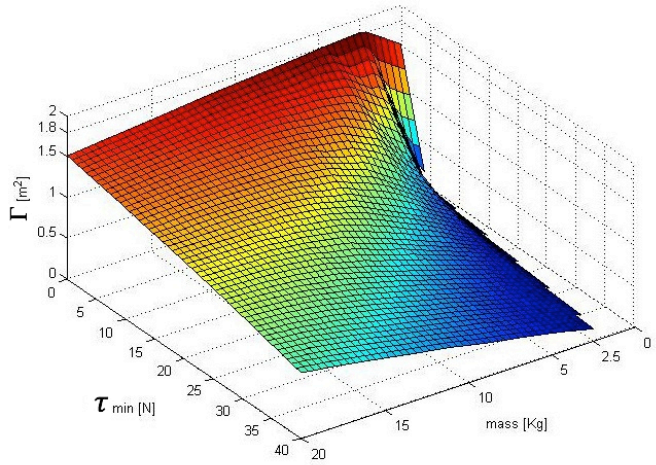

Figure 3.21: Variation of the workspace size of the unconstrained robot.

As it is observed in Figure 3.20, there is a range of payloads where it is possible to magnify the minimum natural frequency by means of the allowable minimum cable tension. For example, at 7 Kg, with a minimum cable tension of 40 N, the natural frequency is almost the same as the case for 2.5 Kg. Based on the results shown in Figure 3.21, a peak of the workspace size at a mass of 2.5 Kg with an admissible minimum cable tension of 0.1 N is observed.

In effect, a small value of the admissible cable tension admits the largest workspaces when the mass is changing. The mass of 2.5 Kg represents a turning point, causing a shift in the variations pace on both criteria. On one hand, a slightly reduction of this mass suddenly brings contradictory results on both plots regardless the value of the admissible minimum cable tension. On the other hand, a gradual decreasing of both criteria is achieved when the mass variations occurs for masses heavier than 2.5 Kg.

3.4.2 Fully-constrained cable-based robot

Extending the analysis for the fully-constrained robot, a mass of 1 Kg is also assumed for the mobile platform. The curves described in Equation (3.11) are delineated in Figure 3.22.

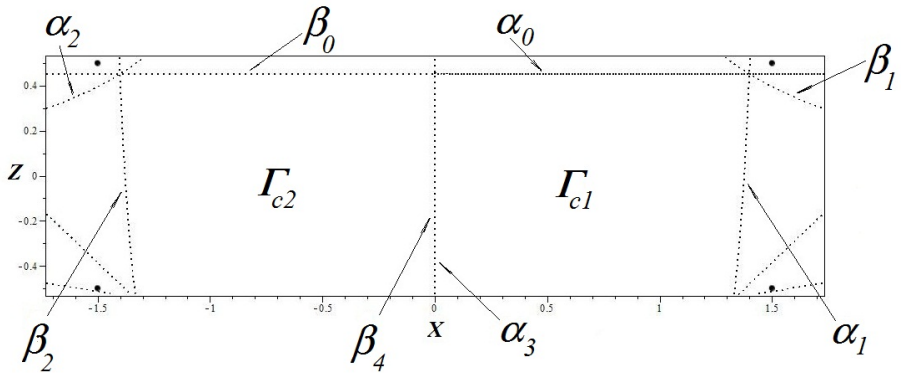

Figure 3.22: Delineation of workspace $\boldsymbol{\Gamma_{c1}}$ by $\boldsymbol{\alpha_0 < 0}$, $\boldsymbol{\alpha_3 < 0}$ and $\boldsymbol{\alpha_1 < 0}$, and workspace $\boldsymbol{\Gamma_{c2}}$ by $\boldsymbol{\beta_0 > 0}$, $\boldsymbol{\beta_4 > 0}$, and $\boldsymbol{\beta_2 > 0}$.

An iterative method analysis verified the above curves as is shown in Figure 3.23. The all-positive workspace cable tension for an unbounded maximum cable tension is depicted by using the proposed method to solve the redundancy resolution.

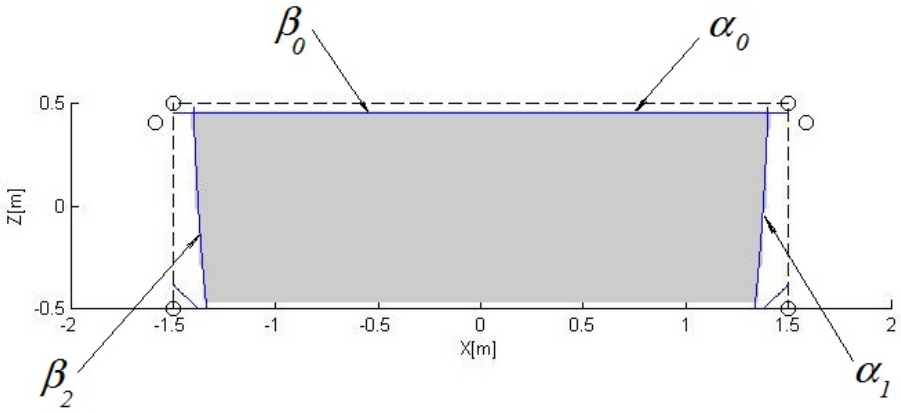

Figure 3.23: The all-positive cable tension area when $\boldsymbol{\tau_{min} > 0}$, and delineated by curves $\boldsymbol{\alpha_0 < 0}$, $\boldsymbol{\beta_0 > 0}$, $\boldsymbol{\alpha_1 < 0}$ and $\boldsymbol{\beta_2 > 0}$.

A minimum cable tension keeps cables taut ensuring a minimum overall stiffness of the robot; however, this constraint affects the workspace size, as is shown in Figure 3.24. In specific, a $\boldsymbol{\tau_{min} \geq 25}$ N with an upper unbounded cable tension is selected for the workspace shown below.

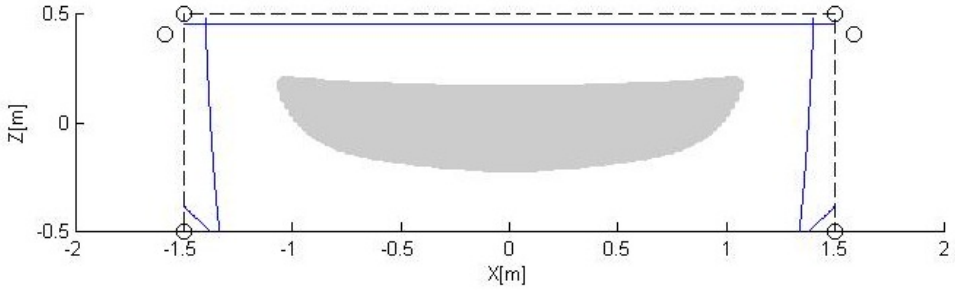

Figure 3.24: Workspaces of the fully-constrained robot for $\boldsymbol{\tau_{min} \geq 25}$ N and $\boldsymbol{\tau_{max}}$ unbounded.

The iterative method based on the minimization of the 2-norm cable tensions results with a workspace reduction of 81.8% of the available workspace.

Chapter 4
Controller development

The control problem is addressed in this chapter. The proposed robot configuration is tested by a control topology so that the positive tensionable condition and optimal cable tensions robot are fulfilled for a given trajectory. The general control scheme and the dynamic model are introduced, followed by a numerical study of the control scheme performance.

4.1 Control system structure

For a pick and place operation, the predominant concern is to make the mobile platform reach a desired target position $\boldsymbol{X}_d$. The control problem is, for the initial position of the mobile platform $\boldsymbol{X}$, to reach the desired position $\boldsymbol{X}_d$. In real applications, the knowledge of the position of the mobile platform can be obtained indirectly by the measurement of the angular position of the robot actuators. In specific, inverse transformations described in equations (3.22) allow to estimate the position of the mobile platform $\boldsymbol{X}_p$ based on the upper cable lengths $\boldsymbol{l}_u = [l_1 \quad l_2]^T$ assuming purely translational motions ($n_T = 2, n_R = 0$) of the mobile platform if conditions (3.16) and (3.17) hold.

Thus, a final transformation of the cable length motion in terms of the actuator motion $\boldsymbol{\theta}, \dot{\boldsymbol{\theta}}$ is required. This transformation involves an analysis of the mechanical transmission between the actuation and reel systems. Specifically, as is shown in Figure 3.8, each upper spool system consists of an electric actuator which shaft is connected to a gear box, which in turn is connected to a timing pulley system to rotate two spool shafts simultaneously (see Figure 3.9).

The cable length between the guide pulleys and the drum l_h is assumed constant as a result of a combined linear and rotational motion of the spool shaft where drums are mounted and fixed, as is shown in Figure 4.1. The combined motion is achieved by manufacturing both lead screw and ball spline grooves in the same shaft. The ball spline nut is constrained to pure rotation motion while the lead screw nut is fixed, such that when the ball spline nut turns, the shaft is forced to rotate and translate a distant established by the pitch of the lead screw mechanism. The guide pulley system (see Figure 4.1), in which a cable is passing through, is composed of four pulleys equally separated around the perimeter of the cable. The proposed guide mechanism reduces cable undesired motions and insures a permanent contact while the cable is collected or released by a drum. Thus, the cable

orientation of the cable between the guide pulleys and the drum can be assumed constant. Note that the above assumption is valid as long as cables have positive tensions.

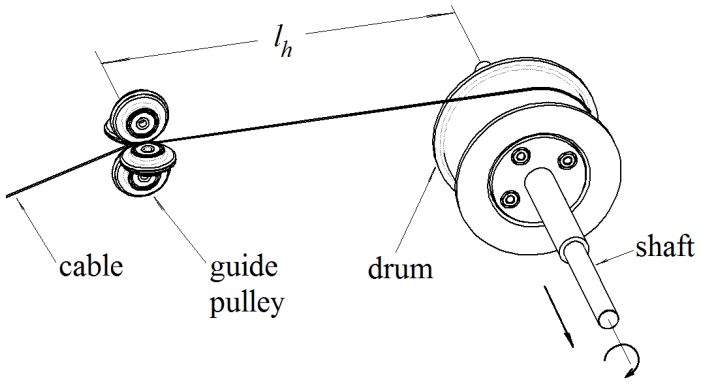

Figure 4.1: Cable displacement between the pulley guides and the drum.

The indirect measurement of the active cable motion is done by optical encoders which measure the relative change of cable lengths. Actual cable lengths are determined by establishing a previous home position of the mobile platform where the initial cable lengths $\boldsymbol{l}_H = [l_{H1} \quad \cdots \quad l_{Hm}]^T$ are known before any experiment can proceed. Then, the cable length vector $\boldsymbol{l}(t) = [l_1 \quad \cdots \quad l_m]^T$ can be related to the angular position of the motor shaft $\boldsymbol{\theta}(t) = [\theta_1 \quad \cdots \quad \theta_m]^T$ with respect to a predetermined home position as follows:

$$\boldsymbol{l}(t) = \boldsymbol{l}_H + \boldsymbol{R}_r\boldsymbol{\theta}(t) \tag{4.1}$$

Note that a negative value of the motor angle means the cable is collected by the drum while its initial cable length is reduced. Conversely, a positive angle produces a rotation in the drum such that the cable is released, increasing its initial cable length. Furthermore, torques as a consequence of the cable tensions can be obtained as follows:

$$\boldsymbol{\tau}_l = \boldsymbol{R}_r\boldsymbol{T}_l \tag{4.2}$$

where the transmission ratio $\boldsymbol{R}_r = [\text{diag}(r_{r1}, \ldots, r_{r4})]$ introduces the gear transmission ratio, the timing pulley transmission ratio, and the radius of the drum for each spool system. The redundancy resolution of the vector of cable tensions $\boldsymbol{\tau}_l$ are calculated by the iterative method described in Chapter 3.

A control formulation for the WCR is shown in Figure 4.2. The control topology follows two objectives, the trajectory tracking motion of the mobile platform and the application of additional forces that give the required constraint (rigidity) to the robot. In this topology, the motion tracking is the main objective and the torque control is a secondary objective. In consequence, the motion tracking is accomplished by means of the position controller block, while the bottom motors apply the forces which constraint the mobile platform based on an optimal torque algorithm block. In other words, the control of the upper motors guarantees the position tracking of the mobile platform, while the bottom actuators administer the torque to ensure a fully-constraint system with a desired stiffness.

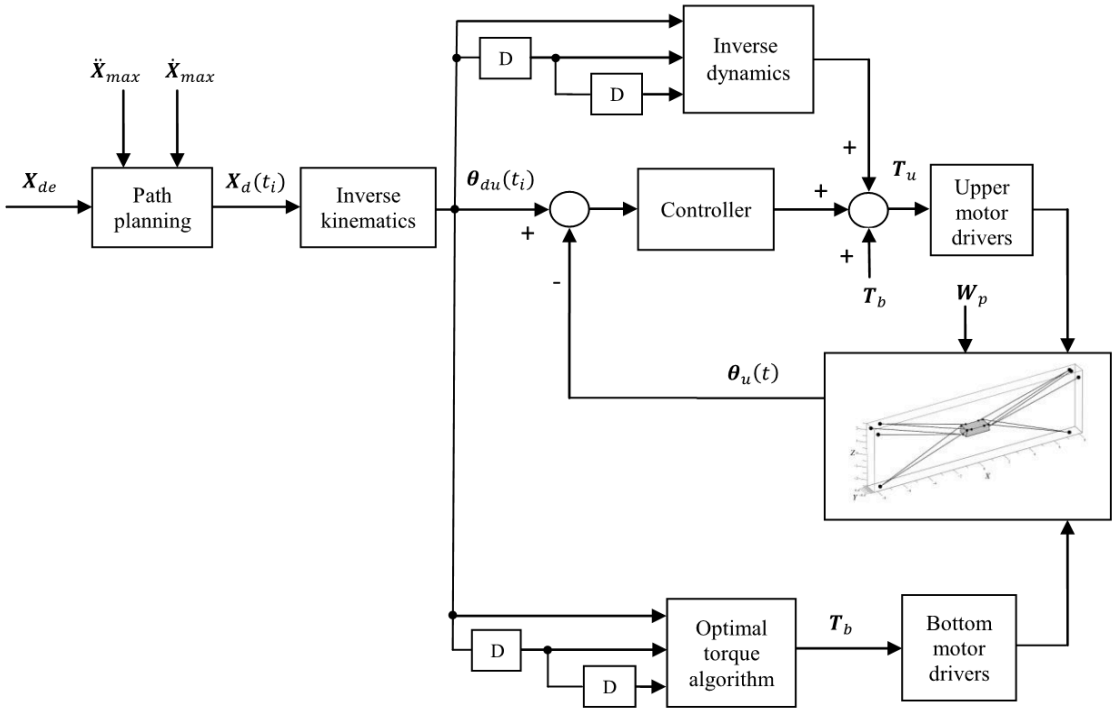

Figure 4.2: Control scheme for the warehousing cable-based robot.

A path planning block generates the trajectory in the work space of the mobile platform based on a desired end position of the mobile platform $\boldsymbol{X}_{de}$. Constraints due to the actuation system are included in the path generator, which can be expressed in terms of the maximum velocity and acceleration of the mobile platform $\dot{\boldsymbol{X}}_{max}$, $\ddot{\boldsymbol{X}}_{max}$, assuming there are not obstacles along the desired path. The output of the path planning is expressed as a sequence of values $\boldsymbol{X}_d(t_i)$ for a

predetermined time interval t_i. The geometrical path for the WCR is developed for warehousing operations such that the mobile platform follows a given set of control points. In this manner, a cubic polynomial is selected such that the first and second derivatives fulfill continuous velocity and acceleration functions.

The sequence of task coordinates $\boldsymbol{X}_d(t_i)$ are transformed into joint coordinates $\boldsymbol{\theta}_{du}(t_i)$ by means of an inverse kinematic block. The desired angular values of the upper motors $\boldsymbol{\theta}_{du}(t_i)$ are compared to the measured angular values of the upper motors $\boldsymbol{\theta}_u(t)$. The angular error is then used by a PID controller block which in turn generates a control torque output. The control torque is compensated with both a torque that comes from the forward dynamics block and the torque due the bottom cables, which result in the commanded torque $\boldsymbol{T}_u$ to drive the upper motors.

Bottom actuators are driven by the torque vector $\boldsymbol{T}_b$ as a result of the optimal torque values from the redundancy cable tension resolution. Dynamic effects of the mobile platform are included in the optimal torque control block such that the resulting cable tensions must balance the mobile platform under dynamic equilibrium.

4.1.1 Dynamics of the mobile platform

The dynamic model of the cable-based robotic system is formulated assuming that the gravitational acceleration is acting along Z axis, cables are massless and straight. Also, the nonlinear effects of friction are ignored to reduce the dynamic equation's complexity. The dynamic model is expressed in Eq. (2.22), and reproduced below for convenience:

$$\boldsymbol{M}_p\,\ddot{\boldsymbol{X}}_p + \boldsymbol{C}_p = \boldsymbol{A}_l\boldsymbol{\tau}_l + \boldsymbol{W}_p \tag{4.3}$$

Equation (4.3) expresses that the dynamic effects, as a consequence of the inertial matrix $\boldsymbol{M}_p$, a vector $\boldsymbol{C}_p$ which includes the gravitational forces assuming pure translational motion of the mobile platform, and an unknown but bounded perturbation wrench $\boldsymbol{W}_p$. The dynamic equilibrium is achieved by the vector force of the cable tensions $\boldsymbol{A}_l\boldsymbol{\tau}_l$. Note that the dynamic equation is valid as long as the cables are always in tension during a prescribed trajectory of the mobile platform $\dot{\boldsymbol{X}}_p, \boldsymbol{X}_p$. The dynamic model is established in terms of the motion of the mobile platform. However, the control topology shown in Figure 4.2 is based on the knowledge of the angular motion of the robot actuators. In consequence, the above dynamic model is reformulated in terms of the actuation

variables by the appropriate transformation equations. Thus, the inverse velocity and acceleration transformation expressed in Eq. (3.15) and Eq. (3.20), respectively, can be rewritten in a forward manner as follows:

$$\frac{d\boldsymbol{X}_p}{dt} = \boldsymbol{J}_u^{-1}\left(\frac{d\boldsymbol{l}_u}{dt}\right) \tag{4.4}$$

$$\frac{d^2\boldsymbol{X}_p}{dt^2} = \boldsymbol{J}_u^{-1}\left(\frac{d^2\boldsymbol{l}_u}{dt^2}\right) - \boldsymbol{J}_u^{-1}\dot{\boldsymbol{J}}_u\left(\frac{d\boldsymbol{X}_p}{dt}\right) \tag{4.5}$$

where

$$\boldsymbol{J}_u = \begin{bmatrix} \dfrac{P_x - \frac{b}{2} + \frac{e}{2}}{l_1} & \dfrac{P_z + c - y_{cp} - \frac{f}{2}}{l_1} \\ \dfrac{P_x + \frac{b}{2} - \frac{e}{2}}{l_2} & \dfrac{P_z + c - y_{cp} - \frac{f}{2}}{l_2} \end{bmatrix}$$

$$\dot{\boldsymbol{J}}_u = \begin{bmatrix} \dfrac{l_1 v_{px} - \dot{l}_{r1}\left(P_x - \frac{b}{2} + \frac{e}{2}\right)}{l_1^2} & \dfrac{l_1 v_{pz} - \dot{l}_{r1}\left(P_z + c - y_{cp} - \frac{f}{2}\right)}{l_1^2} \\ \dfrac{l_2 v_{px} - \dot{l}_{r2}\left(P_x + \frac{b}{2} - \frac{e}{2}\right)}{l_2^2} & \dfrac{l_2 v_{pz} - \dot{l}_{r2}\left(P_z + c - y_{cp} - \frac{f}{2}\right)}{l_2^2} \end{bmatrix}$$

$$\boldsymbol{J}_u^{-1} = \left(\frac{l_1 l_2}{\left(P_x - \frac{b}{2} + \frac{e}{2}\right)\left(P_z + c - y_{cp} - \frac{f}{2}\right) - \left(P_z + c - y_{cp} - \frac{f}{2}\right)\left(P_x + \frac{b}{2} - \frac{e}{2}\right)}\right) \times \begin{bmatrix} \dfrac{\left(P_z + c - y_{cp} - \frac{f}{2}\right)}{l_2} & -\dfrac{\left(P_z + c - y_{cp} - \frac{f}{2}\right)}{l_1} \\ -\dfrac{\left(P_x + \frac{b}{2} - \frac{e}{2}\right)}{l_2} & \dfrac{\left(P_x - \frac{b}{2} + \frac{e}{2}\right)}{l_1} \end{bmatrix}$$

$$\dot{l}_{ri} = \frac{2 l_i \dot{l}_i}{\sqrt{4{l_i}^2 - h^2}} \quad \forall\, i = 1,2$$

Thus, by substituting equations (4.4) and (4.5) into Eq. (4.3), the dynamic model can be expressed in terms of the upper cable motion as

$$\boldsymbol{M}_p\left(\boldsymbol{J}_u^{-1}\ddot{\boldsymbol{l}}_u - \boldsymbol{J}_u^{-1}\,\dot{\boldsymbol{J}}_u\,\boldsymbol{J}_u^{-1}\dot{\boldsymbol{l}}_u\right) + \boldsymbol{C}_p - \boldsymbol{W}_p = \boldsymbol{A}_{lu}\boldsymbol{\tau}_{lu} \tag{4.6}$$

Equation (4.6) states the implicit dynamics of the mobile platform as a function of the upper cable length motion. Finally, Eq. (4.1) and Eq. (4.2) are substituted into Eq. (4.6) to obtain the dynamic model in terms of the angular motion of the upper actuators.

4.2 Simulation results

In this section, the control strategies presented in this chapter are applied to the WCR configuration and evaluated through simulations. A complete description of the proposed robot is presented in detail in Section 3.2, in which the geometric parameters shown in Table 3.3 are adopted in each of the following numerical results. The dynamic parameters of the mobile platform and the actuation system are given in Table 4.1.

Table 4.1: Dynamic parameters for the WCR

Symbol	Description	Value
m_p	Mobile platform mass (Kg)	2.5
I_x	Moment of inertia about axis X (Kg-m^2)	0.057
I_y	Moment of inertia about axis Y (Kg-m^2)	0.029
I_z	Moment of inertia about axis Z (Kg-m^2)	0.030
G_z	Gravitational acceleration (m/s^2)	9.81
r_{ri}	Transmission ratio in motors i = 1 to 3	0.0024
r_{r4}	Transmission ratio in motor 4	0.0016
I_d	Drum inertia (Kg-m^2)	0.0028
I_a	Rotor inertia (Kg-m^2)	2.6×10^{-4}
I_p	Pulley inertia (Kg-m^2)	8.0×10^{-4}
C_v	Viscous friction coefficient (N-m/rad)	0.01
C_s	Dry friction coefficient (N-m)	0.042

A virtual model of the WCR configuration is developed in the Matlab Simulink environment in order to study the performance of the control laws exposed in Section 4.2.

Since the complete architecture of the robot allows the analysis of an underconstrained configuration, two studies are presented in this Section. First, the suspended configuration (see Figure 3.13) is studied such that the analytic boundaries of the feasible workspace are evaluated. Second, the complete control scheme shown in Figure **4.2** is implemented to the fully-constrained configuration. In this control approach an optimal torque is applied to the bottom actuators. The control scheme is tested through simulations in terms of motion tracking and a required stiffness of the mobile platform.

4.2.1 Underconstrained case

As is shown in Figure 3.13, a mobile platform is suspended by eight upper cables and controlled by two independent actuators. Further simulations use a predetermined home position where the initial motion conditions are set to zero. The home position of the mobile platform can be established as a function of the upper cables $\boldsymbol{l}_1$ and $\boldsymbol{l}_2$, as is established in Eq. (3.22). Thus, the home position in terms of the upper cables is established at $\boldsymbol{l}_H = [1.51 \quad 1.54]^T$ m.

4.2.1.1 Controllable workspace

The constraint condition established in Eq. (3.40) defines the region in which the mobile platform of the suspended robot configuration is allowed to move without losing tension in one or more of the upper cables. In consequence, an identification of the all-positive workspace boundaries allows a preliminary evaluation of the robot dynamic model when the mobile platform is approaching to one of these boundaries, as is shown in Figure 4.3.

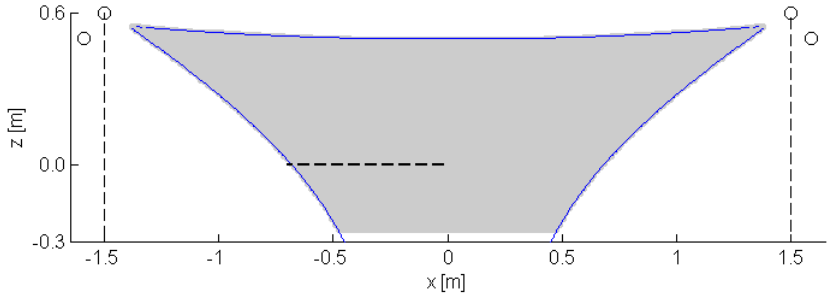

Figure 4.3: Feasible workspace and planned trajectory of the mobile platform.

Curves delimiting the all-positive region are obtained from the formulation established in Section 3.3.1 assuming an absence of perturbations. The target point is defined at $[-0.7 \quad 0.0]^T$ m. A

decentralized PID controller is implemented to regulate the angular position of each upper motor. The PID gains are established as $K_p = 2.5\ \mathbf{1}$, $K_d = 25\ \mathbf{1}$, and $K_i = 0.2\ \mathbf{1}$, where $\mathbf{1} \in \mathbb{R}^{2\times 2}$ is the identity matrix. The position and velocity of the mobile platform are shown in Figure 4.4, in which a discontinuity is observed at the velocity plot when the target position is achieved.

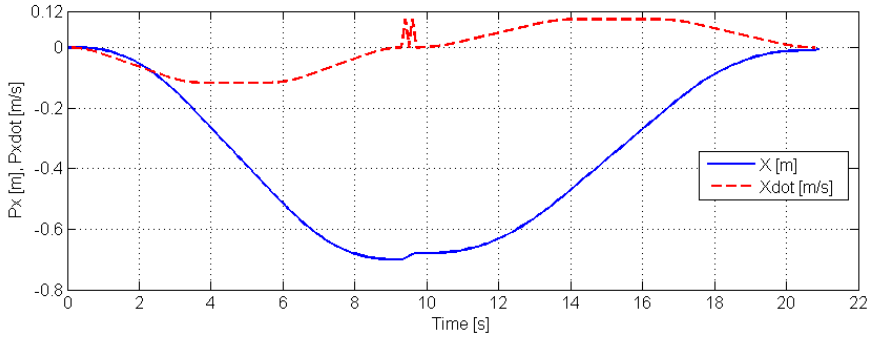

Figure 4.4: Position and velocity of the mobile platform.

Towards the path transition; that is, when the target point is achieved and the returning path is in action, the position of the mobile platform experiences an abruptly change. In effect, when the mobile platform approaches to its left boundary, pair cables 2 and 5 lose tension and only pair cables 1 and 6 are active.

Consider the action of an unknown but bounded perturbation $\boldsymbol{W}_p = [F_{ex} \quad F_{ez} \quad 0]^T$ on the mobile platform, such that $F_{ex} \leq \pm 5$ N, and $F_{ez} \leq \pm 5$ N. Then, analyses of the boundaries of the all-positive workspaces for the worst-case scenarios are depicted in Figure 4.5.

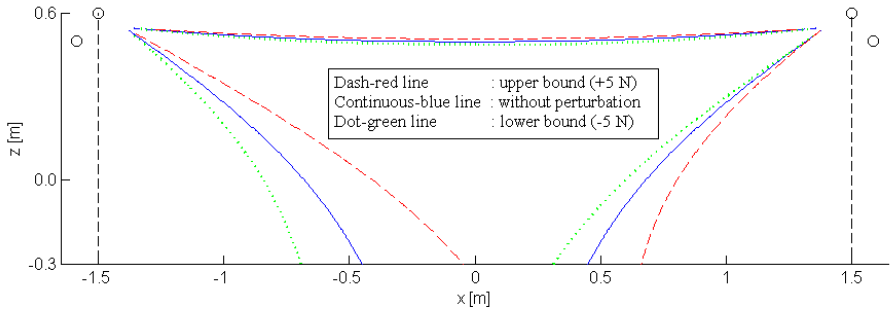

Figure 4.5: All-positive workspace with bounded perturbations.

The all-positive workspace under disturbances (left-dash-red and right-dot-green curves) experiences a reduction with respect to the non-perturbation workspace (continuous-blue curves).

In consequence, any further motion of the mobile platform must be inside the mentioned workspace under disturbances. Although a lower perturbation bound of F_{ez} is established at -5 N, a larger value can benefit the size of the workspace. Conversely, an increment of this disturbance force in the positive sense will shrink the all-positive positions of the mobile platform.

Figure 4.6 depicts the boundaries of the workspaces when the lower bound force of F_{ez} is doubled and the horizontal force is kept constant at $F_{ex} = -5$ N.

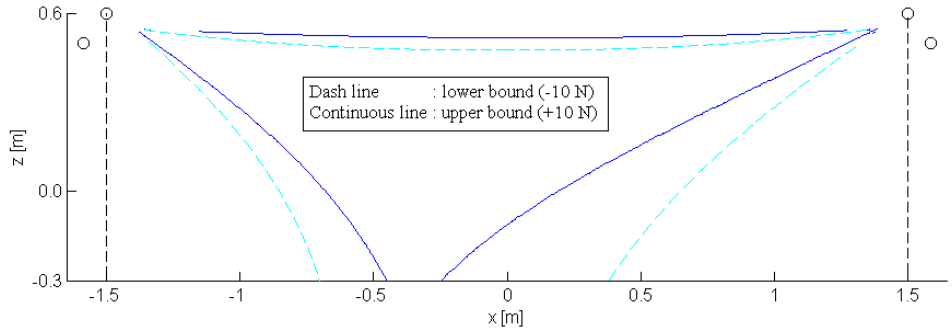

Figure 4.6: All-positive workspaces with a lower bounded of $\boldsymbol{F_{ex} = -5\mathbf{N}}$ and $\boldsymbol{F_{ez} \leq \pm 10\ \mathbf{N}}$.

A larger negative vertical disturbance force (dash curves) has a positive influence in the increment of the wide positions but a reduction of the upper positions of the mobile platform. Finally, an upper force limit can be established as $F_{ez} < |m_g G_z|$ which keep positive cable tensions.

4.2.2 Fully constrained case

In this section, bottom cables are connected to the mobile platform in order to have a fully constrained configuration, as is shown in Figure 3.11. The control strategy shown in Figure 4.2 is implemented to the virtual model developed in Matlab Simulink with the parameters shown in Table 4.1. In consequence, the PID position controller implemented to the upper actuators in the previous section, and the torque calculated in Section 4.2 are studied here. The stiffness matrix has a direct relationship to the amount of tension the upper cables support by the influence of the bottom cables, as is shown in Eq. (3.43). The desired path of the mobile platform is shown in Figure 4.7, in which the

mobile platform is translated from the origin to a target point at $[-0.5 \quad 0.1]^T$ m, and returns again to the origin.

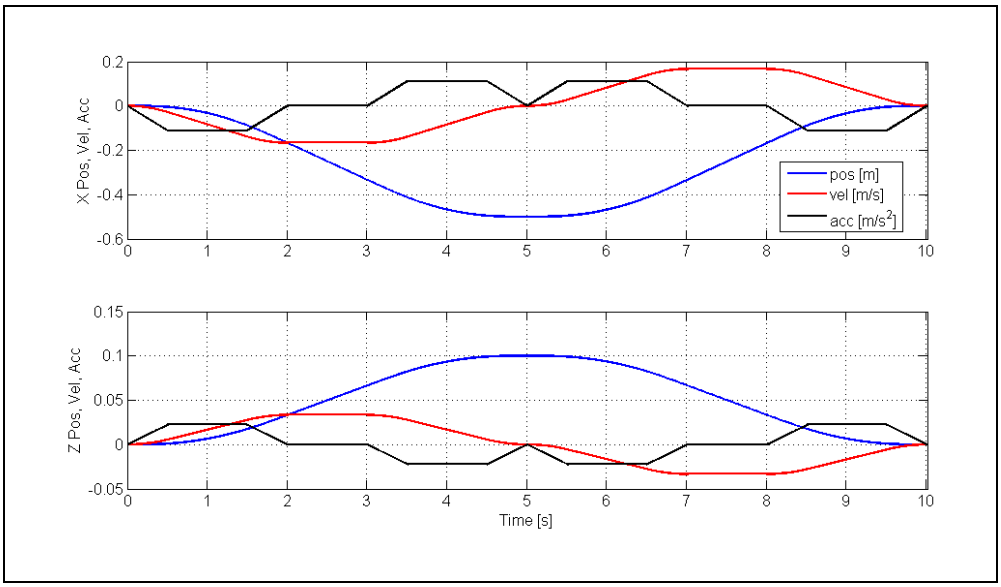

Figure 4.7: Desired path of the mobile platform for a time of 10s.

The maximum velocity and acceleration values are established as 0.17 m/s and 0.113 m/s^2, respectively. The iterative method to solve the cable tension redundancy is implemented for the trajectory, which cable tensions are shown in Figure 4.8.

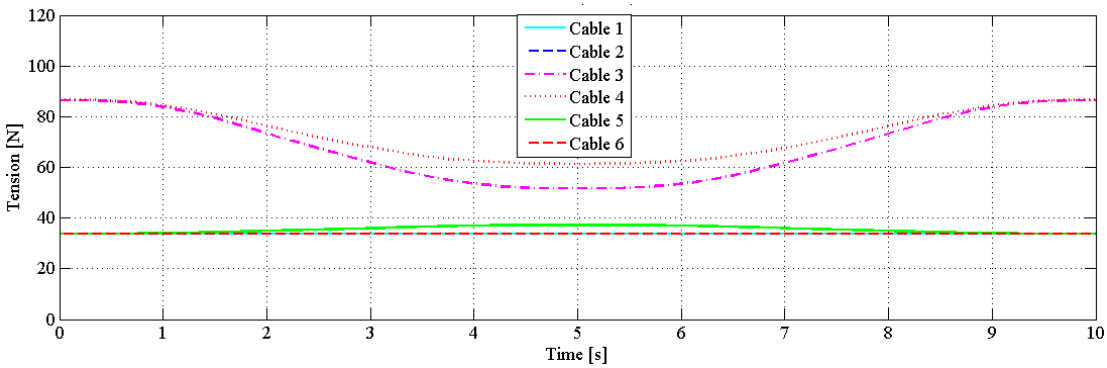

Figure 4.8: Cable tension redundancy resolution for $\boldsymbol{\tau_{min}} = \mathbf{33\ N}$ and $\boldsymbol{\tau_{max}} = \mathbf{220\ N}$.

The cable tensions are bounded to the following cable tensions limits: $\boldsymbol{\tau}_{min} = 33$ N and $\boldsymbol{\tau}_{max} = 220$ N. The 2-norm resolution method causes the cable tensions are close to the minimum tension, resulting to the smallest overall cable tensions. The method requires an analysis of the positions in

which the mobile platform can move with the established tension conditions. Thus, the iterative method described in Section 2.4.1 is used to depict the feasible workspaces in which the proposed trajectory (see Figure 4.7) is defined.

Figure 4.9 shows the feasible workspace when a wrench perturbation $\boldsymbol{W}_p = [50 \quad -50 \quad 0]^T$N is applied to the mobile platform.

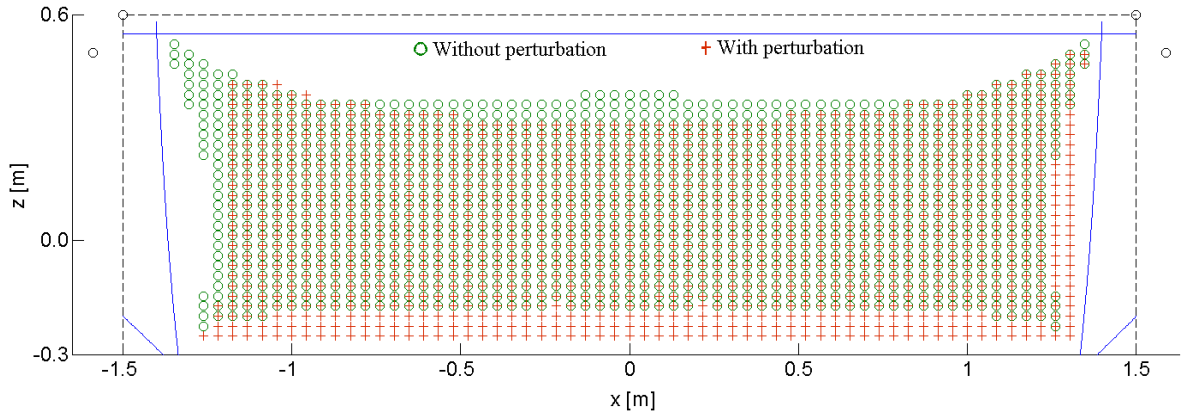

Figure 4.9: Feasible workspaces for $\tau_{min} = 33$ N and $\tau_{max} = 220$ N with/without a wrench perturbation $\boldsymbol{W}_p = [50 \quad -50 \quad 0]^T$N.

This wrench represents the worst-case scenario when the mobile platform is moving from its home position towards its target point at $[-0.5 \quad 0.1]^T$ m. The workspace contains the desired motion of the mobile platform shown in Figure 4.7. These results allow the experimental study of the proposed control topology shown in Figure **4.2**.

For a high-speed simulation, consider the same above trajectory in which the mobile platform is moving from its home position to $[-0.5 \quad 0.1]^T$ m, and then returning to its origin with a maximum velocity of 2.85 m/s as is shown in Figure 4.10. A maximum acceleration of the mobile platform is established at 31.685 m/s^2, with a time of the trajectory of 0.6 s.

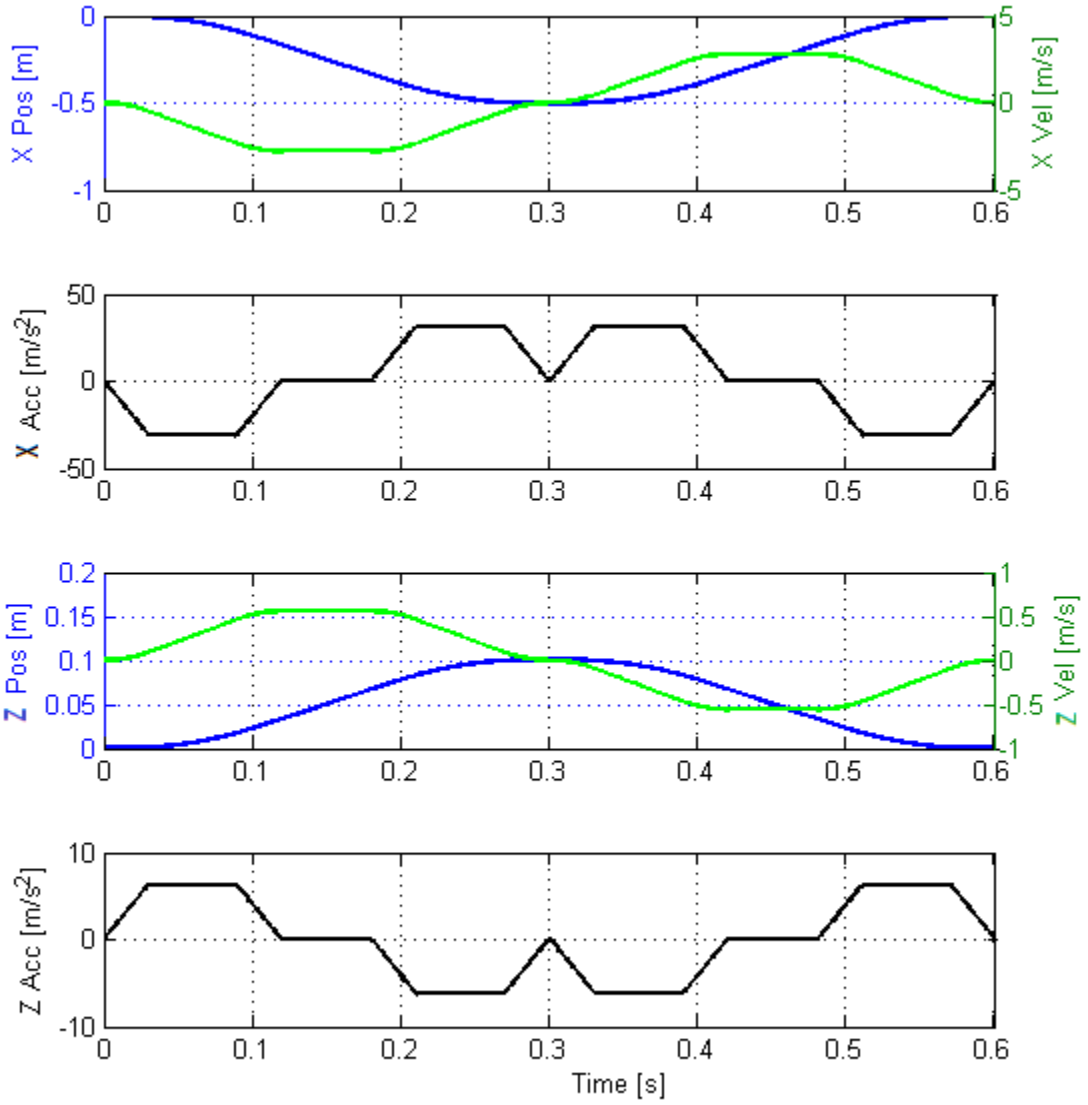

Figure 4.10: Desired path of the mobile platform for a time of 0.6s.

Values of the cable tensions during the trajectory are obtained with the proposed iterative method and shown in Figure 4.11. Cable tension limits are established at $\boldsymbol{\tau}_{min} = 330$ N and $\boldsymbol{\tau}_{max} = 1200$ N which allow to deal with the acceleration requirements.

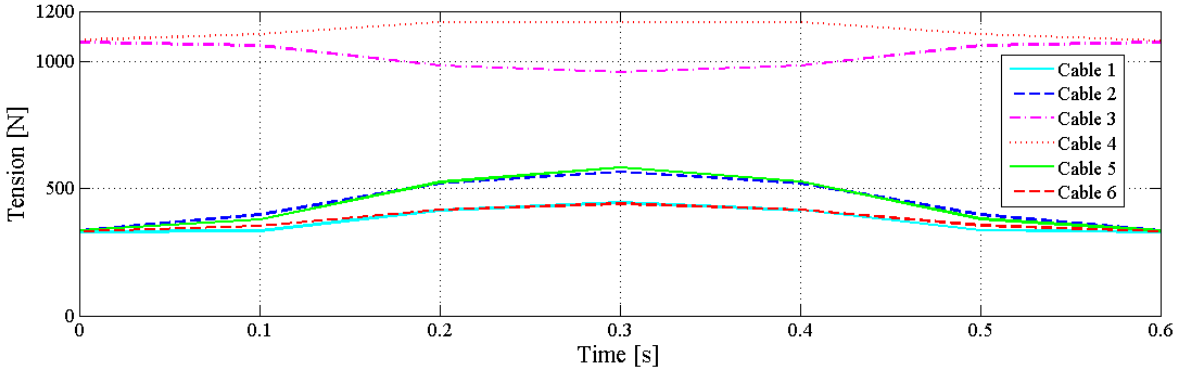

Figure 4.11: Cable tension redundancy resolution for $\boldsymbol{\tau_{min} = 330\ \mathbf{N}}$ and $\boldsymbol{\tau_{max} = 1200\ \mathbf{N}}$.

Bottom pair cables 3, 9 and 4, 10 present the maximum cable tension values. These results give information about the maximum torque capacity of the actuation system. Finally, the position errors of the mobile platform are shown in Figure 4.12.

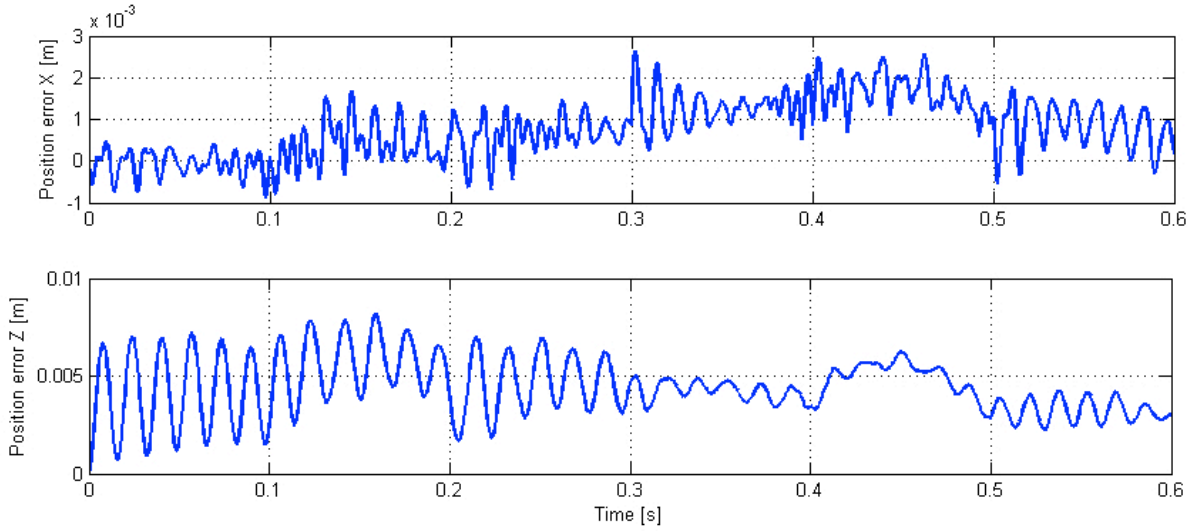

Figure 4.12: Position errors of the mobile platform.

The maximum position error is observed along the Z direction with a peak of 0.008 m and a constant error at the end of the trajectory of 0.003 m. In other hand, the maximum error along the X axis is achieved when the mobile platform reaches its target point.

Chapter 5
Experimental studies

In this chapter, experimental results are obtained so that the proposed configuration design is evaluated. First, the structure of the proposed robotic system is presented for experimental studies. Secondly, the control formulation presented in the previous chapter is implemented and tested for a given trajectory of the mobile platform. Experimental limitations make the necessity to rely on estimates for some data such as the position of the mobile platform and the force applied to the mobile platform. The potential sources of limitations to the experimental studies are mentioned below.

1) A lack of direct sensors to measure the actual position and orientation of the mobile platform, such as laser or camera instruments. In this study, the planar position of the mobile platform is estimated by multiplying the observed change of the upper cable lengths by a direct transformation factor. While encoders can measure the angle of rotation of the drums which indirectly measure the change of the cable lengths, it is not possible to record the actual pose of the mobile platform due to change in the cable routing geometry and also momentarily slackness in the cables. Thus, indirect measurement of the mobile platform limits the accuracy of the experimental results.

2) The constrained forces applied to the mobile platform are estimated based on the torque values supplied by the bottom motors. In other words, the lack of force sensors, such as load cells and strain gauges, do not allow an accurate measurement of the forces applied to the mobile platform by the bottom cables.

3) The architecture of the controller used to drive the motors limits the implementation of custom applications for non-standard robotic systems. The controller is based on a distributed control architecture implemented over Ethernet, which requires of the proper software routines for controlling in Cartesian coordinates (kinematics modules with license) from a built-in library of robot geometries. Kinematic modules, included in the built-in library, are equipped with features that promote the real-time path generation of the controller. In other hand, a robot with unusual kinematic requires the development of an application in the controller software environment that may slow down the robot communication and alter the real-time capabilities of the controller such as execution of subroutines and collection of data values.

The above experimental limitations are related to the measuring instrument and their calibration limits. Thus, these limitations exist and produce unlikely notable errors in some aspects of the obtained results, such that the accuracy must rely on the estimation of some data.

5.1 Experimental setup design

The overall workspace of the proposed prototype is 3 m by 1.5 m by 0.5 m. Three servomotors Tamagawa model TS4813 (motors 1 to 3) and one servomotor Kollmorgen model Emerson DXM-340C (motor 4) are installed in the prototype as is shown in Figure 5.1a. The end-effector, shown in Figure 5.1b, is connected to each cable by a system of a ball-socket joint and a cable tensioner which allow the angular motion of the anchor points and the appropriate tension adjustments previous a motion test.

(a)

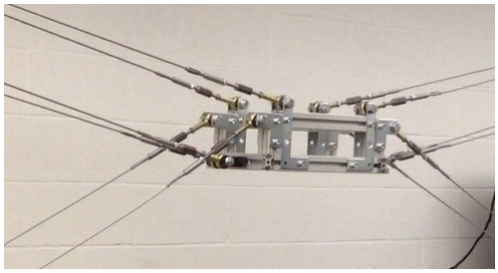

(b)

Figure 5.1: Robot prototype: (a) general structure and (b) the mobile platform.

The Guidance Controller G2420C is used to drive the motors in both position and torque operation modes. Programming codes are written in the Guidance Programming Language (GPL) provided by Precise Automation. The industrial controller comes with a PID formulation to control up to twelve multi-axes robots.

A directly communication to the controller through a computer's Ethernet port is selected. The computer uses a processor Intel(R) Core(TM) i7-2670QM CPU at 2.20 GHz. The PC has an installed memory RAM of 6 GB operating on Windows 7.

Using this prototype, experiments are performed so that the mobile platform follows a desired trajectory within the feasible workspace. The measured position errors of the mobile platform are indirectly obtained by means of the top motor encoders; specifically, absolute optical encoders of 17bit (131,072 divisions).

5.2 Experimental results

Two set of experiments are developed to evaluate the position and torque motion controllers. Position motion experiments are implemented in the underconstrained configuration robotic system; that is, when bottom cables are not connected to the mobile platform. One of the boundaries of the feasible workspace is achieved by horizontally moving the end-effector from its predetermined home position to an extreme point and compared to the theoretical results obtained in Chapter 3. Then, a more complex trajectory is tested to evaluate the tracking error of the position motion control.

The second set of experiments is used to evaluate the fully constrained robot configuration. The end-effector is moved from its home position to follow a desired trajectory. The following experimental results are based on the geometric parameters of the prototype shown in Table 3.2. The mass of the mobile platform is measured at 2.5 Kg.

During experimentation, a friction compensation term is added to the theoretical torque values in order to ensure a good tracking of the mobile platform while cables forces are generated. The friction compensation term comes primarily from the dry friction in the spool systems of the WCR prototype.

5.2.1 Underconstrained case

A proportional derivative integrative (PID) control scheme is used to control the angular motion of the top actuators. The trajectory shown in Chapter 4, Figure **4.3**, is analyzed experimentally. The mobile platform is translated horizontally from the origin to a target point located to its left 0.7 m. and

then comes back to its home position. The indirect measurements of the position and velocity of the mobile platform along X axis are shown in Figure 5.2.

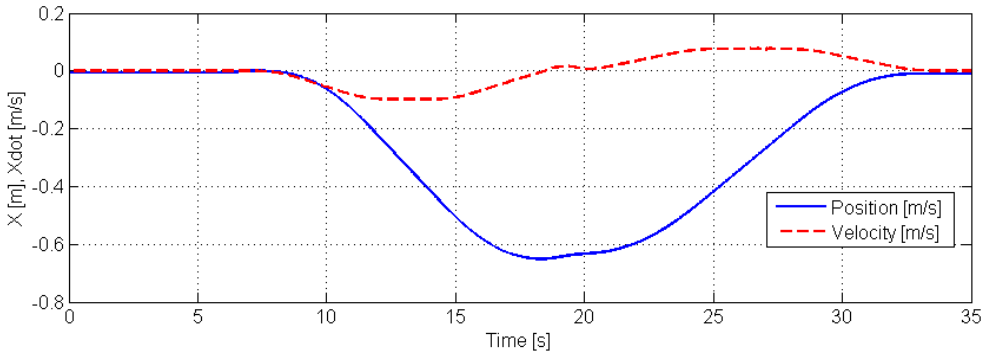

Figure 5.2: The mobile platform position and velocity along X axis.

When the mobile platform is approaching to the target point, the center of mass of the mobile platform is approaching to the boundaries of the controllable workspace. Experimental results in the boundaries of the controllable workspace are similar to the simulated results shown in Chapter 4, Figure 4.4.

The desired position and velocity of the mobile platform is off course when the mobile platform is approximating to the target point. The indirect measurements of position and velocity of the mobile platform expose the consequence of losing position control when the moving platform is translating towards a point outside the feasible workspace; that is, when one or more cables are losing tension.

Next, the experimental results for the trajectory shown in Figure 5.3, are analyzed. PID control gains are established as $\boldsymbol{K}_p = [\text{diag}(3.5,3.5)]$, $\boldsymbol{K}_d = [\text{diag}(20.0,20.0)]$, and $\boldsymbol{K}_i = [\text{diag}(0.3,0.3)]$. The trajectory of the mobile platform is contained inside of the all-positive workspace depicted in Figure **4.5**, in which a bounded perturbation of ± 5 N is acting along the vertical and horizontal axes in the mobile platform. Thus the target point at 0.7 m is determined for the worst case scenario depicted for the dot-green line in Figure 4.5 when a perturbation is established as $\boldsymbol{W}_p = [-5 \quad -5 \quad 0]^T$ N.

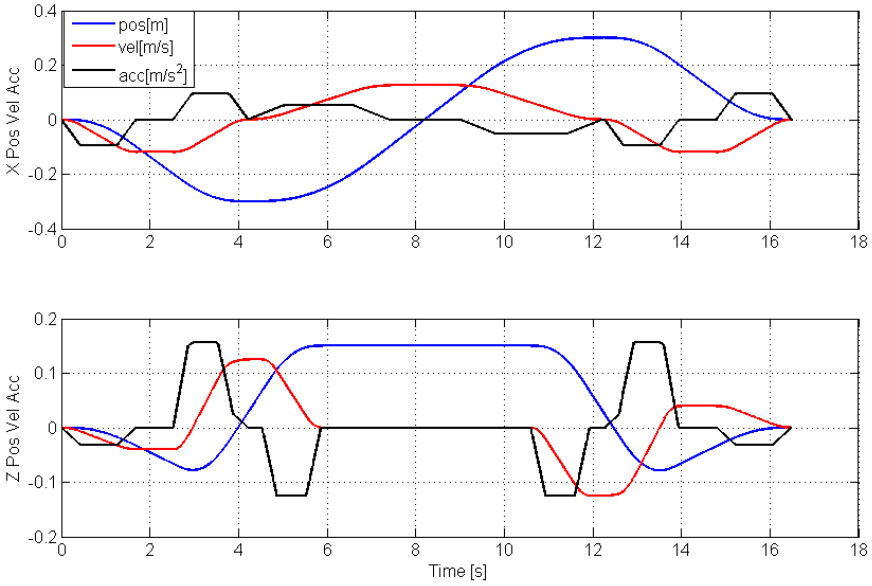

Figure 5.3: Desired path of the mobile platform for the suspended case.

The top motor angular positions are shown in Figure 5.4. The maximum angular errors for motor 1 are 0.012 deg. and 0.015 deg. at 12.49 s. and 22.11 s., respectively. Maximum angular errors for motor 2 are found at 9.82 s and 19.45 s. with values of 0.035 deg. and 0.052 deg., respectively. The maximum angular position errors in both top motors are related to peak angular values. In other words, angular errors are associated to maximum and minimum cable lengths.

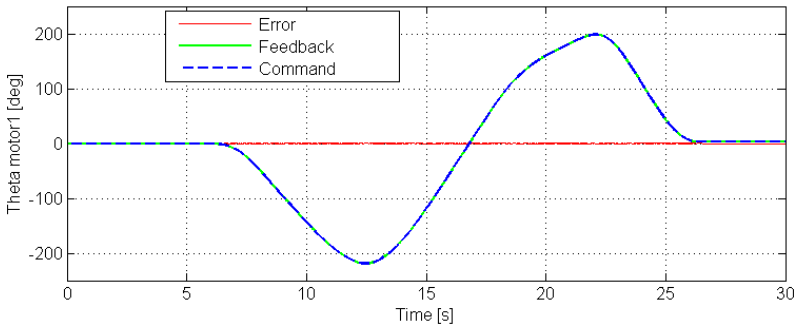

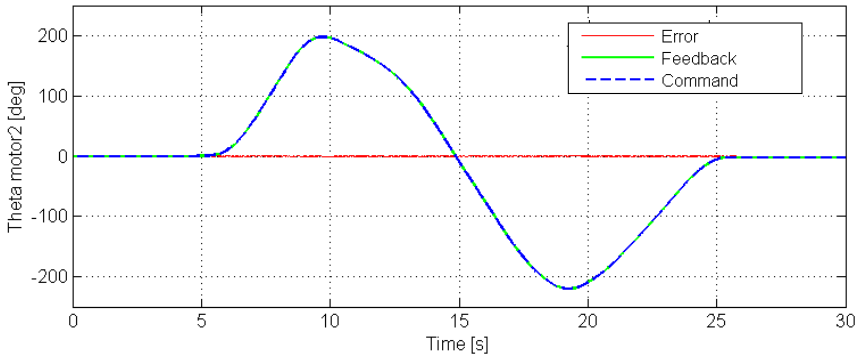

Figure 5.4: Angular position tracking control of top motors.

The top motors angular velocities are shown in Figure 5.5. Abrupt changes of mobile platform in the angular velocity profile result in maximum error values in both top motors. The maximum peak error values are 1.94 deg/s and 1.76 deg/s for motors 1 and 2, respectively.

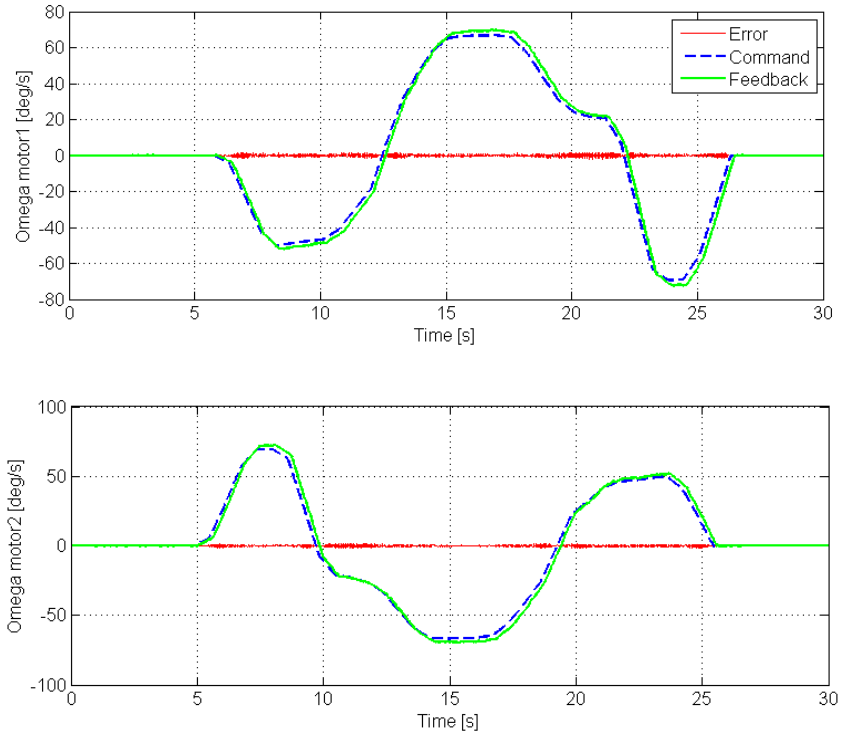

Figure 5.5: Angular velocity tracking control of top motors.

An indirect measurement of the mobile platform is shown in Figure 5.6. The position tracking performance of the mobile platform is obtained based on the actual angular values of the top motors and the direct kinematic formulation.

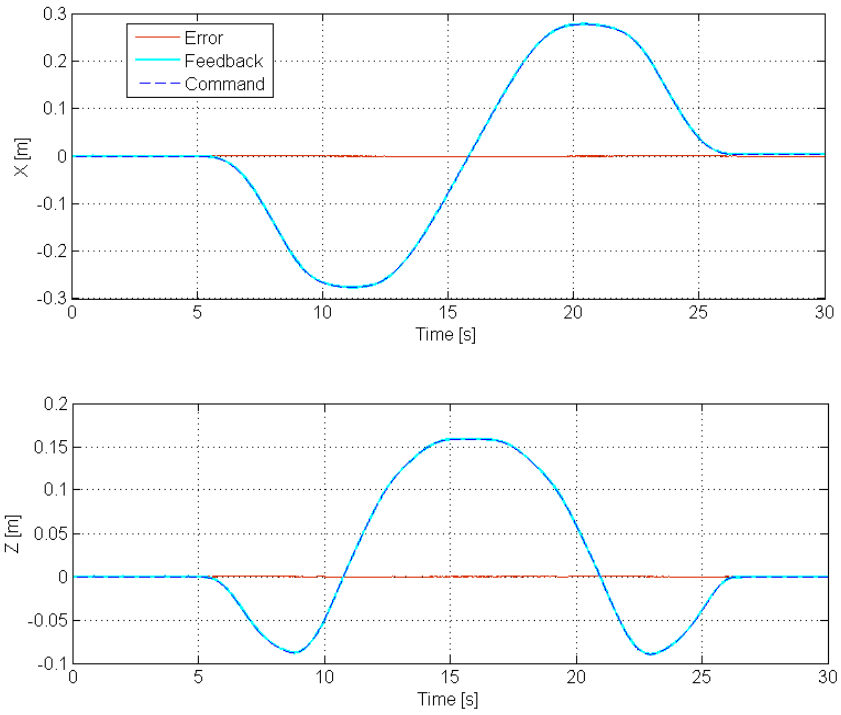

Figure 5.6: Indirect measurement of the position of the mobile platform.

It is observed a good tracking of the position of the mobile platform; that is, the position error is close to zero with peak error values of 4.2×10^{-5} and 1×10^{-4} along axes X and Z, respectively.

Experimental results have shown a good performance of the PID scheme to control the position of the suspended robot configuration.

5.2.2 Fully constrained case

The fully constrained robot configuration shown in Figure 5.1 is experimentally evaluated in this subsection. As is shown in Figure 4.2, the proposed control strategy for the fully constrained robot consists of a control formulation to achieve the desired position of the top actuators while the bottom actuators are controlled to produce a calculated torque. In specific, the PID position control scheme

analyzed in the suspended configuration is combined with a commanded torque calculated with an optimal algorithm.

The input torque to the bottom actuators require the offline cable tension redundancy resolution. The method developed in Chapter 3, to solve the cable tension redundancy, is implemented offline and implemented to the control formulation. The iterative method is based on the minimization of the two-norm of the cable tensions.

The desired trajectory of the mobile platform shown in Figure 4.7 is considered in the following experiments. The total time of the path motion is approximately 10.6 seconds, which the mobile platform is translated from the origin to the target point $[-0.5 \quad 0.1]^T$ m, and then returning to the home position. Gains matrices for the PID position control are the same as established in section 5.2.1. Measured torque values applied to bottom motors during the mobile platform path are shown in Figure 5.7.

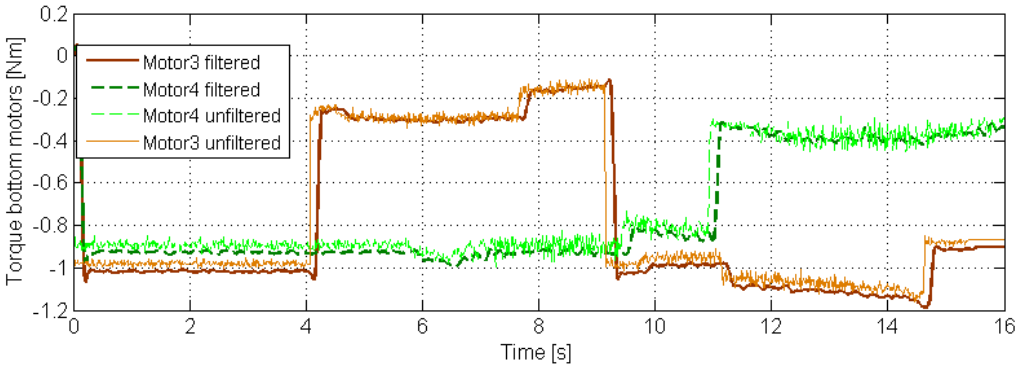

Figure 5.7: Bottom torque motors.

A low-pass filter is applied to the torque signals in order to reduce the noise in the measured signals. The limits of the bottom motors torque values are -0.1 and -1.2 Nm.

The bottom motors present negative torque values along the mobile platform path. During the first part of the trajectory, motor 4 generates a uniform torque of -0.9 Nm, while motor 3 produces a torque of -0.2 Nm. When the mobile platform is returning to its home position, motor 3 torque increases its torque value to a maximum value of -1.2 Nm, while motor 4 reduces its torque value to -0.4 Nm.

An indirect measurement of the mobile platform position based on the angular values of the top motors is shown in Figure 5.8.

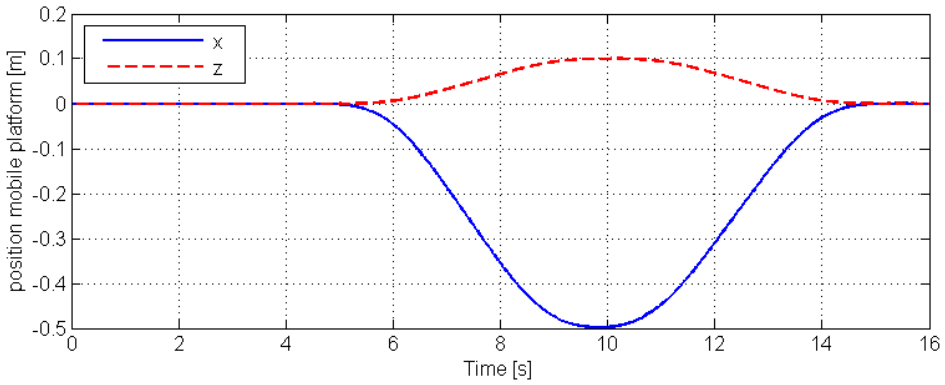

Figure 5.8: Indirect measurement of the position of the mobile platform.

In general a good position tracking is observed along the desired trajectory. However, friction in the pulley system represents one of the most important sources of errors. As a result of this nonlinear behaviour, gain parameters for different trajectories must be tuned experimentally.

5.3 Review of results

The control strategy shown in Figure **4.2** is tested in the WCR prototype which geometrical and dynamics parameters are described in Table 3.3 and Table 4.1, respectively. The control topology follows two objectives, in which position tracking is the main objective and the torque control is a secondary objective.

A PID control law is selected for the position control and implemented to the upper motors, while a commanded torque is generated to control the bottom motors. A cable tension redundancy resolution, based on an iterative method, is included in the torque generation. The iterative method solves the tension distribution by the minimization of the 2-norm cable tension vector. This method provides with a unique cable tension vector solution that is constrained to a given minimum and maximum cable tensions. In practice, selection of the cable tension limits is based on the actuation limitations and cable properties. These tension limits have an influence in the size and shape of the feasible workspace.

The goal of the study is to evaluate the performance of proposed control formulation by means of the indirect measurement of the end effector motion errors when a desired pick and place trajectory is implemented to the WCR prototype. The desired trajectory is shown in Figure 4.7, and is contained into the feasible workspace assuming a perturbation vector of $\boldsymbol{W}_p = [50 \quad -50 \quad 0]^T$ N, and cable tension limits of $\tau_{min} = 33$ N and $\tau_{max} = 220$ N.

In general, experimental results show that the proposed control topology offers a good solution for a redundant cable robot, in which the motion and force requirements are passively regulated. In addition, the proposed iterative redundancy method shows to be an alternative for testing these types of robots.

Chapter 6
Conclusions

In this Thesis the design and control of a novel fully constrained cable-based robot with large workspaces and high stiffness poses were presented. The versatile architecture of the proposed robotic system allowed the analysis of an underconstrained cable robot configuration. Furthermore, design and control theoretical formulations were presented and analyzed by means of numerical simulations. Finally, a prototype, the so-called WCR, was built and used to evaluate the operation and performance of the robot. Experimental results revealed that the proposed robotic system was viable for warehousing applications.

The design problem was divided in two main stages. First, the feasible workspace was optimized for a maximum size and rectangular-type shape of each of the redundant planar architectures. A set of four parameters was selected to fully define the geometry of the mobile platform and the location of its anchor points. In the second design stage, an optimized spatial architecture was obtained for a maximum stiffness by selecting a new set of six parameters that defined the transversal anchor points on both the mobile and static platforms. The simulation results indicated that the maximum size of the workspace could be established by using a planar model, which simplified the number of design parameters. Geometrical parameters of the mobile platform, such as the length and height, could be used to define the size of the planar feasible workspace. On the other hand, the variation of the anchor points, bounded by the optimal geometrical parameters of the mobile platform, allowed to enhance the overall stiffness with a minimum reduction of the size of the workspace.

Once the general architecture of the fully constrained is established, the mechanical modelling and the workspace description of the WCR were addressed. The arrangement of the twelve cables of the proposed robot admitted planar translational motions of the mobile platform for warehousing applications. The feasible workspaces of the suspended and fully constrained cases were described and depicted based on a 2-norm solution. The iterative method was obtained by minimizing the 2-norm of the cable tension. The stiffness attribute was evaluated by means of the minimum fundamental natural frequency. The analysis results showed that the fully constrained system was capable of accomplishing the warehousing requirements of large workspace, high stiffness and low force input.

The WCR control objective was established as follows: generate the motor torque values such that the cable lengths (position control) and the cable tension (force control) were appropriately adjusted for a desired trajectory of the mobile platform which was subjected to unknown but bounded static disturbances. A control topology was proposed in which a PID position control is applied to the upper motors, while an optimal algorithm calculates the torque values to be applied to the bottom motors. The optimal torque block included the cable tension redundancy resolution for a prescribed trajectory. Further simulation results indicated that the proposed control architecture was feasible to be implemented to the WCR.

A prototype of the WCR was manufactured and used to evaluate the performance of the overall robotic system. Experiments were divided into two stages. First, the underconstrained robot configuration was tested by using the PID position control scheme such that the boundaries of the feasible workspace were experimentally detected and compared to the theoretical results. Second, the WCR control topology was implemented to the fully constrained robot. The presented controller topology was experimentally evaluated for a predefined linear trajectory. Performance comparison of the proposed control laws was done by the indirect measurements of the position of the mobile platform. Experimental results supported theoretical formulations and indicated that the proposed control topology was a feasible solution for pick and place applications.

In summary the Thesis contributions are listed below:

1) The design of a novel low mobility cable-based for warehousing applications. The challenge lies in the addition of constraints that eliminate the no desired motions ensuring accuracy and stability of the remaining motions, [137].

2) The analytical solution for the description of the force-closure and feasible workspace of the suspended robot case, and the analytical equations of the force-closure workspace of the fully constrained case [138]. In both cases the minimum two-norm cable tension is used to find a unique solution to the cable tensions.

3) A prototype was developed in order to conduct a series experiments to validate the theoretical results. A proper PID control scheme was used to achieve positive cable tensions with a desired stiffness.

6.1 Future Work

Subsequence topics to continue this work may be focus on improvement the performance of the control robotic system. It is suggested a study related to the implementation and testing of direct sensors that measure the actual position and orientation of the mobile platform. Thus, a more reliable measurement of the mobile platform poses would allow monitoring the effects of momentary slackness in cables and bounded disturbances. Hardware issues related to the architecture of the controller need to be addressed such that the control system can be customized and upgraded as needed.

Next steps should be conducted towards the development of control strategies that reduce the mobile platform vibrations. In specific, a study in passive and active methods to minimize the undesired motions out of the plane of the mobile platform.

Bibliography

[1] Angeles, J., 2003, "Fundamentals of robotic mechanical systems, theory, methods, and algorithms," Springer, New York, .

[2] Merlet, J., 2010, "MARIONET, a Family of Modular Wire-Driven Parallel Robots," ARK, Piran, pp. 53-62.

[3] Oh, S., and Agrawal, S. K., 2005, "Cable Suspended Planar Robots with Redundant Cables: Controllers with Positive Tensions," IEEE Transactions on Robotics, **21**(3) pp. 457-465.

[4] Miermeister, P., Pott, A., and Verl, A., 2010, "Dynamic Modeling and Hardware-in-the-Loop Simulation for the Cable-Driven Parallel Robot IPAnema," Robotics (ISR), 2010 41st International Symposium on and 2010 6th German Conference on Robotics (ROBOTIK), pp. 1-8.

[5] Ebert-Uphoff, I., and Voglewede, P. A., 2004, "On the connections between cable-driven robots, parallel manipulators and grasping," Robotics and Automation, 2004. Proceedings. ICRA '04. 2004 IEEE International Conference on, Anonymous **5,** pp. 4521-4526 Vol.5.

[6] Behzadipour, S., 2005, "Ultra-High-Speed Cable-Based Robots," Ph.D. Thesis, .

[7] Hayward, V., 1989, "A translation in artificial terms of the design of biological manipulators," Engineering in Medicine and Biology Society, 1989. Images of the Twenty-First Century., Proceedings of the Annual International Conference of the IEEE Engineering in, Anonymous pp. 898-899 vol.3.

[8] Gough, V. E., and Whitehall, S. G., 1962, "Universal tyre test machine," Proceedings of the 9th FISITA -- International Automobile Technical Congress, Anonymous pp. 117-137.

[9] Stewart, D., 1965, "Platform with Six Degrees of Freedom," Institution of Mechanical Engineers -- Proceedings, **180**(15) pp. 371-386.

[10] Clavel, R., 1988, "DELTA, a fast robot with parallel geometry," Proceedings of the 18th International Symposium on Industrial Robots, Anonymous IFS Publications, Kempston, Bedford, UK, pp. 91-100.

[11] Merlet, J., and Gosselin, C., 2008, "Parallel Mechanisms and Robots," pp. 269-285.

[12] Okada, T., 1979, "Object-Handling System for Manual Industry," Systems, Man and Cybernetics, IEEE Transactions on, **9**(2) pp. 79-89.

[13] Nguyen, V., 1986, "Constructing force-closure grasps," Robotics and Automation. Proceedings. 1986 IEEE International Conference on, Anonymous **3,** pp. 1368-1373.

[14] Nguyen, V., 1987, "Constructing force-closure grasps in 3D," Robotics and Automation. Proceedings. 1987 IEEE International Conference on, Anonymous **4,** pp. 240-245.

[15] Kawamura, S., Kino, H., and Won, C., 2000, "High-Speed Manipulation by using Parallel Wire-Driven Robots," Robotica, **18**(1) pp. 13-21.

[16] Pfeiffer, F., 1998, "Robots with Unilateral Constraints," Annual Reviews in Control, **22**pp. 121-132.

[17] Han, L., Trinkle, J. C., and Li, Z. X., 2000, "Grasp Analysis as Linear Matrix Inequality Problems," Robotics and Automation, IEEE Transactions on, **16**(6) pp. 663-674.

[18] Andrade-Cetto, J., and Thomas, F., 2008, "A Wire-Based Active Tracker," IEEE Transactions on Robotics, **24**(3) pp. 642-651.

[19] Thomas, F., Ottaviano, E., Ros, L., 2003, "Coordinate-free formulation of a 3-2-1 wire-based tracking device using Cayley-Menger determinants," Robotics and Automation, 2003. Proceedings. ICRA '03. IEEE International Conference on, Anonymous **1,** pp. 355-361 vol.1.

[20] Takemura, F., Enomoto, M., Tanaka, T., 2005, "Development of the balloon-cable driven robot for information collection from sky and proposal of the search strategy at a major disaster," Advanced Intelligent Mechatronics. Proceedings, 2005 IEEE/ASME International Conference on, Anonymous pp. 658-663.

[21] Jordan, B. L., Batalin, M. A., and Kaiser, W. J., 2007, "NIMS RD: A Rapidly Deployable Cable Based Robot," Proceedings 2007 IEEE International Conference on Robotics and Automation, **2007**pp. 144-150.

[22] Takemura, F., Maeda, K., and Tadokoro, S., 2006, "Attitude stability of a cable driven balloon robot," IEEE International Conference on Intelligent Robots and Systems, Anonymous pp. 3504-3509.

[23] Brown, G. W., 1987, "Suspension System for Supporting and Conveying Equipment, such as a Camera," UNITED STATES PATENT AND TRADEMARK OFFICE GRANTED PATENT, (US4710819) .

[24] Bouchard, S., and Gosselin, C. M., 2006, "Kinematic Sensitivity of a very Large Cable-Driven Parallel Mechanism," ASME Conference Proceedings, **2006**(42568) pp. 851-858.

[25] Takemura, F., Enomoto, M., Denou, K., 2004, "Proposition of a human body searching strategy using a cable-driven robot at major disaster," 2004 IEEE/RSJ International Conference on Intelligent Robots and Systems (IROS), Anonymous **2,** pp. 1456-1461.

[26] Gosselin, C. M., and Bouchard, S., 2010, "A Gravity-Powered Mechanism for Extending the Workspace of a Cable-Driven
Parallel Mechanism: Application to the Appearance Modelling of Objects," International Journal of Automation Technology, **4**(4) pp. 372-379.

[27] Duan, B. Y., Qiu, Y. Y., Zhang, F. S., 2009, "On Design and Experiment of the Feed Cable-Suspended Structure for Super Antenna," Mechatronics, **19**(4) pp. 503-509.

[28] Yao, R., Tang, X., Wang, J., 2010, "Dimensional Optimization Design of the Four-Cable-Driven Parallel Manipulator in FAST," IEEE/ASME Transactions on Mechatronics, **15**(6) pp. 932-941.

[29] Mustafa, S. K., Yang, G., Yeo, S. H., 2007, "Self-calibration of a biologically-inspired cable-driven robotic arm," Advanced intelligent mechatronics, 2007 IEEE/ASME international conference on, Anonymous pp. 1-6.

[30] Truong, H., Abdallah, S., Rougeaux, S., 2000, "A Novel Mechanism for Stereo Active Vision," Proceeding of Australian Conference on Robotics Automation ACRA, ARAA, .

[31] Truong, S., Kieffer, J., and Zelinsky, A., 1999, "A Cable-Driven Pan-Tilt Mechanism for Active Vision," In Proc. Australian Conference on Robotics and Automation, pp. 172-177.

[32] Su, H., Dickstein-Fischer, L., Harrington, K., 2010, "Cable-driven elastic parallel humanoid head with face tracking for Autism Spectrum Disorder interventions," Engineering in Medicine and Biology Society (EMBC), 2010 Annual International Conference of the IEEE, Anonymous pp. 467-470.

[33] Mustafa, S. K., Yang, G., Yeo, S. H., 2008, "Kinematic calibration of a 7-DOF self-calibrated modular cable-driven robotic arm," Robotics and Automation, 2008. ICRA 2008. IEEE International Conference on, Anonymous pp. 1288-1293.

[34] Mustafa, S. K., Yang, G., Yeo, S. H., 2006, "Development of a Bio-Inspired Wrist Prosthesis," Robotics, Automation and Mechatronics, 2006 IEEE Conference on, Anonymous pp. 1-6.

[35] Rosati, G., Zanotto, D., Secoli, R., 2009, "Design and Control of Two Planar Cable-Driven Robots for Upper-Limb Neurorehabilitation," 2009 IEEE International Conference on Rehabilitation Robotics, pp. 560-565.

[36] Homma, K., Fukuda, O., Sugawara, J., 2003, "A wire-driven leg rehabilitation system: development of a 4-DOF experimental system," Advanced Intelligent Mechatronics, 2003. AIM 2003. Proceedings. 2003 IEEE/ASME International Conference on, Anonymous **2,** pp. 908-913 vol.2.

[37] Rosati, G., Zanotto, D., and Agrawal, S. K., 2011, "On the Design of Adaptive Cable-Driven Systems," Journal of Mechanisms and Robotics, **3**(2) .

[38] Rosati, G., Zanotto, D., and Rossi, A., 2008, "Performance Assessment of a 3D Cable-Driven Haptic Device," ASME Conference Proceedings, **2008**(48739) pp. 597-606.

[39] Lau, H. Y. K., and Wai, L. C. C., 2005, "Implementation of Position-Force and Position-Position Teleoperator Controllers with Cable-Driven Mechanisms," Robotics and Computer-Integrated Manufacturing, **21**(2) pp. 145-152.

[40] Kawamura, S., and Ito, K., 1993, "A new type of master robot for teleoperation using a radial wire drive system," Intelligent Robots and Systems '93, IROS '93. Proceedings of the 1993 IEEE/RSJ International Conference on, Anonymous **1,** pp. 55-60 vol.1.

[41] Kino, H., Saisyo, K., Hatanaka, Y., 2009, "Torque estimation system for human leg in passive motion using parallel-wire driven mechanism and iterative learning control," Rehabilitation Robotics, 2009. ICORR 2009. IEEE International Conference on, Anonymous pp. 719-724.

[42] Tadokoro, S., Murao, Y., Hiller, M., 2002, "A Motion Base with 6-DOF by Parallel Cable Drive Architecture," Mechatronics, IEEE/ASME Transactions on, **7**(2) pp. 115-123.

[43] Morizono, T., Kurahashi, K., and Kawamura, S., 1997, "Realization of a virtual sports training system with parallel wire mechanism," Robotics and Automation, 1997. Proceedings., 1997 IEEE International Conference on, Anonymous **4,** pp. 3025-3030 vol.4.

[44] Ning, K., Zhao, M., and Liu, J., 2006, "A New Wire-Driven Three Degree-of-Freedom Parallel Manipulator," Journal of Manufacturing Science and Engineering, Transactions of the ASME, **128**(3) pp. 816-819.

[45] Lahouar, S., Ottaviano, E., Zeghoul, S., 2009, "Collision Free Path-Planning for Cable-Driven Parallel Robots," Robotics and Autonomous Systems, **57**(11) pp. 1083-1093.

[46] Fang, S., Franitza, D., Torlo, M., 2004, "Motion Control of a Tendon-Based Parallel Manipulator using Optimal Tension Distribution," IEEE/ASME Transactions on Mechatronics, **9**(3) pp. 561-568.

[47] Ferraresi, C., Paoloni, M., and Pescarmona, F., 2007, "A Force-Feedback Six-Degrees-of-Freedom Wire-Actuated Master for Teleoperation: The WiRo-6.3," Industrial Robot: An International Journal, **34**(3) pp. 195-200.

[48] Albus, J., Bostelman, R., and Dagalakis, N., 1993, "NIST ROBOCRANE," Journal of Robotic Systems, **10**(5) pp. 709-724.

[49] Maeda, K., Tadokoro, S., Takamori, T., 1999, "On design of a redundant wire-driven parallel robot WARP manipulator," Robotics and Automation, 1999. Proceedings. 1999 IEEE International Conference on, Anonymous **2,** pp. 895-900 vol.2.

[50] Fattah, A., and Agrawal, S. K., 2005, "On the Design of Cable-Suspended Planar Parallel Robots," Journal of Mechanical Design, Transactions of the ASME, **127**(5) pp. 1021-1028.

[51] Miermeister, P., and Pott, A., 2010, "Modelling and Real-Time Dynamic Simulation of the Cable-Driven Parallel Robot IPAnema," **5**pp. 353-360.

[52] Kamishima, H., Arai, T., Yuasa, K., 2000, "Hybrid drive parallel arm and its motion control," Intelligent Robots and Systems, 2000. (IROS 2000). Proceedings. 2000 IEEE/RSJ International Conference on, Anonymous **1,** pp. 516-521 vol.1.

[53] Alp, A. B., and Agrawal, S. K., 2002, "Cable suspended robots: design, planning and control," Robotics and Automation, 2002. Proceedings. ICRA '02. IEEE International Conference on, Anonymous **4,** pp. 4275-4280 vol.4.

[54] Dagalakis, N. G., Albus, J. S., Wang, B. -., 1989, "Stiffness Study of a Parallel Link Robot Crane for Shipbuilding Applications," Journal of Offshore Mechanics and Arctic Engineering, **111**(3) pp. 183-193.

[55] Dekker, R., Khajepour, A., and Behzadipour, S., 2006, "Design and Testing of an Ultra-High-Speed Cable Robot," International Journal of Robotics and Automation, **21**(1) pp. 25-34.

[56] Behzadipour, S., and Khajepour, A., 2005, "A New Cable-Based Parallel Robot with Three Degrees of Freedom," Multibody System Dynamics, **13**(4) pp. 371-383.

[57] Behzadipour, S., Khajepour, A., Dekker, R., 2003, "DeltaBot: A new cable-based ultra high speed robot," American Society of Mechanical Engineers, Dynamic Systems and Control Division (Publication) DSC, Anonymous **72,** pp. 533-537.

[58] Hassan, M., and Khajepour, A., 2007, "Minimum-Norm Solution for the Actuator Forces in Cable-Based Parallel Manipulators Based on Convex Optimization," Proceedings 2007 IEEE International Conference on Robotics and Automation, **2007**pp. 1498-1503.

[59] Bostelman, R., Jacoff, A., and Proctor, F., 2000, "Cable-Based Reconfigurable Machines for Large Scale Manufacturing," Japan/USA Flexible Automation Conference Proc., University of Michigan, Ann Arbor, .

[60] Verhoeven, R., Hiller, M., and Tadokoro, S., 1998, "Workspace, Stiffness, Singularities and Classification of Tendon-Driven Stewart Platforms," 6th International Symposium on Advances in Robot Kinematics, pp. 105-114.

[61] Alikhani, A., Behzadipour, S., Ghahremani, F., 2010, "Modeling, control and simulation of a new large scale cable-driven robot," Proceedings of the ASME International Design Engineering Technical Conferences and Computers and Information in Engineering Conference 2009, DETC2009, Anonymous **7,** pp. 11-16.

[62] Merlet, J., 2008, "Kinematics of the wire-driven parallel robot MARIONET using linear actuators," Robotics and Automation, 2008. ICRA 2008. IEEE International Conference on, Anonymous pp. 3857-3862.

[63] Ming, A. and Higuchi, T., 1994, "Study on Multiple Degree-of-Freedom Positioning Mechanism using Wires (Part 1) - Concept, Design and Control," International Journal of the Japan Society for Precision Engineering, **28**(2) pp. 131-138.

[64] Yamamoto, M., Yanai, N., and Mohri, A., 1999, "Inverse dynamics and control of crane-type manipulator," Intelligent Robots and Systems, 1999. IROS '99. Proceedings. 1999 IEEE/RSJ International Conference on, Anonymous **2,** pp. 1228-1233 vol.2.

[65] Bosscher, P. M., and Ebert-Uphoff, I., 2004, "A stability measure for underconstrained cable-driven robots," Robotics and Automation, 2004. Proceedings. ICRA '04. 2004 IEEE International Conference on, Anonymous **5,** pp. 4943-4949 Vol.5.

[66] Campbell, P. D., Swaim, P. L., and and Thompson, C. J., 1993, "Charlotte Robot Technology for Space and Terrestrial Applications," SAE Technical Series, (paper 951520) .

[67] Kawamura, S., Choe, W., Tanaka, S., 1995, "Development of an ultrahigh speed robot FALCON using wire drive system," Robotics and Automation, 1995. Proceedings., 1995 IEEE International Conference on, Anonymous **1,** pp. 215-220 vol.1.

[68] Landsberger, S. E., and and Sheridan, T. B., 1993, "A Minimal, Minimal Linkage: The Tension-Compression Parallel Link Manipulator," Robotics, Mechatronics and Manufacturing Systems, pp. 81-88.

[69] Yanai, N., Yamamoto, M., and Mohri, A., 2001, "Inverse dynamics analysis and trajectory generation of incompletely restrained wire-suspended mechanisms," Robotics and Automation, 2001. Proceedings 2001 ICRA. IEEE International Conference on, Anonymous **4,** pp. 3489-3494 vol.4.

[70] Ferraresi, C., Paoloni, M., Pastorelli, S., 2004, "A New 6-DOF Parallel Robotic Structure Actuated by Wires: The WiRo-6.3," Journal of Robotic Systems, **21**(11) pp. 581-595.

[71] Bosscher, P. M., Williams II, R. L., Bryson, L. S., 2007, "Cable-Suspended Robotic Contour Crafting System," Automation in Construction, **17**(1) pp. 45-55.

[72] Behzadipour, S., and Khajepour, A., 2006, "Cable-Based Robot Manipulators with Translational Degrees of Freedom, Industrial Robotics: Theory, Modelling and Control,"InTech, pp. 211-236.

[73] Gosselin, C. M., and Angeles, J., 1990, "Singularity Analysis of Closed-Loop Kinematic Chains," Robotics and Automation, IEEE Transactions on, **6**(3) pp. 281-290.

[74] Zlatanov, D., Fenton, R. G., and Benhabib, B., 1994, "Singularity analysis of mechanisms and robots via a velocity-equation model of the instantaneous kinematics," Robotics and Automation, 1994. Proceedings., 1994 IEEE International Conference on, Anonymous pp. 986-991 vol.2.

[75] Gosselin, C. M., and Wang, J., 1997, "Singularity Loci of Planar Parallel Manipulators with Revolute Actuators," Robotics and Autonomous Systems, **21**(4) pp. 377-398.

[76] Wang, J., and Gosselin, C. M., 1998, "Kinematic Analysis and Singularity Loci of Spatial Four-Degree-of-Freedom Parallel Manipulators using a Vector Formulation," Journal of Mechanical Design, **120**(4) pp. 555-558.

[77] Dash, A. K., Chen, I., Yeo, S. H., 2003, "Singularity-free path planning of parallel manipulators using clustering algorithm and line geometry," Robotics and Automation, 2003. Proceedings. ICRA '03. IEEE International Conference on, Anonymous **1,** pp. 761-766 vol.1.

[78] Kumar, M., and Dash, A. K., 2006, "Elimination of singularities in parallel robotic manipulators," Anonymous **3,** pp. 1635-1641.

[79] Arakelian, V., Briot, S., and Glazunov, V., 2008, "Increase of Singularity-Free Zones in the Workspace of Parallel Manipulators using Mechanisms of Variable Structure," Mechanism and Machine Theory, **43**(9) pp. 1129-1140.

[80] Kotlarski, J., Abdellatif, H., Ortmaier, T., 2009, "Enlarging the useable workspace of planar parallel robots using mechanisms of variable geometry," Reconfigurable Mechanisms and Robots, 2009. ReMAR 2009. ASME/IFToMM International Conference on, Anonymous pp. 63-72.

[81] Li, B., Cao, Y., Zhang, Q., 2010, "Singularity elimination of Stewart Platform using redundant actuation," Computer Application and System Modeling (ICCASM), 2010 International Conference on, Anonymous **10,** pp. V10-156-V10-159.

[82] Yang, Y., and O'Brien, J. F., 2008, "A sequential method for the singularity free workspace design of a planar 3-arm parallel robot," Intelligent Robots and Systems, 2008. IROS 2008. IEEE/RSJ International Conference on, Anonymous pp. 1977-1982.

[83] Campos, L., Bourbonnais, F., Bonev, I. A., 2010, "Development of a Five-Bar Parallel Robot with Large Workspace," ASME Conference Proceedings, **2010**(44106) pp. 917-922.

[84] Yang, Y., and O'Brien, J. F., 2010, "A Sequential Method for the Singularity-Free Workspace Design of a Three Legged Parallel Robot," Mechanism and Machine Theory, **45**(11) pp. 1694-1706.

[85] Yang, G., Yeo, S. H., and Pham, C. B., 2004, "Kinematics and singularity analysis of a planar cable-driven parallel manipulator," Intelligent Robots and Systems, 2004. (IROS 2004). Proceedings. 2004 IEEE/RSJ International Conference on, Anonymous **4,** pp. 3835-3840 vol.4.

[86] Hiller, M. H., Fang, S., Mielczarek, S., 2005, "Design, Analysis and Realization of Tendon-Based Parallel Manipulators," Mechanism and Machine Theory, **40**(4) pp. 429-445.

[87] Diao, X., Ma, O., and Lu, Q., 2008, "Singularity Analysis of Planar Cable-Driven Parallel Robots," Robotics, Automation and Mechatronics, 2008 IEEE Conference on, Anonymous pp. 272-277.

[88] Su, Y. X., Duan, B. Y., Nan, R. D., 2001, "Development of a Large Parallel-Cable Manipulator for the Feed-Supporting System of a Next-Generation Large Radio Telescope," Journal of Robotic Systems, **18**(11) pp. 633-643.

[89] Qiu, Y. Y., Duan, B. Y., Wei, Q., 2002, "Elimination of Force Singularity of the Cable and Cabin Structure for the Next Generation Large Radio Telescope," Mechatronics, **12**(7) pp. 905-918.

[90] Alikhani, A., Behzadipour, S., Alasty, A., 2011, "Design of a Large-Scale Cable-Driven Robot with Translational Motion," Robotics and Computer-Integrated Manufacturing, **27**(2) pp. 357-366.

[91] Hassan, M., and Khajepour, A., 2009, "Analysis of Hybrid Cable-Actuated Parallel Manipulators with a Constraining Leg for Lower-Degree-of-Freedom Operation," ASME Conference Proceedings, **2009**(49040) pp. 93-100.

[92] Hiller, M. H., and Hirsch, K., 2006, "Multibody System Dynamics and Mechatronics," ZAMM, **86**(2) pp. 87-109.

[93] Bruckmann, T., Mikelsons, L., Brandt, T., 2008, "Wire Robots Part II: Dynamics, Control & Application," Parallel Manipulators, New Developments, pp. 41-56.

[94] Behzadipour, S., and Khajepour, A., 2006, "Time-Optimal Trajectory Planning in Cable-Based Manipulators," Robotics, IEEE Transactions on, **22**(3) pp. 559-563.

[95] Pham, C. B., Yang, G., and Yeo, S. H., 2005, "Dynamic analysis of cable-driven parallel mechanisms," Advanced Intelligent Mechatronics. Proceedings, 2005 IEEE/ASME International Conference on, Anonymous pp. 612-617.

[96] Bedoustani, Y. B., Taghirad, H. D., and Aref, M. M., 2008, "Dynamics analysis of a redundant parallel manipulator driven by elastic cables," Control, Automation, Robotics and Vision, 2008. ICARCV 2008. 10th International Conference on, Anonymous pp. 536-542.

[97] Du, J., Bao, H., Duan, X., 2010, "Jacobian Analysis of a Long-Span Cable-Driven Manipulator and its Application to Forward Solution," Mechanism and Machine Theory, **45**(9) pp. 1227-1238.

[98] Gouttefarde, M., Merlet, J., and Daney, D., 2006, "Advances in Robot Kinematics (10th ARK International Symposium), Springer,"pp. 315-322.

[99] Roberts, R. G., Graham, T., and Lippitt, T., 1998, "On the Inverse Kinematics, Statics, and Fault Tolerance of Cable-Suspended Robots," Journal of Robotic Systems, **15**(10) pp. 581-597.

[100] Verhoeven, R., 2004, "Analysis of the Workspace of Tendon-Based Stewart Platforms," .

[101] Gouttefarde, M., and Gosselin, C., 2004, "
on the Properties and the Determination of the Wrench-Closure Workspace of Planar Parallel Cable-Driven Mechanisms," ASME Des. Eng. Tech Conf. Computer Inf. Eng. Conf., pp. 337-346.

[102] Diao, X., and Ma, O., 2007, "A Method of Verifying Force-Closure Condition for General Cable Manipulators with Seven Cables," Mechanism and Machine Theory, **42**(12) pp. 1563-1576.

[103] Lim, W. B., Yang, G., Yeo, S. H., 2009, "A Generic Tension-Closure Analysis Method for Fully-Constrained Cable-Driven Parallel Manipulators," 2009 IEEE International Conference on Robotics and Automation, pp. 2187-2192.

[104] Gouttefarde, M., 2009, "Characterizations of fully constrained poses of parallel cable-driven robots: A review," 2008 ASME International Design Engineering Technical Conferences and Computers and Information in Engineering Conference, DETC 2008, Anonymous **2,** pp. 21-30.

[105] Pham, C. B., Yeo, S. H., Yang, G., 2009, "Workspace Analysis of Fully Restrained Cable-Driven Manipulators," Robotics and Autonomous Systems, **57**(9) pp. 901-912.

[106] Pott, A., Bruckmann, T., and Mikelsons, L., 2009, "Closed-Form Force Distribution for Parallel Wire Robots," pp. 25-34.

[107] Gosselin, C. M., and Grenier, M., 2011, "On the Determination of the Force Distribution in Overconstrained Cable-Driven Parallel Mechanisms," Meccanica, **46**(1) pp. 3-15.

[108] Angeles, J., and Park, F. C., 2008, "Performance Evaluation and Design Criteria," pp. 229-244.

[109] Merlet, J., 2006, "Parallel robots," Dordrecht ;Boston, MA : Kluwer Academic Publishers, c2006, .

[110] De Luca, A., and Book, W., 2008, "Robots with Flexible Elements," pp. 287-319.

[111] Svinin, M. M., Kaneko, M., and Tsuji, T., 1999, "Internal Forces and Stability in Multi-Finger Grasps," Control Engineering Practice, **7**(3) pp. 413-422.

[112] Bruckmann, T., Mikelsons, L., Brandt, T., 2008, "Wire Robots Part I: Kinematics, Analysis & Design," Parallel Manipulators, New Developments, pp. 109-132.

[113] Merlet, J., 2009, "Analysis of Wire Elasticity for Wire-Driven Parallel Robots," pp. 471-478.

[114] Behzadipour, S., and Khajepour, A., 2006, "Stiffness of Cable-Based Parallel Manipulators with Application to Stability Analysis," Journal of Mechanical Design, Transactions of the ASME, **128**(1) pp. 303-310.

[115] Yu, K., Lee, L., and Krovi, V. N., 2009, "Simultaneous Trajectory Tracking and Stiffness Control of Cable Actuated Parallel Manipulator," ASME Conference Proceedings, **2009**(49040) pp. 55-63.

[116] Liu, X., Qiu, Y., and Sheng, Y., 2009, "Stiffness Enhancement and Motion Control of a 6-DOF Wire-Driven Parallel Manipulator with Redundant Actuations for Wind Tunnels," Hangkong Xuebao/Acta Aeronautica Et Astronautica Sinica, **30**(6) pp. 1156-1164.

[117] Yang, Y., Chen, W., Wu, X., 2010, "Stiffness analysis Of 3-DOF spherical joint based on cable-driven humanoid arm," Industrial Electronics and Applications (ICIEA), 2010 the 5th IEEE Conference on, Anonymous pp. 99-103.

[118] Howard, W. S., and Kumar, V., 1996, "On the Stability of Grasped Objects," Robotics and Automation, IEEE Transactions on, **12**(6) pp. 904-917.

[119] Svinin, M. M., Ueda, K., and Kaneko, M., 1999, "On the stability of an object in multi-finger grasping," Intelligent Robots and Systems, 1999. IROS '99. Proceedings. 1999 IEEE/RSJ International Conference on, Anonymous **1,** pp. 412-417 vol.1.

[120] Hanafusa, H., and Adli, M. A., 1991, "Effect of internal forces on stiffness of closed mechanisms," Advanced Robotics, 1991. 'Robots in Unstructured Environments', 91 ICAR., Fifth International Conference on, Anonymous pp. 845-850 vol.1.

[121] Svinin, M. M., Ueda, K., and Uchiyama, M., 2000, "On the stability conditions for a class of parallel manipulators," Robotics and Automation, 2000. Proceedings. ICRA '00. IEEE International Conference on, Anonymous **3,** pp. 2386-2391 vol.3.

[122] Stump, E., and Kumar, V., 2006, "Workspaces of Cable-Actuated Parallel Manipulators," Journal of Mechanical Design, **128**(1) pp. 159-167.

[123] Bosscher, P. M., and Ebert-Uphoff, I., 2004, "Wrench-based analysis of cable-driven robots," Robotics and Automation, 2004. Proceedings. ICRA '04. 2004 IEEE International Conference on, Anonymous **5,** pp. 4950-4955 Vol.5.

[124] Barrette, G., and Gosselin, C. M., 2000, "Kinematic Analysis and Design of Planar Parallel Mechanism Actuated with Cables," ASME Design Engineering Technical Conference, .

[125] Barrette, G., and Gosselin, C. M., 2005, "Determination of the Dynamic Workspace of Cable-Driven Planar Parallel Mechanisms," Journal of Mechanical Design, **127**(2) pp. 242-248.

[126] Tadokoro, S., Nishioka, S., Kimura, T., 1996, "On Fundamental Design of Wire Configurations of Wire-Driven Parallel Manipulators with Redundancy," ASME JapanUSA Symposium on Flexible Automotion, **1**pp. 151-158.

[127] Hassan, M., and Khajepour, A., 2010, "Analysis of a large-workspace cable-actuated manipulator for warehousing applications," Proceedings of the ASME International Design Engineering Technical Conferences and Computers and Information in Engineering Conference 2009, DETC2009, Anonymous **7,** pp. 45-53.

[128] Bosscher, P. M., and Ebert-Uphoff, I., 2006, "Disturbance Robustness Measures for Underconstrained Cable-Driven Robots," Proceedings 2006 IEEE International Conference on Robotics and Automation, 2006.ICRA 2006., **2006**pp. 4205-4212.

[129] Shiang, W., Cannon, D., and Gorman, J., 1999, "Dynamic analysis of the cable array robotic crane," Robotics and Automation, 1999. Proceedings. 1999 IEEE International Conference on, Anonymous **4,** pp. 2495-2500 vol.4.

[130] Oh, S., and Agrawal, S. K., 2003, "Cable-suspended planar parallel robots with redundant cables: controllers with positive cable tensions," Robotics and Automation, 2003. Proceedings. ICRA '03. IEEE International Conference on, Anonymous **3,** pp. 3023-3028 vol.3.

[131] Yu, K., Lee, L., Tang, C. P., 2010, "Enhanced trajectory tracking control with active lower bounded stiffness control for cable robot," Robotics and Automation (ICRA), 2010 IEEE International Conference on, Anonymous pp. 669-674.

[132] Kino, H., Yahiro, T., Takemura, F., 2006, "Adaptive Position Control for Fully Constrained Parallel Wire Driven Systems," Intelligent Robots and Systems, 2006 IEEE/RSJ International Conference on, Anonymous pp. 79-84.

[133] Zeinali, M., and Khajepour, A., 2010, "Design and Application of Chattering-Free Sliding Mode Controller to Cable-Driven Parallel Robot Manipulator: Theory and Experiment," ASME Conference Proceedings, **2010**(44106) pp. 319-327.

[134] Ghasemi, A., Eghtesad, M., and Farid, M., 2008, "Constrained model predictive control of the redundant cable robots," Automation Congress, 2008. WAC 2008. World, Anonymous pp. 1-6.

[135] Gholami, P., Aref, M. M., and Taghirad, H. D., 2008, "On the control of the KNTU CDRPM: A cable driven redundant parallel manipulator," Intelligent Robots and Systems, 2008. IROS 2008. IEEE/RSJ International Conference on, Anonymous pp. 2404-2409.

[136] Stump, E., and Kumar, V., 2004, "Workspace delineation of cable-actuated parallel manipulators," Anonymous **2 B,** pp. 1303-1310.

[137] Torres-Mendez, Sergio J. and Khajepour A., "Design Optimization of a Warehousing Cable-Based Robot," Proceedings of the ASME 2014 International Design Technical Conference & Computers and Information in Engineering Conference IDETC/CIE, August 17-20, 2014, Buffalo, New York, USA, **2014**.

[138] Torres-Mendez, Sergio J. and Khajepour A., "Analysis of a High Stiffness Warehousing Cable-Based Robot," Proceedings of the ASME 2014 International Design Technical Conference & Computers and Information in Engineering Conference IDETC/CIE, August 17-20, 2014, Buffalo, New York, USA, **2014**.

[139] Gungor G., Torres-Mendez S., Fidan B., and Khajepour A., "Estimation of Anchor Points for Fully-Constrained and Redundant Planar Cable Robts," Proceedings of the ASME 2014 International Mechanical Engineering Congress & Exposition IMECE2014, to be presented at November 8-13, Montreal, Quebec, Canada, **2014**.

[140] Torres-Mendez S., Gungor G., Fidan B., and Khajepour A., "Comparison of adaptive and Robust Controllers for Fully-constrained and Redundant Planar Cable Robots," Proceedings of the

ASME 2014 International Mechanical Engineering Congress & Exposition IMECE2014, to be presented at November 8-13, Montreal, Quebec, Canada, **2014**.

Appendix A

MatLab code

The detailed MatLab code based on the iterative algorithm described in Section 2.4.1 is as follows:

```
%*****************************************************
%           m_spatial_confi09e.m
% This program calculates motor torque values for
% a given path of the mobile platform of a
% cable-robot station for warehousing tasks.
% Sergio Javier Torres Mendez(2014)
%-----------------------------------------------------
function m_spatial_confi09e01
clc;%Clean screen
clear all;%Clean memory
%---------------------------------------
% Data
[a b c d e f g h i j ina inb inc zc ing inh1 inh2 ini inj1 inj2 scale]=geo();
%calling functions
[mi mp mt m ycp cablep cablet
anchorm]=para(a,b,c,d,e,f,g,h,i,j,ina,inb,inc,zc,ing,inh1,inh2,ini,inj1,inj2);
[Pv Rm VELv ACCv WEv Kv Mm taulimit distmin PATHv as am anchors mass taumin
taumax]=data(mi,mp,mt,a,b,c,d,e,f,g,h,i,j,ina,inb,inc,ing,inh1,inh2,ini,inj1,inj2,ycp,
cablep,cablet,anchorm);
%Data for controller with information
[ppx vpx apx ppz vpz apz size_points dt]=path_DemoTraj;
data_controller(ppx,vpx,apx,ppz,vpz,apz,size_points,dt);
%---------------SUBFUCTIONS-----------------------------------
%function that read data
function [a b c d e f g h i j ina inb inc zc ing inh1 inh2 ini inj1 inj2 scale]=geo()
  %Give dimensions of the static platform
  scale=1/5;d=3.0;e=3.0;f=1.0;i=0.2;j=0.2;
  %Give Dimensions of the mobile platform
  a=0.38;b=0.205;c=0.110;zc=0.045;g=0.125;h=g;
  %Give Dimensions to anchor points on mobile platform
  ina=a;inb=0.345;
  %optimal parameters
  ing=0.0;inh1=h;inh2=h;ini=0.0;inj1=0.0;inj2=j;
  %Compute center of mass of the mobile platform
```

```
  amax=max(a,ina);bmax=max(b,inb);ycp=((2*bmax+amax)/(amax+bmax))*(c/3);inc=c-ycp;%[m]
end
%-----------------------------------------------------------------
function [mi mp mt m ycp cablep cablet
anchorm]=para(a,b,c,d,e,f,g,h,i,j,ina,inb,inc,zc,ing,inh1,inh2,ini,inj1,inj2)
  %Calculate total number of cables
  mi=6;mp=0;mt=6;m=mi+mp+mt;
  amax=max(a,ina);bmax=max(b,inb);ycp=((2*bmax+amax)/(amax+bmax))*(c/3);
  cablet1=1;cablet2=2;cablet3=3;cablet4=4;cablet5=5;cablet6=6;
     %WCR CONFIGURATION
        anchorm1=[-b/2;-inh1/2;c-ycp];anchorm2=[b/2;-inh1/2;c-ycp];
        anchorm3=[inb/2;-inh2/2;zc-ycp];anchorm4=[-inb/2;-inh2/2;zc-ycp];
        anchorm5=[-ina/2;-ing/2;-ycp];anchorm6=[ina/2;-ing/2;-ycp];
        anchorm7=[-b/2;inh1/2;c-ycp];anchorm8=[b/2;inh1/2;c-ycp];
        anchorm9=[inb/2;inh2/2;zc-ycp];anchorm10=[-inb/2;inh2/2;zc-ycp];
        anchorm11=[-ina/2;ing/2;-ycp];anchorm12=[ina/2;ing/2;-ycp];
  %Anchor points on both platforms
  anchorm=zeros(3,m);cablep=zeros(mp,1);cablet=zeros(mt,1);
  for ii=1:mp
      cablep(ii,1)=eval(strcat('cablep',int2str(ii)));
  end
  for ii=1:mt
      cablet(ii,1)=eval(strcat('cablet',int2str(ii)));
  end
  for ii=1:m
      anchorm(:,ii)=eval(['anchorm',int2str(ii)]);
  end
end%end function para
%-----------------------------------------------------------------
%Function that reads data
function [Pv Rm VELv ACCv WEv Kv Mm taulimit distmin PATHv as am anchors mass taumin
taumax]=data(mi,mp,mt,a,b,c,d,e,f,g,h,i,j,ina,inb,inc,ing,inh1,inh2,ini,inj1,inj2,ycp,
cablep,cablet,anchorm)
  %HOME
  Dxh=-0.016368515205724;Dyh=0.0;Dzh=-0.163066720328403;%[m]
  Hv=[Dxh;Dyh;Dzh];%m
  Areasp=(f/2)*(d+e);%reachable area
  %Compute Initial points on static platform
  as1=[-e/2;-j/2;f/2]-Hv;as2=[e/2;-j/2;f/2]-Hv;as3=[d/2;-i/2;-f/2]-Hv;
  as4=[-d/2;-i/2;-f/2]-Hv;as5=[-e/2;j/2;f/2]-Hv;as6=[e/2;j/2;f/2]-Hv;
```

```
  as7=[d/2;i/2;-f/2]-Hv;as8=[-d/2;i/2;-f/2]-Hv;
  %Compute Anchor points on static platform
  anchors1=[-e/2;-inj1/2;f/2]-Hv;anchors2=[e/2;-inj1/2;f/2]-Hv;
  anchors3=[d/2;-ini/2;-f/2]-Hv;anchors4=[-d/2;-ini/2;-f/2]-Hv;
  anchors5=[-e/2+b/2-ina/2;-inj2/2;f/2-c]-Hv;
  anchors6=[e/2-b/2+ina/2;-inj2/2;f/2-c]-Hv;
  %Give mass of the mobile platform
  mass=2.5;%50.0*scale;
  Massm=[mass 0 0;0 mass 0;0 0 mass];
  %Compute center of mass
  amax=max(a,ina);bmax=max(b,inb);ycp=((2*bmax+amax)/(amax+bmax))*(c/3);
  %Inertia matrix
  Ixx=1/12*mass*(g*g+c*c);
  Iyy=(mass/(18*(amax+bmax)))*(3*bmax*(bmax*bmax+c*c+12*(c/2-ycp)*(c/2-ycp))+...
      (amax-bmax)*(((amax-bmax)/2)*...
      ((amax-bmax)/2)+c*c+18*(((2*bmax+amax)/6)*((2*bmax+amax)/6)+(ycp-c/3)*(ycp-
c/3))));
  Izz=(mass/(36*(amax+bmax)))*(6*bmax*(bmax*bmax+g*g)+...
      (amax-bmax)*(2*((amax-bmax)/2)*((amax-
bmax)/2)+3*g*g+(2*bmax+amax)*(2*bmax+amax)));
  Ixy=0;Ixz=0;Iyz=0;
  %Compute Centroidal Inertia mass tensor
  Tmp=[Ixx -Ixy -Ixz;-Ixy Iyy -Iyz;-Ixz -Iyz Izz];
  %Compute corners of the mobile platform
  am1=[-bmax/2;-h/2;c-ycp];am2=[bmax/2;-h/2;c-ycp];
  am3=[amax/2;-g/2;-ycp];am4=[-amax/2;-g/2;-ycp];
  am5=[-bmax/2;h/2;c-ycp];am6=[bmax/2;h/2;c-ycp];
  am7=[amax/2;g/2;-ycp];am8=[-amax/2;g/2;-ycp];
  %Compute additional anchor points for parallel cables on static platform
  anchors7=[];anchors8=[];anchors9=[];anchors10=[];anchors11=[];anchors12=[];
  for ii=1:mp
      asig=eval(strcat('anchors',num2str(cablep(ii))))-...
          (anchorm(:,cablep(ii))-anchorm(:,mi+ii));
      eval(['anchors',int2str(mi+ii),'=',mat2str(asig),';'])
  end
  %Compute additional anchor points for triang cables on static platform
  mmatrix=[1,0,0;0,-1,0;0,0,1];
  for ii=1:mt
      asig=mmatrix*eval(strcat('anchors',num2str(cablet(ii))));
      eval(['anchors',int2str(mi+mp+ii),'=',mat2str(asig),';'])
```

```
  end
%Input data of the mobile box.
px=0.0;py=0.0;pz=0.0;theta1=0.0;theta2=0.0;theta3=0.0;
%Rotational transformation matrix of the mobile box
Rm=[cos(theta1) -sin(theta1) 0;sin(theta1) cos(theta1) 0;0 0 1]*...
   [1 0 0;0 cos(theta2) -sin(theta2);0 sin(theta2) cos(theta2)]*...
   [cos(theta3) 0 sin(theta3);0 1 0;-sin(theta3) 0 cos(theta3)];
%mobile platform linear and angular velocities
vpx=0.0;vpy=0.0;vpz=0.0;Vv=[vpx;vpy;vpz];wpx=0.0;wpy=0.0;wpz=0.0;Wwv=[wpx;wpy;wpz];
%mobile platform linear and angular accelerations
apx=0.0;apy=0.0;apz=0.0;Av=[apx;apy;apz];alfapx=0.0;alfapy=0.0;alfapz=0.0;ALFAwv=[alfa
px;alfapy;alfapz];
%mobile platform external forces
Gz=-1.0;%gravity along z
fex=0.0;fey=0.0;fez=0.0;mex=0.0;mey=0.0;mez=0.0;
FEv=[fex;fey;fez+mass*Gz*9.81];MEv=[mex;mey;mez];
k=300000.0;taumin=33.0;taumax=220.0;distmin=0.5*scale;
%INFORMATION TO SEND
as=zeros(3,8);am=zeros(3,8);anchors=zeros(3,m);
%Initial values of the mobile platform
Pv=[px;py;pz];VELv=[Vv;Wwv];ACCv=[Av;ALFAwv];WEv=[FEv;MEv];
Mm=[Massm zeros(3);zeros(3) Tmp];%Inertia matrix
taulimit=[taumin taumax];
pxd=0.2;pyd=0.0;pzd=0.0;tf=4.0;PATHv=[pxd;pyd;pzd;tf];
%Independent points on both platforms
for ii=1:8
    as(:,ii)=eval(['as',int2str(ii)]);am(:,ii)=eval(['am',int2str(ii)]);
end
for ii=1:m
    anchors(:,ii)=eval(['anchors',int2str(ii)]);
end
end%end function data
%-----------------------------------------------------------------
%Function that calculates the inverse kinematics
function [Uv LENv Lv]=ikinematics(Pv,m,anchors,anchorm)
  Lv=zeros(3,m);LENv=zeros(m,1);Uv=zeros(3,m);
  for ii=1:m
      Lv(:,ii)=Pv+anchorm(:,ii)-anchors(:,ii);
      LENv(ii,:)=sqrt(Lv(:,ii)'*Lv(:,ii));
      Uv(:,ii)=Lv(:,ii)/LENv(ii,:);
```

```
  end
end %End of function ikinematics
%-------------------------------------------------------
%Function that compute the cable length rates velocities
function [Jm Vlv]=velocity(m,anchorm,Uv,VELv)
crossUv=zeros(m,3);
for ii=1:m
    crossUv(ii,:)=(cross(anchorm(1:3,ii),Uv(1:3,ii)))';%3D
end
Jm=[Uv(1,:)' Uv(2,:)' Uv(3,:)' crossUv];%3D
Vlv=Jm*VELv;
end %End of function velocity
%-------------------------------------------------------
%Function that compute the cable length rates acceleration
function [dJm Alv]=acceleration(m,anchorm,Uv,VELv,ACCv,Jm,Vlv,LENv,Lv)
crossUv=zeros(m,3);
for ii=1:m
    crossUv(ii,:)=(cross(anchorm(1:3,ii),Uv(1:3,ii)))';%3D
end
for ii=1:m
    crosswr(ii,:)=(cross(VELv(4:6),anchorm(1:3,ii)))';%3D
    crosswrl(ii,:)=(cross(crosswr(ii,:)',Lv(:,1)))';%3D
    crossav(ii,:)=(cross(anchorm(1:3,ii),VELv(4:6)))';%3D
    crossrl(ii,:)=(cross(anchorm(1:3,ii),Lv(:,1)))';%3D
    dJm1(ii,:)=(LENv(ii)*(VELv(4:6)'+crosswr(ii,:))-
Vlv(ii)*Lv(:,ii)')/(LENv(ii)*LENv(ii));
    dJm2(ii,:)=(LENv(ii)*(crosswrl(ii,:)+crossav(ii,:))-
Vlv(ii)*crossrl(ii,:))/(LENv(ii)*LENv(ii));
end
dJm=[dJm1 dJm2];%Derivative of Jacobian
Alv=Jm*ACCv+dJm*VELv;
end %End of function acceleration
%-------------------------------------------------------
%function that calculates interfere
 function [dist]=interference(Pv,anchors,anchorm,cablep)
    %Checking parallelism
    %independent cables (1 and 2)
    L1xf=[anchors(1,1) Pv(1)+anchorm(1,1)];L1zf=[anchors(3,1) Pv(3)+anchorm(3,1)];
    L2xf=[anchors(1,2) Pv(1)+anchorm(1,2)];L2zf=[anchors(3,2) Pv(3)+anchorm(3,2)];
    %Parallel to virtual cable of triangular cables (5 and 6)
```

```
    L5xf=[anchors(1,5) Pv(1)+anchorm(1,5)];L5zf=[anchors(3,5) Pv(3)+anchorm(3,5)];
    L6xf=[anchors(1,6) Pv(1)+anchorm(1,6)];L6zf=[anchors(3,6) Pv(3)+anchorm(3,6)];
    %Compute slopes
    m1=((L1zf(1)-L1zf(2))/(L1xf(1)-L1xf(2)));% pendiente of independent cable
    m2=((L2zf(1)-L2zf(2))/(L2xf(1)-L2xf(2)));% pendiente of independent cable
    m5=((L5zf(1)-L5zf(2))/(L5xf(1)-L5xf(2)));% pendiente of parallel cable
    m6=((L6zf(1)-L6zf(2))/(L6xf(1)-L6xf(2)));% pendiente of parallel cable
    if ((abs(m1-m5)<0.001)&&(abs(m2-m6)<0.001))
        mp1=-1/m1; mp2=-1/m2;
        Point1x=(mp1*L1xf(2)-m5*L5xf(2)+L5zf(2)-L1zf(2))/(mp1-m5);
        Point1y=mp1*(Point1x-L1xf(2))+L1zf(2);
        distpar1=sqrt((L1xf(2)-Point1x)*(L1xf(2)-Point1x)+(L1zf(2)-Point1y)*(L1zf(2)-
Point1y));
        Point2x=(mp2*L2xf(2)-m6*L6xf(2)+L6zf(2)-L2zf(2))/(mp2-m6);
        Point2y=mp2*(Point2x-L2xf(2))+L2zf(2);
        distpar2=sqrt((L2xf(2)-Point2x)*(L2xf(2)-Point2x)+(L2zf(2)-Point2y)*(L2zf(2)-
Point2y));
        dist=[distpar1 distpar2];
    else
        dist=[0.0 0.0];
    end
 end %End of function interference
%-------------------------------------------------------------------------
%function that calculates cable tensions
function [TAUva,x2]=forcea(anchorm,Uv,WEv,taumin,taumax)
clear Am;clear TAUva;clear x2;clear x1;clear x1a;clear x2a;clear y1a;
clear y2a;clear x3;clear t;clear I;clear NN;clear x1c;clear x2c;
crossUv=zeros(3,m);
for ii=1:m
    crossUv(:,ii)=(cross(anchorm(1:3,ii),Uv(1:3,ii)))';%3D
end
Am=[Uv(1,:);Uv(2,:);Uv(3,:);crossUv];%3D
%DYSTRA algorithm
    I=eye(m);
    NN=I-((pinv(Am))*Am);
    ii=0;x1a=0.0*ones(m,1);x2a=0.0*ones(m,1);
    y1a=0.0*ones(m,1);y2a=0.0*ones(m,1);
    error=0.0001;error1=100000.0;taumin=32.9;taumax=220.0;
    %**********************
    while error1>error
```

```
        ii=ii+1;error1a=error1;x3=x1a;
        %first projection
        t=x3-y2a;x2=((pinv(Am))*WEv)+NN*(t);y2=x2-t;t=x2-y1a;
        for kk=1:m
            if (t(kk)<=taumin)
                t(kk)=taumin;
            else
                if (t(kk)>=taumax)
                    t(kk)=taumax;
                end
            end
        end
        x1=t;y1=x1-t;error1=norm(x1-x1a,2)+norm(x2-x2a,2)+norm(y2-y2a,2);
        if (error1<=error1a)
            x1a=x1;x2a=x2;y1a=y1;y2a=y2;
        else
            break
        end
    end %end of while
if ((abs(x1-x2))<=(error*ones(m,1)))
    %disp('feasible solution')
    TAUva=x1;
else
    %disp('****no feasible solution****')
    TAUva=x2;
end
end%End of function forcea
%-------------------------------------------------------------------------
%function that calculates the stiffness
 function [Km]=stiffness(m,anchorm,Uv,LENv,Kv,TAUv)
    clear Km;clear Kk;clear Kt;clear Ksi;clear Kfi;
    clear aux1;clear aux2;clear rcrossi;clear ucrossi;clear I;
    I=eye(3,3);%Identity matrix
    Km=zeros(6,6);
    for ii=1:m
        rcrossi=[0 -anchorm(3,ii) anchorm(2,ii);anchorm(3,ii) 0 -anchorm(1,ii);-
anchorm(2,ii) anchorm(1,ii) 0];
        ucrossi=[0 -Uv(3,ii) Uv(2,ii);Uv(3,ii) 0 -Uv(1,ii);-Uv(2,ii) Uv(1,ii) 0];
        aux1=Uv(1:3,ii)*Uv(1:3,ii)';
        Kk=(Kv(ii)/LENv(ii))*[aux1 aux1*rcrossi';...
```

```
                    rcrossi*aux1 rcrossi*aux1*rcrossi'];
        Kt=(TAUv(ii)/LENv(ii))*[I-aux1 (I-aux1)*rcrossi';...
                               rcrossi*(I-aux1) rcrossi*(I-aux1)*rcrossi'-
(LENv(ii))*ucrossi*rcrossi'];
        Km=Km+(Kk+Kt);
    end
 end%End of function stiffness
%-------------------------------------------------------------------------
% %%%%%%%%%%%%%%%%%%%%%%%% LINEAR PATH %%%%%%%%%%%%%%%%%%%%%%%%%%%%
function [ppx vpx apx ppz vpz apz size_points dt]=path_DemoTraj
    dt=0.001;
    %%All paths must return to the zero point
%
%       ^     |
%       |     |
%       |     v
%       +     +
%
%1) Home-UP-Home as fast as possible
    %Trajectory
    Pt=[[0;0] [0.0;0.25] [0;0]];%[m]
    VelOR=1/4.9;
    Vel=[0.9 0.9 0.9]*VelOR;
    dmind = [1.0 1.0 1.0];
    NTr=size(Pt,2)-1;
    %Traj Definition
    for i=1:NTr;
        Traj(i).TP=[0.1 0.3 0.4];%slopes of pos vel and acce curves
        Traj(i).dt=dt;
        Traj(i).dQc=Pt(:,i+1)-Pt(:,i);
        Traj(i).dS=norm(Traj(i).dQc);
        Traj(i).dQc=Traj(i).dQc/Traj(i).dS;
        Traj(i).dV=Vel(i);
        Traj(i).dmind=dmind(i);
        Traj(i).iCrit=zeros(1,8);
        Traj(i).iTc=0;
    end
    %%PreCalculation of the trajectory
    for i=1:NTr
        [dSnd,dVnd]=NDTP_Prop(Traj(i));
```

```
        Traj(i).dTc= Traj(i).dS / Traj(i).dV * dVnd/dSnd;
        Traj(i).dTc = ceil(Traj(i).dTc/Traj(i).dt)*Traj(i).dt;
        Traj(i).dAmax = Traj(i).dS / dSnd / Traj(i).dTc^2;
        [xp Tr vp ap]=TPDimen(Traj(i),Traj(i).dt);
        Traj(i)=Tr;
        Traj(i).iTc=Tr.iCrit(8);
        Xp{i}=xp; Vp{i}=vp; Ap{i}=ap;
    end
    %%%%%%%%%%%%%Merging%%%%%%%%%%%%%%%%
    X=Pt(:,1);
    V=[0;0];
    A=[0;0];
    iInd=1;
    for i=1:NTr
        NSpan=Traj(i).iTc-size(X,2)+iInd-1;
        XpTemp=Traj(i).dQc*Xp{i};
        X=[X X(:,end)*ones(1,NSpan)];
        X(:,iInd:end)=X(:,iInd:end)+XpTemp;
        VpTemp=Traj(i).dQc*Vp{i};
        V=[V V(:,end)*ones(1,NSpan)];
        V(:,iInd:end)=V(:,iInd:end)+VpTemp;
        ApTemp=Traj(i).dQc*Ap{i};
        A=[A A(:,end)*ones(1,NSpan)];
        A(:,iInd:end)=A(:,iInd:end)+ApTemp;
        iInd=iInd+floor(Traj(i).dmind*Traj(i).iTc);
    end
    Time=size(X,2)*dt;
    %Plot trajectory of mobile platform (points each second)
    figure;
    drawxysb(anchors); hold on %draws static box
    plot(X(1,:),X(2,:)); grid on; hold on %draws line path
    plot(X(1,1:1000:end),X(2,1:1000:end),'.');axis equal; %draws points path
    title('Trajectory of end effector (points each second)')
    axis tight
    hold off
    division=100.0;%Every dt*division seconds
    disp('Mobile platform pos, vel, acc along horizontal axis (X)')
    ppx=X(1,1:division:end);
    vpx=V(1,1:division:end);
```

```
    apx=A(1,1:division:end);
    disp('Mobile platform pos, vel, acc along vertical axis (Z)')
    ppz=X(2,1:division:end);
    vpz=V(2,1:division:end);
    apz=A(2,1:division:end);
    %[dimension_points,size_points]=size(ppx);
    size_points = size(ppx,2);
    %new division
    dt=dt*division;
end %end of function path_DemoTraj
%-------------------------------------------------------------------------
function data_controller(ppx,vpx,apx,ppz,vpz,apz,size_points,dt)
    %Start calculating path for each step
    for nn=1:1:size_points
        %Assign linear position vector of the mobile platform
        Pv=[ppx(1,nn);0;ppz(1,nn)];
        %Assign velocity vector of the mobile platform
        Vv=[vpx(1,nn);0;vpz(1,nn)];%linear velocity
        wpx=0.0;wpy=0.0;wpz=0.0;
        Wwv=[wpx;wpy;wpz];VELv=[Vv;Wwv];
        %Assign acceleration vector of the mobile platform
        apy=0.0;
        Av=[apx(1,nn);apy;apz(1,nn)];%linear acceleration
        alfapx=0.0;alfapy=0.0;alfapz=0.0;
        ALFAwv=[alfapx;alfapy;alfapz];ACCv=[Av;ALFAwv];
        %Calculate cable lengths
        [Uv LENv Lv]=ikinematics(Pv,m,anchors,anchorm);
        for ii=1:12
            LENpv(nn,ii)=LENv(ii);
        end
        %Calculate cable velocities
        [Jm Vlv]=velocity(m,anchorm,Uv,VELv);
        for ii=1:12
            Vlpv(nn,ii)=Vlv(ii);
        end
        %Calculate cable accelerations
        [dJm Alv]=acceleration(m,anchorm,Uv,VELv,ACCv,Jm,Vlv,LENv,Lv);
         for ii=1:12
            Alpv(nn,ii)=Alv(ii);
```

```
            PISpv(nn,ii)=LENpv(1,ii)-LENv(ii);%cable displacement
        end
        %Checking first singularity when cable length is zero or negative
        if (min(LENv(:)))>0
            XXPv(nn)=Pv(1);ZZPv(nn)=Pv(3);
            %Calculate the cable tensions
            Gz=-1.0;%gravity along z
            fex=mass*apx(1,nn);fey=mass*apy;fez=mass*apz(1,nn);
            mex=0.0;mey=0.0;mez=0.0;
            %Includes externals forces on center mass in a vector WENCH\
            FEv=[fex;fey;fez+mass*Gz*9.81];%External linear forces
            MEv=[mex;mey;mez];%External Moments vector
            WEv=[FEv;MEv];
            %Dystra min 2-norm or min 2-norm-average tau
            [TAUva,x2]=forcea(anchorm,Uv,WEv,taumin,taumax);
            for ii=1:12
                TENpv(nn,ii)=TAUva(ii);
            end
            %Calculate the dynamic stiffness matrix K
            [Km]=stiffness(m,anchorm,Uv,LENv,Kv,TAUva);
            %Calculating eigenvalues
            EIGv=eig(Km);
        else
            TENpv(nn,1)=0;TENpv(nn,2)=0;TENpv(nn,3)=0;
            TENpv(nn,4)=0;TENpv(nn,5)=0;TENpv(nn,6)=0;
        end
    end
timep=size_points*dt;
%Data to controller
drum_diameter=0.095;pulley_ratio1=48/30;ratio_gear1=1/31;
%For motor1
theta_motor1=(180.0/pi)*(2.0/drum_diameter)*PISpv(:,1)/pulley_ratio1;%degrees
omega_motor1=(180.0/pi)*(2.0/drum_diameter)*Vlpv(:,1)/pulley_ratio1;%degrees/s
alfa_motor1=(180.0/pi)*(2.0/drum_diameter)*Alpv(:,1)/pulley_ratio1;%degrees/s^2
%For motor2
theta_motor2=(180.0/pi)*(2.0/drum_diameter)*PISpv(:,2)/pulley_ratio1;%degrees
omega_motor2=(180.0/pi)*(2.0/drum_diameter)*Vlpv(:,2)/pulley_ratio1;%degrees/s
alfa_motor2=(180.0/pi)*(2.0/drum_diameter)*Alpv(:,2)/pulley_ratio1;%degrees/s^2
%For motor3
```

```
  tension_motor3=TENpv(:,3);%Newton
  %For motor4
  tension_motor4=TENpv(:,4);%Newton
  nn=0;
  for tt=0:dt:timep-dt
      nn=nn+1;
      data(nn,:)=[...
          tt,...
          theta_motor1(nn,1),omega_motor1(nn,1),alfa_motor1(nn,1),...
          theta_motor2(nn,1),omega_motor2(nn,1),alfa_motor2(nn,1),...
          tension_motor3(nn,1),...
          tension_motor4(nn,1)];
  end
  disp('columns of data=(tt,theta1,omega1,alfa1,theta2,omega2,alfa2,tau3,tau4)')
  data
  %for the MAT-file
  pos1_matrix=[0:dt:timep-dt;PISpv(:,1)'];vel1_matrix=[0:dt:timep-dt;Vlpv(:,1)'];
  acc1_matrix=[0:dt:timep-dt;Alpv(:,1)'];tau1_matrix=[0:dt:timep-dt;TENpv(:,1)'];
  pos2_matrix=[0:dt:timep-dt;PISpv(:,2)'];vel2_matrix=[0:dt:timep-dt;Vlpv(:,2)'];
  acc2_matrix=[0:dt:timep-dt;Alpv(:,2)'];tau2_matrix=[0:dt:timep-dt;TENpv(:,2)'];
  pos3_matrix=[0:dt:timep-dt;PISpv(:,3)'];vel3_matrix=[0:dt:timep-dt;Vlpv(:,3)'];
  acc3_matrix=[0:dt:timep-dt;Alpv(:,3)'];tau3_matrix=[0:dt:timep-dt;TENpv(:,3)'];
  pos4_matrix=[0:dt:timep-dt;PISpv(:,4)'];vel4_matrix=[0:dt:timep-dt;Vlpv(:,4)'];
  acc4_matrix=[0:dt:timep-dt;Alpv(:,4)'];tau4_matrix=[0:dt:timep-dt;TENpv(:,4)'];
  pos5_matrix=[0:dt:timep-dt;PISpv(:,5)'];vel5_matrix=[0:dt:timep-dt;Vlpv(:,5)'];
  acc5_matrix=[0:dt:timep-dt;Alpv(:,5)'];tau5_matrix=[0:dt:timep-dt;TENpv(:,5)'];
  pos6_matrix=[0:dt:timep-dt;PISpv(:,6)'];vel6_matrix=[0:dt:timep-dt;Vlpv(:,6)'];
  acc6_matrix=[0:dt:timep-dt;Alpv(:,6)'];tau6_matrix=[0:dt:timep-dt;TENpv(:,6)'];
  %for the MAT-file
  pos1_motor_matrix=[0:dt:timep-
dt;(180.0/pi)*(2.0/drum_diameter)*PISpv(:,1)'/pulley_ratio1];
  vel1_motor_matrix=[0:dt:timep-
dt;(180.0/pi)*(2.0/drum_diameter)*Vlpv(:,1)'/pulley_ratio1];
  acc1_motor_matrix=[0:dt:timep-
dt;(180.0/pi)*(2.0/drum_diameter)*Alpv(:,1)'/pulley_ratio1];
  torque1_motor_matrix=[0:dt:timep-
dt;(2*TENpv(:,1)'+2*TENpv(:,5)')*(drum_diameter/2)*pulley_ratio1*ratio_gear1];
  pos2_motor_matrix=[0:dt:timep-
dt;(180.0/pi)*(2.0/drum_diameter)*PISpv(:,2)'/pulley_ratio1];
  vel2_motor_matrix=[0:dt:timep-
dt;(180.0/pi)*(2.0/drum_diameter)*Vlpv(:,2)'/pulley_ratio1];
  acc2_motor_matrix=[0:dt:timep-
```

```
dt;(180.0/pi)*(2.0/drum_diameter)*Alpv(:,2)'/pulley_ratio1];
  torque2_motor_matrix=[0:dt:timep-
dt;(2*TENpv(:,2)'+2*TENpv(:,6)')*(drum_diameter/2)*pulley_ratio1*ratio_gear1];
  tau3_motor_matrix=[0:dt:timep-dt;TENpv(:,3)'];
  tau4_motor_matrix=[0:dt:timep-dt;TENpv(:,4)'];
  Xpos_matrix=[0:dt:timep-dt;ppx(1,:)];Zpos_matrix=[0:dt:timep-dt;ppz(1,:)];
end%end of function path_controller
%--------------------------------------------------------------------------
end %fin de la función principal "m_spatial_confi09d"
```

Appendix B
Suspended robot workspace

The all-positive workspace boundaries of the underconstrained robot configuration are addressed in this Appendix. The analytic equations of the suspended cable-based robot for warehousing applications are developed so that its workspace fulfills the tensionable condition for a given set of minimum and maximum tension limits. The suspended robot cable is based on the configuration shown in Figure 3.13, where the mobile platform is suspended by the upper four cables. The structure matrix, the cable tension vector, and the wrench of the suspended cable robot is defined by

$$\boldsymbol{A}_s = \begin{bmatrix} \frac{q_1}{2l_1} & \frac{q_2}{2l_2} & \frac{q_1}{2l_5} & \frac{q_2}{2l_6} \\ \frac{q_5}{2l_1} & \frac{q_5}{2l_2} & \frac{q_5}{2l_5} & \frac{q_5}{2l_6} \\ \frac{q_7}{4l_1} & \frac{q_8}{4l_2} & \frac{q_{11}}{4l_5} & \frac{q_{12}}{4l_6} \end{bmatrix}, \quad \boldsymbol{\tau}_s = \begin{bmatrix} \tau_{s1} \\ \tau_{s2} \\ \tau_{s5} \\ \tau_{s6} \end{bmatrix}, \quad \boldsymbol{W}_s = \begin{bmatrix} F_x \\ \left(F_z + m_p G_z\right) \\ M_y \end{bmatrix} \tag{A.1}$$

where

$$q_1 = 2P_x + (e - b)$$
$$q_2 = 2P_x - (e - b)$$
$$q_5 = 2P_z + 2\left(c - y_{cp}\right) - f$$
$$q_7 = 2\left(c - y_{cp}\right)(2P_x + e) + b(2P_z - f)$$
$$q_8 = 2\left(c - y_{cp}\right)(2P_x - e) - b(2P_z - f)$$
$$q_{11} = a\, q_5 - 2y_{cp}\, q_1$$
$$q_{12} = -a\, q_5 - 2y_{cp}\, q_2$$
$$y_{cp} = \frac{(2d + a)c}{3(d + a)}$$

The all-positive workspace, $\boldsymbol{\Gamma}_s$ can be obtained by analyzing slackness conditions with constant orientation of the mobile platform ($\theta_y = 0$), and by solving the all-positive cable tension redundancy. Indeed, the loss of one cable makes $\boldsymbol{A}_s$ square, which might admit an exact positive tension solution for the remaining three cable pairs. When cable 1 has no tension, then $\tau_{s1} = 0$ and the system transforms into an equivalent three-tension system. The unique solution, $\boldsymbol{\Gamma}_{s1}$, is defined by the feasible area of curves $\boldsymbol{\delta}_0 > 0$, $\boldsymbol{\delta}_2 > 0$, and $\boldsymbol{\delta}_6 > 0$. Symmetrically, the area defined by curves $\boldsymbol{\varepsilon}_0 < 0$, $\boldsymbol{\varepsilon}_1 < 0$ and $\boldsymbol{\varepsilon}_5 < 0$

represents the feasible workspace, $\boldsymbol{\Gamma}_{s2}$, when cable 2 is slack ($\tau_{s2} = 0$). Equations of the curves are shown below.

$$\boldsymbol{\delta}_0 = -\frac{1}{8}\left(-2y_{cp} + 2c + 2P_z - f\right)(b-e)(bf + 2by_{cp} - 2bP_z - af + 2aP_z + 2ac - 2ay_{cp} + 4cP_x - 2ce).$$

$$\boldsymbol{\delta}_2 = -\frac{1}{4}(2F_x ac - 2F_x ey_{cp} + 2M_y b - F_x af - 2M_y e - 2F_x ay_{cp} - 2F_z aP_x + 2am_p G_z P_x + 2F_x aP_z + 2F_x by_{cp})(2c - f + 2P_z - 2y_{cp}).$$

$$\begin{aligned}\boldsymbol{\delta}_5 = \frac{1}{8}\big(&bm_p G_z - em_p G_z + 2m_p G_z P_x + 2F_x c - F_x f + 2F_x P_z - 2F_x y_{cp} - F_z b + F_z e \\ &- 2F_z P_x\big)\big(2ac - af + 2aP_z - 2ay_{cp} + bf - 2bP_z + 2by_{cp} - 2ce \\ &+ 4cP_x\big)\end{aligned}$$

$$\begin{aligned}\boldsymbol{\delta}_6 = {} & c\left(F_z - m_p G_z\right)P_x^2 + \frac{F_x}{2}(a+b)P_z^2 \\ &+ \Big(\frac{1}{2}F_x cf + \frac{1}{4}F_z bf - \frac{1}{2}F_z ac - \frac{1}{2}m_p G_z by_{cp} + \frac{1}{2}m_p G_z ac - \frac{1}{2}F_z bc \\ &+ \frac{1}{4}F_z af + \frac{1}{2}F_z by_{cp} + \frac{1}{2}F_z ay_{cp} - F_x c^2 - \frac{1}{2}m_p G_z ay_{cp} + F_x cy_{cp} \\ &+ \frac{1}{2}m_p G_z bc - \frac{1}{4}m_p G_z af - \frac{1}{4}m_p G_z bf\Big)P_x \\ &+ \Big(-\frac{1}{4}m_p G_z b^2 - \frac{1}{4}F_z ab - M_y e + \frac{1}{4}F_z ae + \frac{1}{4}F_z b^2 + F_x ac - \frac{1}{4}F_z be \\ &- \frac{1}{2}F_x af + \frac{1}{4}m_p G_z ab - F_x ay_{cp} + M_y b + \frac{1}{2}F_x bc - \frac{1}{4}m_p G_z ae \\ &- \frac{1}{2}F_x bf - F_x ey_{cp} + \frac{1}{2}F_x ce + \frac{1}{4}m_p G_z be\Big)P_z \\ &+ \Big(\frac{1}{2}m_p G_z a - \frac{1}{2}F_z a + \frac{1}{2}bm_p G_z - F_x c - \frac{1}{2}F_z b\Big)P_x P_z + \frac{1}{8}m_p G_z b^2 f + \frac{1}{4}m_p G_z b^2 y_{cp} \\ &+ \frac{1}{4}m_p G_z ce^2 - \frac{1}{4}F_z abc + \frac{1}{8}F_z abf + \frac{1}{4}F_z aby_{cp} + \frac{1}{4}F_z ace - \frac{1}{8}F_z aef \\ &- \frac{1}{4}F_z aey_{cp} + \frac{1}{4}F_z bce + \frac{1}{8}F_z bef + \frac{1}{4}F_z bey_{cp} - \frac{1}{2}F_x acf - F_x acy_{cp} \\ &+ \frac{1}{2}F_x afy_{cp} - \frac{1}{4}F_x bcf + \frac{1}{2}F_x bcfy_{cp} - \frac{1}{4}F_x cef - \frac{3}{2}F_x cey_{cp} \\ &+ \frac{1}{2}F_x efy_{cp}\end{aligned} \tag{A.2}$$

$\boldsymbol{\varepsilon_0} = \frac{1}{8}\left(-2y_{cp} + 2c + 2P_z - f\right)(b-e)(bf + 2by_{cp} - 2bP_z - af + 2aP_z + 2ac - 2ay_{cp} - 4cP_x - 2ce)$.

$\boldsymbol{\varepsilon_1} = \boldsymbol{\delta_2}$.

$$\begin{aligned}\boldsymbol{\varepsilon_5} = {} & \left(cm_pG_z - F_zc\right)P_x^2 \\ & + \left(\left(-\frac{1}{2}F_zb + \frac{1}{2}am_pG_z - \frac{1}{2}F_za + \frac{1}{2}bm_pG_z + F_xc\right)P_z + \frac{1}{4}F_zaf\right. \\ & + \frac{1}{4}F_zbf + \frac{1}{2}m_pG_zbc - F_xcy_{cp} + \frac{1}{2}F_zby_{cp} + \frac{1}{2}F_zay_{cp} + F_xc^2 \\ & + \frac{1}{2}am_pG_zc - \frac{1}{2}F_zbc - \frac{1}{2}F_zac - \frac{1}{2}F_xcf - \frac{1}{4}am_pG_zf - \frac{1}{2}am_pG_zy_{cp} \\ & \left. - \frac{1}{4}bm_pG_zf - \frac{1}{2}bm_pG_zy_{cp}\right)P_x + \left(\frac{1}{2}F_xb + \frac{1}{2}aF_x\right)P_z^2 \\ & + \left(-\frac{1}{4}F_zb^2 + acF_x - \frac{1}{2}fbF_x - ay_{cp}F_x - \frac{1}{4}m_pG_zbe - eM_y\right. \\ & + \frac{1}{4}m_pG_zb^2 + \frac{1}{4}F_zab - \frac{1}{2}faF_x - \frac{1}{4}m_pG_zab - y_{cp}eF_x - \frac{1}{4}F_zae \\ & \left. + \frac{1}{2}cbF_x + \frac{1}{4}am_pG_ze + bM_y + \frac{1}{4}F_zbe + \frac{1}{2}ecF_x\right)P_z - \frac{1}{8}m_pG_zb^2f \\ & - \frac{1}{8}F_zbef + \frac{1}{8}F_zaef - \frac{1}{8}F_zabf - \frac{1}{4}F_zbey_{cp} - \frac{1}{4}F_zbce + \frac{1}{4}F_zaey_{cp} \\ & - \frac{1}{4}F_zace - \frac{1}{4}F_zaby_{cp} + \frac{1}{4}F_zabc - \frac{1}{4}F_xbcf - \frac{1}{4}F_xcef - \frac{1}{4}m_pG_zce^2 \\ & - \frac{1}{4}m_pG_zb^2y_{cp} - aF_xcy_{cp} + \frac{1}{8}F_zb^2f + \frac{1}{8}F_xbf^2 + \frac{1}{8}F_xaf^2 + \frac{1}{4}F_zce^2 \\ & + \frac{1}{4}F_zb^2y_{cp} + \frac{1}{2}F_xc^2e - \frac{1}{2}F_xby_{cp}^2 + \frac{1}{2}F_xay_{cp}^2 + \frac{1}{2}F_xac^2 + \frac{1}{2}M_yef - \frac{1}{2}M_ybf \\ & + \frac{1}{2}F_xefy_{cp} + \frac{1}{2}F_xbcy_{cp} + \frac{1}{2}F_xafy_{cp} - \frac{1}{2}F_xacf + F_xey_{cp}^2 + eM_yy_{cp} \\ & - M_yce - bM_yy_{cp} + bM_yc - \frac{3}{2}F_xcey_{cp} - \frac{1}{8}m_pG_zaef + \frac{1}{8}m_pG_zabf \\ & + \frac{1}{4}m_pG_zbce + \frac{1}{4}m_pG_zbey_{cp} - \frac{1}{4}m_pG_zaey_{cp} + \frac{1}{4}m_pG_zace \\ & - \frac{1}{4}m_pG_zabc + \frac{1}{4}m_pG_zaby_{cp} + \frac{1}{8}m_pG_zbef\end{aligned}$$

$\boldsymbol{\varepsilon_6} = \frac{1}{8}(-bm_pG_z + em_pG_z + 2m_pG_zP_x + 2F_xc - F_xf + 2F_xP_z - 2F_xy_{cp} + F_zb - F_ze -$

$2F_zP_x)(2ac - af + 2aP_z - 2ay_{cp} + bf - 2bP_z + 2by_{cp} - 2ce - 4cP_x)$.

Conditions $\boldsymbol{\delta}_0 > 0$ and $\boldsymbol{\varepsilon}_0 < 0$ ensure that the structure matrices are not singular. In addition, conditions (3.27) guarantee a nonsingular position of the mobile platform. Cable tensions can be obtained by

$$\overline{\tau}_{si} = \begin{cases} \left(\frac{l_i\delta_i}{\delta_0}\right) & \forall\, i = 2,5,6.\ \ 0 < P_x < \delta_6 \\ \left(\frac{l_i\varepsilon_i}{\varepsilon_0}\right) & \forall\, i = 1,5,6.\ \ \varepsilon_5 < P_x \leq 0 \end{cases} \tag{A.3}$$

These results provide information about the amount of tension applied at each top projected parallel cable set by

$$\tau_{spi} = \overline{\tau}_{si} + \overline{\tau}_{s(i+4)} \ \ \forall\, i = 1,2 \tag{A.4}$$

with the tension orientation as follows:

$$\boldsymbol{\tau}_{spi} = \tau_{spi}[\ \hat{l}_{ix} \quad 0 \quad \hat{l}_{iz}\ ]^T \quad \forall \ \ i = \ \ 1,2 \tag{A.5}$$

The location of virtual cables in the mobile platform permits a better understanding of the problem. The virtual cables represent the action of the top parallel cables on the mobile platform. Figure A.1 shows the virtual cables acting on the suspended cable robot.

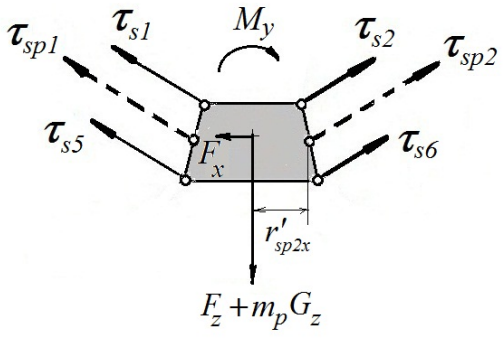

Figure A.1: Virtual cables acting in the suspended planar cable robot.

The virtual anchor points can be written in function of the anchor horizontal distance r'_{sp2x}, by using geometrical parameters of the mobile platform and moment balance equations as follows:

$$r'_{sp2z} = \rho\left(r_{6x} - r'_{sp2x}\right) - y_{cp} \tag{A.6}$$

$$r'_{sp1z} = \rho\left(r'_{sp1x} - r_{5x}\right) - y_{cp} \tag{A.7}$$

$$r'_{sp1x} = \frac{r_{5x}\rho(F_x\theta_2 - \alpha) + (F_x\theta_1 - \alpha)\left(r_{6x}\rho - r'_{sp2x}(\rho + \theta_2)\right) + (\theta_1 - \theta_2)(\Delta_{mx}\alpha - F_x y_{cp})}{(\rho - \theta_1)(F_x\theta_2 - \alpha)} \tag{A.8}$$

$$\forall\ \rho \neq \theta_1$$

where

$$\rho = \frac{2c}{(a-b)}, \quad \forall\ a > b, c > 0$$

$$\theta_i = \frac{\hat{l}_{iz}}{\hat{l}_{ix}}, \quad \forall\ \hat{l}_{ix} \neq 0, i = 1, 2.$$

$$\Delta_{mx} = \frac{M_y}{\alpha\sqrt{F_x^2 + \alpha^2}} \quad \forall\ \alpha \neq 0$$

$$\alpha = F_z - m_p G_z \quad \forall\ m_p \neq 0$$

In other words, the virtual anchor points are changing accordingly to find a positive cable tension solution. Thus, cable tensions can be expressed in function of these virtual anchor points as:

$$\begin{bmatrix}\tau_{s1}\\ \tau_{s5}\end{bmatrix} = \left(\frac{\tau_{sp1}}{r_{1x}r_{5z} - r_{1z}r_{5x}}\right)\begin{bmatrix} r_{5z} & -r_{5x}\\ -r_{1z} & r_{1x}\end{bmatrix}\begin{bmatrix} r'_{sp1x}\\ r'_{sp1z}\end{bmatrix} \tag{A.9a}$$

$$\begin{bmatrix}\tau_{s2}\\ \tau_{s6}\end{bmatrix} = \left(\frac{\tau_{sp2}}{r_{2x}r_{6z} - r_{2z}r_{6x}}\right)\begin{bmatrix} r_{6z} & -r_{6x}\\ -r_{2z} & r_{2x}\end{bmatrix}\begin{bmatrix} r'_{sp2x}\\ r'_{sp2z}\end{bmatrix} \tag{A.9b}$$

The distances r_{ix} are the known anchor points on the mobile platform. The solution of equations (A.9a) and (A.9b) are function of the geometrical parameter r'_{sp2x} which value for positive tensions can be found between the geometric limits $r_{2x} < r'_{sp2x} < r_{6x}$.

The minimum two-norm cable tension problem expressed in Eq. (2.15) can be rewritten as:

$$\text{minimize } \mathrm{F}^2 = \tau_{sp1}^2 + \tau_{sp2}^2 - 2(\tau_{s1}\tau_{s5} + \tau_{s2}\tau_{s6}) \tag{A.10}$$

By substituting equations (A.9a) and (A.9b) into Eq. (A.10), a quadratic equation is obtained which admits a minimum value by equaling its derivative to zero,

$$\frac{\partial(\tau_{s1}\tau_{s5} + \tau_{s2}\tau_{s6})}{\partial(r'_{sp2x})} = 0 \tag{A.11}$$

The optimal value of r'_{sp2x} for the minimum cable tensions requires the solution of Eq. (A.11), such as

$$^{*}r'_{sp2x} = -\frac{N_m}{2D_m} \tag{A.12}$$

where

$N_m = \left(\frac{\tau_{sp1}}{(r_{1x}r_{5z} - r_{1z}r_{5x})}\right)^2 \left(\frac{1}{(\theta_1 - \rho)(F_x\theta_2 - \alpha)}\right)^2 (\theta_2 + \rho)(F_x\theta_1 - \alpha)(2r_{1x}r_{5x}^2\theta_1\theta_2\rho^2 + 2r_{1x}r_{5x}r_{6x}\theta_1\rho^3 - r_{1x}r_{5x}r_{5z}\theta_1\theta_2\rho - r_{1x}r_{5x}r_{5z}\theta_2\rho^2 + 2r_{1x}r_{5x}\theta_1\theta_2\rho y_{cp} - 2r_{1x}r_{5x}\theta_1\rho^2 y_{cp} - 2r_{1x}r_{5z}r_{6x}\theta_1\rho^2 - r_{1z}r_{5x}^2\theta_1\theta_2\rho - r_{1z}r_{5x}^2\theta_2\rho^2 - 2r_{1z}r_{5x}r_{6x}\theta_1\rho^2 - r_{1x}r_{5z}\theta_1\theta_2 y_{cp} + 2r_{1x}r_{5z}\theta_1\rho y_{cp} - r_{1x}r_{5z}\theta_2\rho y_{cp} + 2r_{1z}r_{5x}r_{5z}\theta_2\rho - r_{1z}r_{5x}\theta_1\theta_2 y_{cp} + 2r_{1z}r_{5x}\theta_1\rho y_{cp} - r_{1z}r_{5x}\theta_2\rho y_{cp} + 2r_{1z}r_{5z}r_{6x}\theta_1\rho - 2r_{1z}r_{5z}\theta_1 y_{cp} + 2r_{1z}r_{5z}\theta_2 y_{cp})F_x + (2r_{1x}r_{5z}r_{6x}\rho^2 - 2r_{1x}r_{5x}^2\theta_1\rho^2 - 2r_{1x}r_{5x}r_{6x}\rho^3 + r_{1x}r_{5z}\theta_1 y_{cp} + 2r_{1x}r_{5x}\rho^2 y_{cp} - r_{1x}r_{5z}\rho y_{cp} - 2r_{1x}r_{5x}\theta_1\rho y_{cp} - 2r_{1z}r_{5x}r_{5z}\rho + 2r_{1z}r_{5x}r_{6x}\rho^2 + 2\Delta_{mx}r_{1z}r_{5z}\theta_1 - 2\Delta_{mx}r_{1z}r_{5z}\theta_2 + r_{1z}r_{5x}\theta_1 y_{cp} - r_{1z}r_{5x}\rho y_{cp} - 2r_{1z}r_{5z}r_{6x}\rho + r_{1z}r_{5x}^2\theta_1\rho + 2\Delta_{mx}r_{1x}r_{5x}\theta_1\rho^2 - 2\Delta_{mx}r_{1x}r_{5z}\theta_1\rho + r_{1x}r_{5x}r_{5z}\rho^2 + r_{1z}r_{5x}^2\rho^2 + r_{1x}r_{5x}r_{5z}\theta_1\rho + 2\Delta_{mx}r_{1z}r_{5x}\theta_1\rho + 2\Delta_{mx}r_{1z}r_{5x}\theta_2\rho - 2\Delta_{mx}r_{1x}r_{5x}\theta_2\rho^2 + 2\Delta_{mx}r_{1x}r_{5z}\theta_2\rho)\alpha + \left(\frac{\tau_{sp2}}{r_{2x}r_{6z} - r_{2z}r_{6x}}\right)^2 (\rho\, r_{6x} - y_{cp})(2\rho\, r_{2x}r_{6x} + r_{2x}r_{6z} + r_{2z}r_{6x})$.

$D_m = \left(\frac{\tau_{sp1}}{(r_{1x}r_{5z} - r_{1z}r_{5x})}\right)^2 \left(\frac{(\theta_2 + \rho)(F_x\theta_1 - \alpha)}{(\theta_1 - \rho)(F_x\theta_2 - \alpha)}\right)^2 (\rho r_{1x} - r_{1z})(r_{5z} - \rho r_{5x}) - \left(\frac{\tau_{sp2}}{r_{2x}r_{6z} - r_{2z}r_{6x}}\right)^2 (\rho\, r_{2x} + r_{2z})(\rho\, r_{6x} + r_{6z})$.